Nuno Manuel Ortega Amaro

Mestre em Engenharia Electrotécnica e de Computadores

Study of AC losses in medium-sized high temperature superconducting coils

Dissertação para obtenção do Grau de Doutor em Engenharia Electrotécnica e de Computadores

Orientador: João Miguel Murta Pina, Professor Doutor,
Universidade Nova de Lisboa
Co-orientadores: João Francisco Alves Martins, Professor Doutor,
Universidade Nova de Lisboa
José Maria Ceballos Martinez, Professor Doutor,
Universidad de Extremadura

Júri:

Presidente: Prof. Doutor Paulo da Costa Luís da Fonseca Pinto
Arguentes: Prof. Doutor Mário Fernando da Silva Ventim Neves
Prof. Doutor Xavier Granados Garcia

Vogais: Prof. Doutor Alfredo Álvarez Garcia
Prof. Doutor Paulo José da Costa Branco
Prof. Doutor João Miguel Murta Pina

FACULDADE DE CIÊNCIAS E TECNOLOGIA
UNIVERSIDADE NOVA DE LISBOA

Dezembro 2015

Study of AC losses in medium-sized High Temperature Superconducting Coils

To my family and friends…

Looking back, I have to thank to so many people that it is almost impossible to write it down in a few lines. First of all I would like to thank to my three supervisors: Prof. João Murta Pina, Prof. João Martins and Prof. José Ceballos. Although the necessary hierarchical structure defines one supervisor and two co-supervisors I feel that this was really a team work and the experience and knowledge I gain from the three is similar. Thank you for all the moments, professional and personal, we had together.

To Doctors Fedor Gomory, Enric Pardo, Jan Souc and the remaining personnel from the Slovak Academy of Sciences, thank you for everything during my visit of three months to your laboratory. It was truly an honour to have the opportunity to work with you and to share some goods moments during my stay there.

I also would like to express my gratitude to the remaining professors in our section, from Faculdade de Ciências e Tecnologia da Universidade Nova de Lisboa. Prof. Mário Ventim, Prof. Anabela Pronto, Prof. Pedro Pereira and Prof. Stanimir Valtchev, and the remaining organization of the Electrical Engineering department. Thank you all not only for the help during the PhD work but also in the undergraduate and Masters Studies. It was that path that brought me here, today. A very warm and special thanks also for the remaining Professors of the Benito Mahedero – Group of Electrical applications of Superconductors from Universidad de Extremadura, Spain, for all the help given and kindness demonstrated during our many visits to Badajoz.

I also acknowledge the financial support given by Fundação para a Ciência e Tecnologia, through a PhD Scholarship with the reference SFRH/BD/78418/2011.

To my friends, Fábio Januário, Pedro Arsénio and Nuno Vilhena, thank you for walking alongside me during this long journey and for everything, in the good and not so good moments. Your time will come soon guys! To remaining colleagues, whose names are too many to state but the non-inclusion of a name does not necessarily means a forgetfulness of all help during these last four years.

Finally, I need to thank to all my family for supporting my choices and always being there when I needed.

Ana Rita, you cannot be included in this list. My thanks to you could not be expressed in words even if I had a true writing gift. To you I owe what I am today, and no matter what I will become you will always be there.

Thank you all, this work and this document is the result of what I am and what I am is the result of all I received from everyone that crossed my path during my life. Thank you all…

Abstract

The study of AC losses in superconducting pancake coils is of utmost importance for the development of superconducting devices. Due to different technical difficulties this study is usually performed considering one of two approaches: considering superconducting coils of few turns and studying AC losses in a large frequency range vs. superconducting coils with a large number of turns but measuring AC losses only in low frequencies. In this work, a study of AC losses in 128 turn superconducting coils is performed, considering frequencies ranging from 50 Hz till 1152 Hz and currents ranging from zero till the critical current of the coils. Moreover, the study of AC losses considering two different simultaneous harmonic components is also performed and results are compared to the behaviour presented by the coils when operating in a single frequency regime.

Different electrical methods are used to verify the total amount of AC losses in the coil and a simple calorimetric method is presented, in order to measure AC losses in a multi-harmonic context. Different analytical and numerical methods are implemented and/or used, to design the superconducting coils and to compute the total amount of AC losses in the superconducting system and a comparison is performed to verify the advantages and drawbacks of each method.

Keywords:, HTS Coils, AC losses, analytical modelling, numerical modelling, multi-harmonic behaviour.

Resumo

O estudo de perdas AC em bobinas supercondutoras é de elevada importância para o desenvolvimento de dispositivos associados a esta tecnologia. Devido a diversas dificuldades de foro técnico os estudos presentes na literatura enquadram-se em uma de duas diferentes aproximações: estudo de perdas AC em bobinas com reduzido número de espiras mas considerando um espectro de frequências elevado ou estudo realizado em bobinas com um maior número de espiras, mas realizados apenas a frequências baixas, nomeadamente as frequências industriais de 50 ou 60 Hz. Neste trabalho, um estudo de perdas AC em bobinas de tamanho médio com um total de 128 espiras foi realizado, considerando um espectro de frequências desde 50 Hz até 1152 Hz e considerando correntes desde zero até à corrente crítica da bobina supercondutora. Adicionalmente, um outro estudo considerando mais do que uma harmónica de corrente a fluir em simultâneo na bobina também foi realizado, para verificar o efeito que este comportamento multi-harmónica poderá ter no valor total de perdas AC apresentado pela bobina.

Diferentes métodos de carácter eléctrico foram considerados para a medição das perdas AC nas bobinas supercondutoras e um método calorimétrico foi implementado para a determinação de perdas no contexto multi-harmónicas. Diferentes modelos analíticos e numéricos foram implementados e/ou utilizados, tanto para verificar as características das bobinas supercondutoras como para calcular a totalidade de perdas AC apresentadas pelas mesmas. Finalmente, foi efectuada uma comparação entre os diversos métodos e modelos utilizados, a fim de extrair as vantagens e desvantagens de cada um, no estudo de perdas AC em bobinas supercondutoras.

Palavras-chave: Bobinas supercondutoras, Perdas AC, modelos analíticos, modelos numéricos, comportamento multi-harmónicas.

List of Contents

List of Figures

List of Tables

Symbology

B	Magnetic flux density (T).
B_i	Experimentally verified constant used in Kim Model.
C	Capacitance (F).
C_1	Cylindrical Capacitor 1.
C_2	Cylindrical Capacitor 2.
C_{1LN2}	Capacitance of cylindrical capacitor 1 when fully immersed in liquid nitrogen (pF)
C_{2LN2}	Capacitance of cylindrical capacitor 2 when fully immersed in liquid nitrogen (pF)
d	thickness of superconducting tape or superconducting layer (mm).
D	Internal diameter of a superconducting coil (mm).
ΔH_{vap}	Latent heat of vaporization of nitrogen (198.99 kJ/kg).
E	Energy (J).
E	Electric Field (V/m).
E_C	Critical Electric Field (1 µV/cm).
$\mathbf{E_{sc}}$	Electric field inside a superconductor.
esp	Thickness of a superconducting tape.
f	Frequency (Hz).
g	distance between two adjacent superconducting coils (mm).
H	Magnetic Field (A/m).
H	Height of nitrogen in a cryostat (m).
h	distance between superconducting regions of two adjacent superconducting tapes (mm).
H_C	Critical Magnetic Field (A/m).
I	DC current applied to a superconducting tape or coil (A).
I_p (or I_m)	Amplitude of an AC current flowing in a superconductor (A).
J	Current Density (A/m^2).
J_C	Critical Current Density (A/m^2).

J_{C0}	Critical Current Density achieved in self-field conditions (A/m^2).
J_{SC}	Critical Current Density inside a superconductor (A/m^2).
L	Self-inductance (H).
l	Perimeter of outer filament in a superconducting tape (mm) or length of superconducting tape used in a coil (m).
L_C	Loss Power per cycle per unit of length (W/m).
L_M	Mutual Inductance (H).
m	Mass (kg).
n	coefficient of the power law in a superconductor.
N	number of turns in a coil.
P_{ed}	Loss power due to eddy currents per cycle per unit of length (W/m).
Pr	Resistive loss power per cycle per unit of length (W/m).
Q	Energy loss per cycle per unit length (J/m).
R	Electrical resistance (Ω).
$R_{connection}$	Resistance of an electric connection between two superconducting coils (Ω).
r_1	Internal radius of a cylindrical capacitor (mm).
r_2	External radius of a cylindrical capacitor (mm).
R_i	Internal radius of a superconducting coil (mm).
R_e	External radius of a superconducting coil (mm).
S	Section of superconductor (mm^2).
S_C	Section of a cryostat (mm^2).
T	Working Temperature (K).
T_C	Critical Temperature (K).
U	Voltage (V).
w	width of a superconduting tape (mm).
ε	Permittivity of medium (F/m).
ε_0	Permittivity of vacuum (8.854×10^{-12} F/m).
μ_0	Vacuum permeability ($4 \times \pi \times 10^{-7}$ H/m).
ρ	Resistivity (Ω.m).
τ	Time constant (s).

Acronyms

1G	Superconducting tape of first generation, in Bi-2212 or Bi-2223.
2G	Second generation superconducting tape manufactured from YBCO.
AC	Alternating current.
AMSC	American Superconductor.
BaLaCuo	First high temperature superconductor discovered.
BLCO	same as BaLaCuO.
Bi-2201	High temperature superconductor with a chemical composition of $Bi_2Sr_2Ca_0Cu_1O_6$.
Bi-2212	High temperature superconductor with a chemical composition of $Bi_2Sr_2Ca_1Cu_2O_8$.
Bi-2223	High temperature superconductor with a chemical composition of $Bi_2Sr_2Ca_2Cu_3O_{12}$.
BSCCO	One of the three forms of the superconductor above.
BiSrCaCuO	same as BSCCO.
DC	Direct Current, in opposition to alternative current.
FEA	Finite Element Analysis.
FEM	Finite Element Method or Finite Element Modelling.
HBCCO	High temperature superconductor with a chemical composition of $HgBa_2Ca_2Cu_3O_{1+x}$.
HgBaCaCuO	same as HBCCO.
HTBCCO	High temperature superconductor with a chemical composition of $Hg_{0.8}Tl_{0.2}Ba_2Ca_2Cu_3O_{8+\delta}$.
HgTlBaCaCuO	same as HTBCCO.
HTS	High Temperature Superconductivity / Superconductor.
IBAD	Ion Beam Assisted Deposition.
LIA	Lock-In Amplifier.
MEMEP	Minimum Electro-Magnetic Entropy Production.
MOCVD	Metal-Organic Chemical Vapour Deposition.

PDE	Partial Differential Equation.
PIT	Powder In Tube.
RABiTS	Rolling-Assisted Biaxially Textured Substrate.
SFCL	Superconducting Fault Current Limiter.
SFCLT	Superconducting Fault Current Limiting Transformer.
SMES	Superconducting Magnetic Energy Storage.
TFA-MOD	Trifluoroacetate Metal Organic Deposition.
XPS	Extruded polystyrene.
Y-123	Superconducting phase of YBCO.
YBaCuO	High temperature superconductor with a chemical constitution of $YBa_2Cu_3O_{7-\delta}$.
YBCO	Same as YBaCuO.

1

Introduction

1.1 Background and Motivation

Electric grids are operating in a particular challenging context in the last years. The necessity for a high quality power and different environmental protection laws are forcing grid operators to surpass different technological challenges and to change completely the concept of electric grid. With this change arises the opportunity for new devices and new technologies, having always as goals the improvement of power quality while reaching a sustainable energy system. One such technology, whose applications are envisaged to promote this change in electric grids, is superconductivity.

Different superconducting devices can be applied in power grids and their unique characteristics make them valid candidates to solve different problems in the existing grids. Through the whole world, different research groups focus their interest in these devices and their applications to power systems (Tixador 2010; Fujiwara et al. 2010; Xiao et al. 2012). However, superconductors still have different technological problems that need to be solved, in order to reach a maturity state to apply in a large scale context. One of such challenges, which concentrate a huge investigation effort, is the existence of AC losses. When operating in DC conditions, superconductors present a virtual zero resistance, a unique and very important characteristic which by itself could solve different problems in power grids such as transport losses. However, when operating in AC conditions a component of AC losses is generated. Considering that superconductors operate at cryogenic temperatures, it is necessary to extract all heat generated in the system and the existence of AC losses results in a higher amount of heat loss, which evidently results in the need to have higher power cryogenic systems, when comparing with DC operation. Therefore, the study of AC losses, which includes the mechanisms that originate them, creation and development of methods to measure them and minimization strategies, is a key to improve the performance of superconducting devices and their applicability. In addition to this, superconducting materials are still costly, which results in high implementation costs for any project. Considering this, the creation of accurate models is a very important step, in order to allow the simulation of superconducting devices and extract their behavioural characteristics to apply to real systems. Different models, with different levels of complexity can be used, not only to calculate AC losses but so simulate the overall system.

One of the superconducting elements that is most vastly used in devices is the superconducting pancake coil. Therefore, the study of AC losses in pancake coils is of utmost importance. Although this study has been already performed for years, there is still space for innovation in this area. The coil inductance allied to the high currents that can flow through the superconductor will result in high voltages at the coil ends, making the process of measuring AC losses a complex one. The need for accurate models is even more important considering this aspect.

Taking into account the different considerations present in the last few paragraphs, this work aims to contribute to the study of AC losses in medium-sized (more than one hundred turns) superconducting coils, through the implementation of measuring processes and validation of different models. The study of AC losses is usually performed considering two different conditions: small coils considering a large frequency spectrum or larger coils, but considering only the industrial frequency (50 Hz or 60 Hz). In this work, a study of AC losses in medium sized coils will be performed for a frequency range of 50 Hz to 1152 Hz considering different measuring methods and different models.

1.2 Research Question and General Approach

As mentioned before, the application of superconducting devices in power systems in order to increase power quality is desirable. Many of these devices use a common superconducting element: superconducting pancake coils. Although they have unique characteristics, superconductors present AC losses when in present of an AC magnetic field, or when flown by an AC current. Since these losses will generate heat that must be extracted from the cryogenic system in which the superconducting device is immersed, the study of AC losses in superconducting pancake coils is of upmost importance to the development of superconducting devices. Considering this, the main research question chosen to guide this work is the following:

Research Question (Q1)

What is the behavior demonstrated by AC losses in medium-sized superconducting coils when subjected to currents considering a high frequency range, in comparison to that demonstrated by smaller coils and samples of superconducting tape?

Proposed hypothesis to address this research question is:

Hypothesis

If measuring methods used to measure AC losses in other superconducting components can be applied to medium-sized coils at high frequencies, within safe operating conditions, then the behavior presented by these coils can be correctly evaluated and compared to that obtained by other superconducting elements, providing an advance in the study of AC losses in superconducting pancake coils.

In addition to this research question, some more specific research questions can be formulated:

Q1 a)

Are methods used to measure AC losses in samples of superconducting tape applicable to coils with a high number of turns and a high working frequency?

Q1 b)

Do existing models, both analytical and numerical, present good results when considering AC losses in superconducting coils with a high number of turns?

Q1 c)

Do AC losses have a linear behavior when more than one current harmonic is flowing in the superconducting coil, i.e., is the total amount of AC losses the sum of the losses components originated by the different frequency harmonics or is there a new component?

To answer these questions, all the following steps must be taken into account:

- Consider the different existing methods to measure AC losses and apply them to medium-sized superconducting coils;
- Compare results obtained with the different methods and if necessary try to adjust the existing methods to improve results, or consider the creation of new measuring methods;
- Simulate the behavior of a test superconducting coil, in order to verify the applicability of numerical and analytical models.

1.3 Contents of this document

This thesis is organized in five different chapters, excluding the present one and one for conclusions, which aims not only to summarize results obtained but also to give some future work possibilities within this line of research and present the original contributions of this work to the scientific field in study. A brief description of the remaining chapters is now given, in order to give the reader an overall view of the document organization.

- Chapter 2 – **Theoretical Background**: this section is made of a literature revision of superconducting devices systems and associated technologies. Since superconductivity is not a conventional field in the framework of Electrical Engineering, a brief historical perspective is presented. After that, the literature review is focused in AC losses, describing their origins, measuring methods and evolution when increasing the superconducting device complexity.
- Chapter 3 – **Modelling of High Temperature Superconductors**: for a successful application of superconducting devices in power systems, a first phase of modelling is usually performed in order to achieve the desirable system characteristics. Different implemented models in this work are contained in this section of the document, together with other models that are used here but whose implementation was performed by other research groups along the years. All models described have as a goal the computation of AC losses, even if they can easily be used for other goals.
- Chapter 4 – **Experimental Setups**: different experimental setups were implemented, with the objective of verifying the main characteristics of the different elements used in this thesis. The implementation process of every experimental setup is described in this section.
- Chapter 5 – **HTS Coils Prototypes**: this section contains a description of the implementation process of different superconducting coils, which are the test elements in this work. Measurements performed in those coils, in order to verify their characteristics, are also presented in this chapter.
- Chapter 6 – **AC Losses**: main chapter of this document, in which the measurement of AC losses in the test coils is performed and results are compared to those obtained using the different models.

2

Theoretical Background

2.1. Superconductivity as a state of Matter

Superconductivity is a vast field of knowledge, with more than 100 years of associated research. Consequently it is not feasible to describe in a document such as a thesis all associated phenomena and characteristics of superconducting materials. However, it is also not logical to realize a work in this area without addressing the main phenomena related to it. Thus, a short description of superconductivity and basic characteristics of materials used in this work will be presented.

2.1.1. Historical Perspective

Figure 2.1 shows a summarized timeline with the most significant discoveries related to superconductivity. Some of these discoveries, although very important to the general knowledge of this phenomenon, are out of the scope of this thesis, thus will not be addressed.

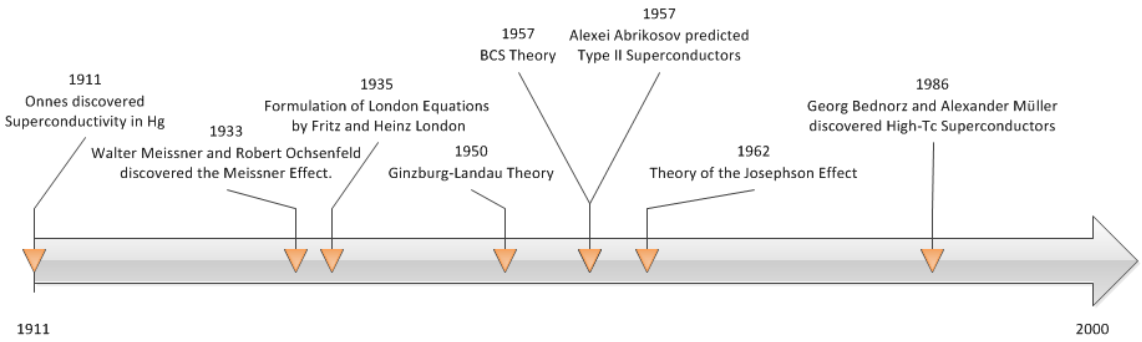

Figure 2.1. Superconductivity concise timeline

The term “superconductivity” was first used by Heike Onnes, in 1911. In his laboratory in the Netherlands, this scientist verified that the electrical resistance of capillaries of mercury abruptly disappeared at temperatures below 4.2 K. This was the discovery of a new state of matter, as Onnes stated at his Nobel Prize winning speech in 1913 (Onnes 1913):

“*Thus the mercury at 4.2 K has entered a new state, which, owing to its particular electrical properties, can be called the state of superconductivity*”

Figure 2.2 depicts the experiments made by Onnes, where an abrupt loss of resistivity in Mercury can be clearly seen at 4.2 K. The temperature below which a material becomes superconducting is called critical temperature.

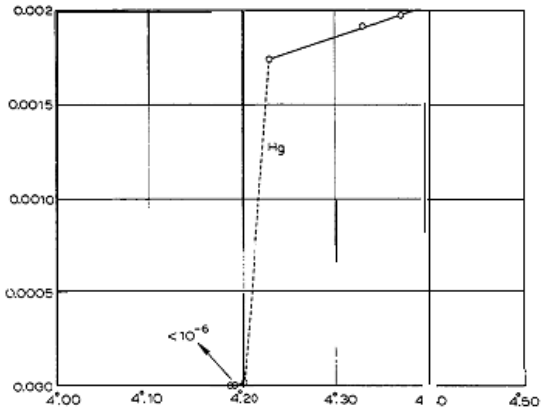

Figure 2.2. Experiments made by Onnes using Mercury. Abscissa is resistance (as a fraction of resistance value at 0 °C) and ordinate is temperature in Kelvin. Source: (Onnes 1913).

In 1933, Walter Meissner and Robert Ochsenfeld discovered that superconductors exhibit perfect diamagnetism, i.e. they fully expel magnetic flux from their core (Meissner & Ochsenfeld 1933). This effect, henceforth known as Meissner Effect, fully separates superconductivity from perfect conductivity (in which a material has zero resistance, but is a perfect flux conservation medium, rather than a perfect diamagnet).

Two decades later, in 1957, Alexei Abrikosov foretold the existence of a new type of superconductors, to which he called type II superconductors, in opposition to the already known superconductors (then known as type I). These new superconductors allowed the existence of a mix state, in which the material would undergo a progressive penetration of the magnetic flux in its interior in flux quanta well defined (flux vortices). A superconducting state and a normal state would then co-exist in the material. Also in 1957, John Bardeen, Leon Cooper and John Schrieffer elaborated a theory known as BCS theory to explain the microscopic behaviour of superconductors. This is the more consensual theory in superconductivity and states that pairs of electrons (known as Cooper pairs) act as charge carriers in superconductors.

In 1986 two IBM researchers, Georg Bednorz and Alexander Müller, discovered High Temperature Superconductivity (HTS) in ceramic compounds (Bednorz & Müller 1986). This was a breakthrough because some of these compounds are superconductors at temperatures above 77 K (liquid nitrogen boiling temperature), thus allowing the utilization of nitrogen instead of helium as a cryogenic fluid. Due to their discoveries, these researchers were awarded the Nobel Prize in Physics in 1987. The discovery of HTS was the initial step to conceive technical and economically viable applications of superconductivity in power systems.

2.1.2. Macroscopic properties of Superconductors

Superconductivity presents unique macroscopic properties. These properties include:

Zero resistivity

Below a temperature defined as critical temperature, T_C, superconductors present virtually zero resistivity. The absence of electrical resistance can be experimentally verified by measuring the flux density caused by persistent currents flowing in the superconductor.

Considering a superconducting ring with resistance R and inductance L, imposing a current I_0 in the ring, the evolution of current flowing in the ring is given by

$$i(t) = I_0 e^{-\frac{t}{\tau}} \tag{2.1}$$

where $\tau = \frac{L}{R}$ is the time constant of the ring. Being the ring in a superconducting state it can be seen that $\tau \to \infty$ while $R \to 0$. This means that $i(t) = I_0, t \geq 0$, i.e. the current does not decay with time. Measurements indicate that resistivity in a superconductor in which flows a DC current is at the order of 10^{-25} Ω·m, 17 orders of magnitude below copper (Orlando & Delin 1991).

Meissner Effect

Meissner Effect is a fundamental characteristic to distinguish superconductivity from perfect conductivity. Discovered by Meissner and Ochsenfeld (Meissner & Ochsenfeld 1933) this effect verifies an expulsion of magnetic field from the interior of a superconductor. This expulsion is due to the appearance of shielding currents flowing in the surface of the superconductor which completely shield the superconducting core.

T – J – H phase diagram

In order not to lose superconductivity, i.e. in order not to achieve a phenomenon designated as quench, superconductors must stay between certain working limits. These limits include not only the already mentioned current density and temperature but also the magnetic field. These three quantities are not independent from each other. Instead, they relate in a phase diagram usually called $T - J - H$ diagram. Figure 2.3 shows a typical surface of a $T - J - H$ phase diagram.

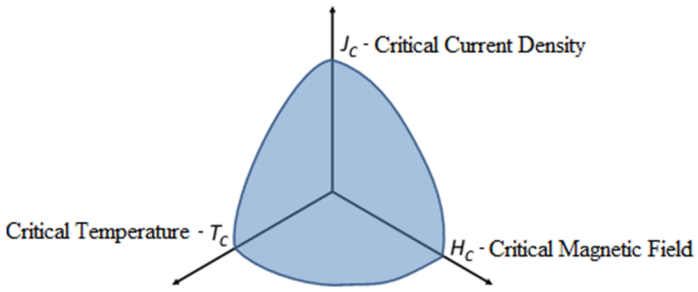

Figure 2.3. T - J - H phase diagram

It is important to notice that in order to maintain superconductivity, a superconducting material must obey simultaneously the three following conditions:

- $T < T_C$;
- $H < H_C$;
- $J < J_C$;

where T, H, J are respectively: working temperature, applied magnetic field and operating current density.

2.1.3. Types of Superconductors

Since the discovery of Onnes in 1911, further investigations during the 20th century found that superconductivity is a thermodynamic phase that many elements can achieve. In fact, around half of known elements can act as superconductors. However, some of these elements require high pressures to achieve a superconducting state whilst others can achieve it at atmospheric pressure. Figure 2.4 shows a periodic table of elements where elements that can reach a superconducting state are highlighted and in which pressure conditions they can achieve such state.

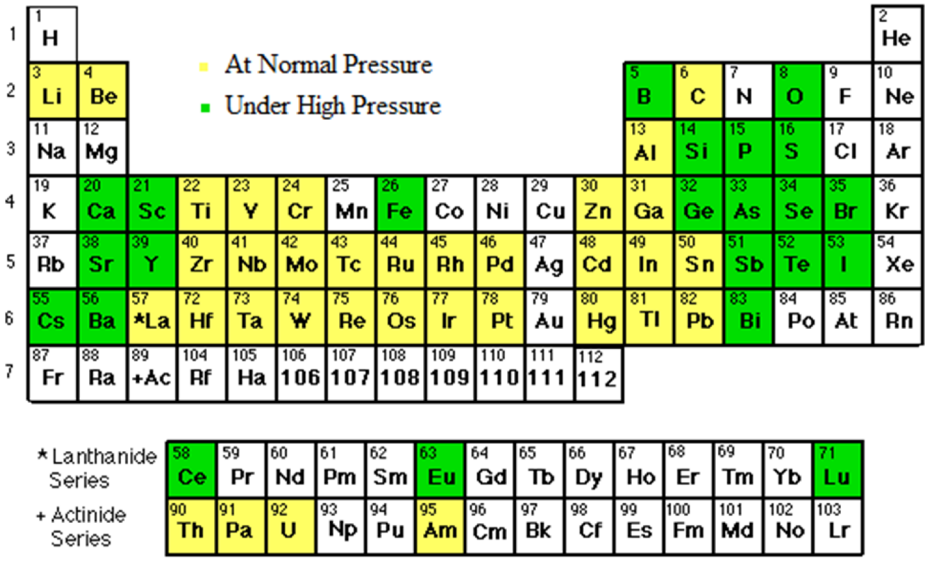

Figure 2.4. Known elements with superconductivity properties. Source: www.superconductors.org

Even if there are many elements that can reach a superconducting state, in real applications only a few are used. These are often compounds involving several elements, not pure elements. The discovery of superconductivity in the diverse known elements happened during several decades and were the foundation to discover microscopic and macroscopic properties of superconductivity. Nonetheless, all superconductors can be included in one of two types:

Type I Superconductors

The first superconductors to be discovered were type I superconductors (the designation of type I was only used when type II superconductors were found, later on). This type of superconductors obey Meissner Effect and are not penetrated by magnetic flux till a certain value of applied magnetic field (critical magnetic field), in which the material loses superconductivity and then become fully penetrated by flux lines. These materials (usually pure metals and some metalloids) act as perfect diamagnets till superconductivity is lost. Being perfect diamagnets, the magnetization is symmetric to the applied magnetic field. This behaviour can be seen in Figure 2.5.

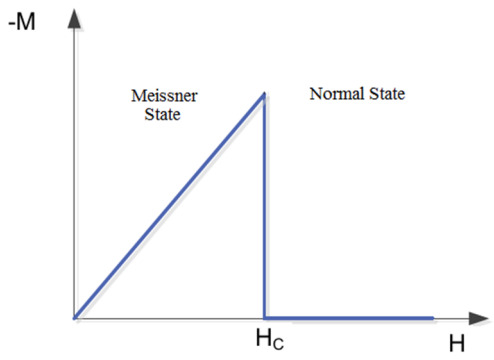

Figure 2.5. Type I superconductor

Type II Superconductors

In 1957, Alexei Abrikosov theoretically predicted a different kind of superconductors from those already known (Abrikosov 1957). With this discovery, aroused the need for a separation of types of superconductors, which originated the designation of type I and type II. Abrikosov defended that a third state could exist in the material, besides Meissner and normal states. This was called mix state and it consisted in the coexistence of a superconducting and a normal state in the material. This means that some parts of the superconductor are penetrated by magnetic flux in well-defined flux quanta while others are not. The typical behaviour of type II superconductors is illustrated in Figure 2.6.

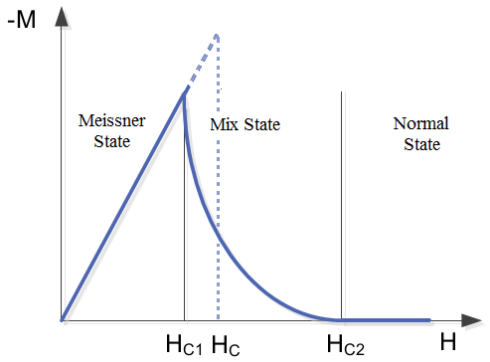

Figure 2.6. Type II superconductor

Type II superconductors are usually metal compounds and alloys with the exception of Niobium (French 1968), Technetium (Daunt & Cobble 1953) and Vanadium (Wexler & Corak 1952). These (type II) are the only superconductors with real applications. One very important kind of superconductors included in type II are the high temperature superconductors, described in next section.

2.1.4. High Temperature Superconductivity

2.1.4.1 Historical perspective

In 1986, Georg Bednorz and Alexander Müller discovered superconductivity in a ceramic compound of $Ba_{0.15}La_{1.85}CuO_4$ (or BLCO) with a critical temperature around 30 K (Bednorz & Müller 1986). BLCO was the first superconductor designated as high temperature superconductor. This was a great breakthrough for two reasons: first these ceramic materials

were poor conductors at room temperature and offered a new perspective because till that time it was thought that superconductivity was associated to good electric conductors (at room temperature). In addition to this, it was thought that the critical temperature of superconductors would not increase much above 20 K (Burns 1992). One important thing to notice is that high temperature superconductors do not obey BCS theory and the current transport mechanism in this superconductors is still not clear (Burns 1992).

The discovery of BLCO led to a search for superconducting characteristics in ceramic materials, increasing critical temperatures in several dozens of degrees in the last 30 years. Table 2.1 contains a list of some high temperature superconductors discovered in the last three decades. Although this is not a consensual opinion for all authors, in this work it is considered high temperature superconductors as materials whose critical temperatures are above 77 K (boiling temperature of Nitrogen), with the exception of BLCO.

Table 2.1. High temperature superconductors

Material (acronym)	Critical Temperature (K)	Reference
$Ba_xLa_{5-x}Cu_5O_{5-(3-y)}$ (BLCO)	30	(Bednorz & Müller 1986)
$Y_{1.2}Ba_{0.8}CuO_{4-\delta}$ (YBCO)	93	(Wu et al. 1987)
$BiSrCaCu_2O_x$ (BSCCO)	105	(Maeda et al. 1988)
$TlBa_2Ca_3Cu_4O_{11}$ (TBCCO)	128	(Ihara et al. 1988)
$HgBa_2Ca_2Cu_3O_{1+x}$ (HBCCO)	133	(Schilling et al. 1993)
$Hg_{0.8}Tl_{0.2}Ba_2Ca_2Cu_3O_{8+\delta}$ (HTBCCO)	138	(Dai et al. 1995)
$HgBa_2Ca_2Cu_3O_{8+\delta}$ (HBCCO)*	153	(Chu et al. 1993)

* at a pressure of 150 kbar (148 katm).

2.1.4.2 Materials

From all discovered high temperature superconductors there are two compounds with greater importance, in terms of their applicability to industrial systems:

- $Bi_2Sr_2Ca_nCu_{n+1}O_{6+2n}$ (BSCCO) with n = 0, 1, 2.
- $YBa_2Cu_3O_{7-\delta}$ (YBCO).

BSCCO is usually present in two of three phases where it presents superconductivity. These two phases, Bi-2212 (n = 1) and Bi-2223 (n = 2), have critical temperatures of respectively 92 K and 110 K. Despite the fact that Bi-2223 has higher critical temperature (110 K comparing to 92 K) and higher critical current density than Bi-2212, this one has the advantage of having a lower degradation in its properties in the presence of magnetic fields, so both phases are produced and commercialized. Bi-2201 (n = 0) is also superconductor but its critical temperature is around 40 K thus cannot be cooled using liquid nitrogen.

In $YBa_2Cu_3O_{7-\delta}$, δ defines the amount of oxygen present in the material. In order to present superconductivity it must obey $x = 7 - \delta \geq 6.6$ (Jorgensen et al. 1991).

Superconducting Tapes

Superconductors used in power systems applications are usually presented in two forms, either bulk or tape.

Since this work is based only in superconducting tapes, no further description of bulk materials is made. Nonetheless, the characteristics of materials here presented are valid for both tapes and bulk superconductors. The most common types of HTS tape available on the market are made using one of two materials:

- BSCCO ($Bi_2Sr_2Ca_nCu_{n+1}O_{6+2n}$ with n = 1, 2) – also called first generation (1G) tape.
- YBCO ($YBa_2Cu_3O_{7-\delta}$) – used more recently than the BSCCO tape, forms the basis of the second generation (2G) tape.

A short description of production processes and characteristics of both 1G and 2G tapes are presented in this section, to verify the differences between these materials.

First Generation HTS Tapes

BSCCO tapes (or 1G tapes) are manufactured using a technique called Powder In Tube (PIT) (Grivel & Flükiger 1996). PIT process can be described very shortly as follows. Small silver tubes are filled with a precursor powder of superconducting material with one or more filaments (the number of superconducting filaments depends on the manufacturer). Obtained tubes are then brought together in a larger silver capsule which is then subjected to a process of drawing and rolling. The tape is then sintered at a temperature around 850 °C which allows a controlled growth of the superconductor with high degree of alignment between the grain boundaries, fundamental characteristic to achieve a high critical current density. PIT process is schematized in Figure 2.7. Even considering the additional robustness given by silver, 1G HTS tapes are still fragile due to the fact that the superconducting material is ceramic. These tapes have a maximum bending radius of a few dozen of millimetres which can limit their applications.

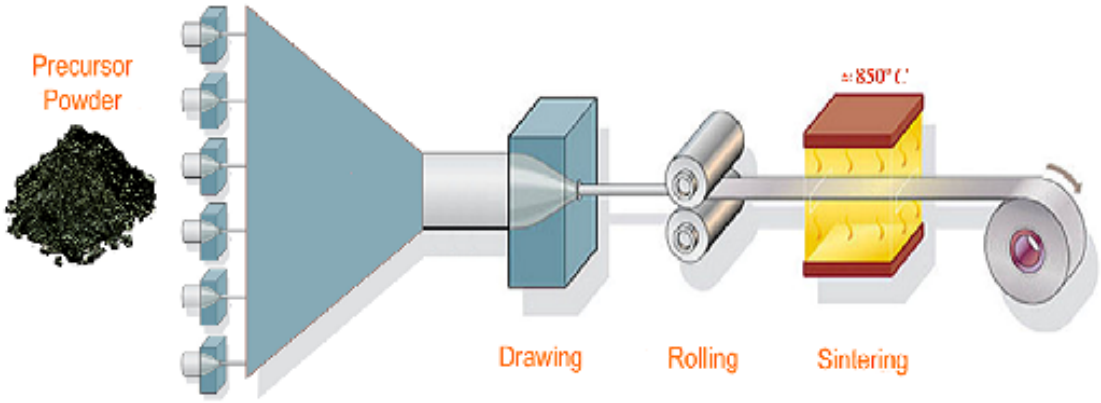

Figure 2.7. PIT process. Source: (Ceballos 2010)**.**

Figure 2.8 a) shows a BSCCO HTS tape where superconducting filaments embedded in a silver matrix can be easily seen. The real aspect of this tape is showed in Figure 2.8 b). Despite the existence of commercially available 2G tapes, BSCCO tapes are still produced (with lengths of around one kilometre) and are still very used in power systems applications of superconductivity.

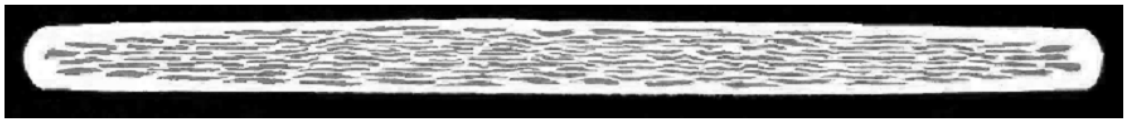

a) Cross section of a Bi-2223 tape with 121 superconducting filaments (grey) embedded in a silver matrix (white).

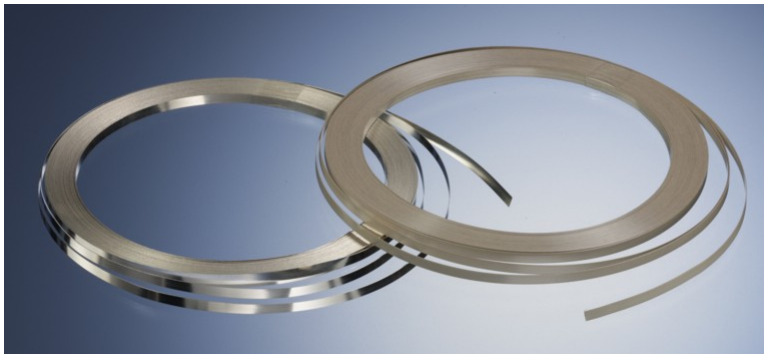

b) Aspect of Bi-2223 superconducting tape

Figure 2.8. Bi-2223 superconducting tape produced by Bruker HTS GmbH (http://bruker-est.com/).

One of the main issues of 1G superconducting tapes is the fast degradation of its critical current value with increasing applied magnetic field. This behaviour can be seen in Figure 2.9. Even considering temperatures around 20 K it is possible to see this fast degradation. Continuous research efforts regarding superconducting materials led to the creation of a new kind of superconducting tape – 2G HTS tape – with an improved behaviour under magnetic fields.

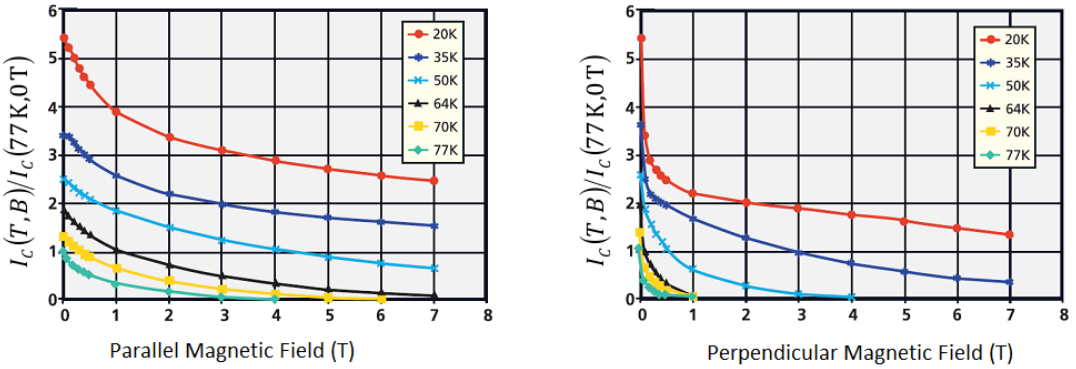

Figure 2.9. Degradation of critical current value with the increase of magnetic field in a Bi-2223 tape manufactured by American Superconductor (AMSC) (http://www.amsc.com/).

Second Generation HTS Tapes

2G HTS tapes appeared as an alternative to 1G tapes because they can withstand higher magnetic fields and higher critical current densities, without losing superconductivity (Selvamanickam et al. 1998). Figure 2.10 depicts a comparison between 1G and 2G HTS tapes, regarding the influence of magnetic field in the critical current value.

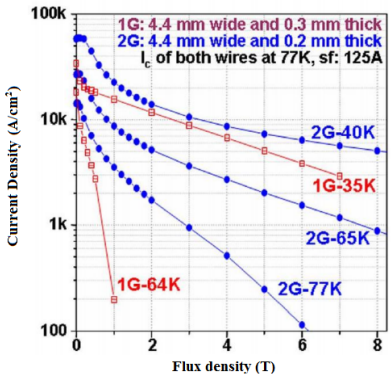

Figure 2.10. Performance of 1G and 2G tapes under applied magnetic field. Source: http://www.theva.com

These tapes are manufactured using YBCO (phase Y-123), and are commonly designated as coated conductors. The process has four main steps:

- Preparation of the substrate;
- Deposition of intermediate layers;
- Deposition of superconducting layer (YBCO);
- Addition of connection and stabilizing layers.

Step 1 – Preparation of the Substrate

There are two different techniques to do the preparation of substrate for 2G tapes. One is to use an alloy of nickel-tungsten subjected to a technique called Rolling-Assisted Biaxially Textured Substrate (RABiTS™). This method, schematized in Figure 2.11, is used by several manufacturers including American Superconductor (AMSC) (Rupich et al. 2007).

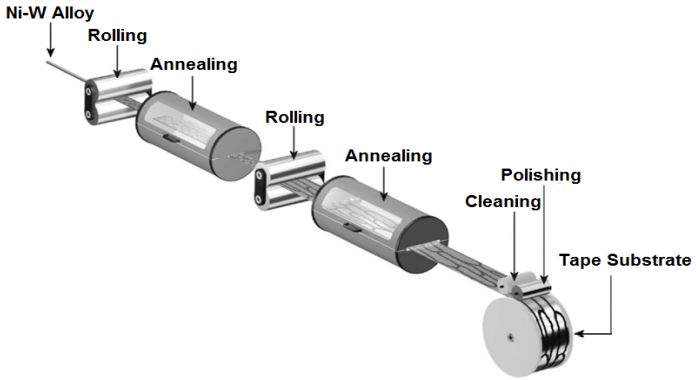

Figure 2.11. RABiTS™ technique (adapted from (Hammerl et al. 2002)**).**

One major disadvantage of RABiTS™ technique is that Ni-W substrate is ferromagnetic at 77 K, which introduces an important component in tape losses (Duckworth et al. 2003) as will be seen later on. As an alternative to this process, other manufacturers including SuperPower use a different technique for the preparation of the substrate. In this case, an untextured substrate is used and the surface of the substrate that will receive the deposition of superconductor is electro-polished. The main advantage of this process is that it can be used almost any metal alloy, in particular non-ferromagnetic alloys. In the specific case of SuperPower a nickel alloy known as Hastelloy® is used.

Step 2 – Deposition of intermediate layers

After the preparation of substrate it is necessary to implant a series of layers prior to the deposition of the superconducting layer. These layers are called Epitaxial Buffer Layers. Main functions of buffer layers include:

- Provide a surface for the epitaxial growth of the superconductor;
- Protect the superconductor of possible contaminations from the substrate;
- Facilitate the adhesion of the superconductor, avoiding a possible peeling effect.

Since there are two different methods for preparing the substrate, the deposition of intermediate layers is also different for each case. In the case where RABiTS™ was used to prepare the substrate, a sputtering technique is used for the deposition of the intermediate layers (Goyal et al. 2004). In the case of manufacturers that used an untextured substrate sputtering is insufficient to implant the intermediate layers. In this case, a technique called Ion Beam Assisted Deposition (IBAD) is used. This technique combines ion implantation with sputtering, allowing an adequate deposition of the different intermediate layers (Selvamanickam et al. 2001).

Step 3 – Deposition of superconducting layer

Deposition of YBCO layer is also implemented using different techniques depending on the manufacturer. AMSC uses a technique denominated as Trifluoroacetate Metal Organic Deposition (TFA-MOD) (McIntyre et al. 1995). This technique consists in a chemical deposition of the YBCO layer using a trifluoroacetate precursor and subsequent pyrolysis. In the case of SuperPower, a different method called Metal-Organic Chemical Vapour Deposition (MOCVD) is used (Selvamanickam et al. 2001). In this method, a chemical vapour is deposited in the substrate and pyrolysis is used to form the epitaxial layer of YBCO.

Step 4 Addition of connection and stabilizing layers

In order to protect the superconducting layer and to add mechanical stability to the HTS tape a series of connection and stabilizing layers are added. A silver layer is added to permit electrical connections and a coating (usually copper) is added to minimize tape deterioration due to mechanical stresses.

The complete schemas of layers used in 2G HTS tapes manufactured by SuperPower and AMSC are depicted in Figure 2.12 and Figure 2.13, respectively.

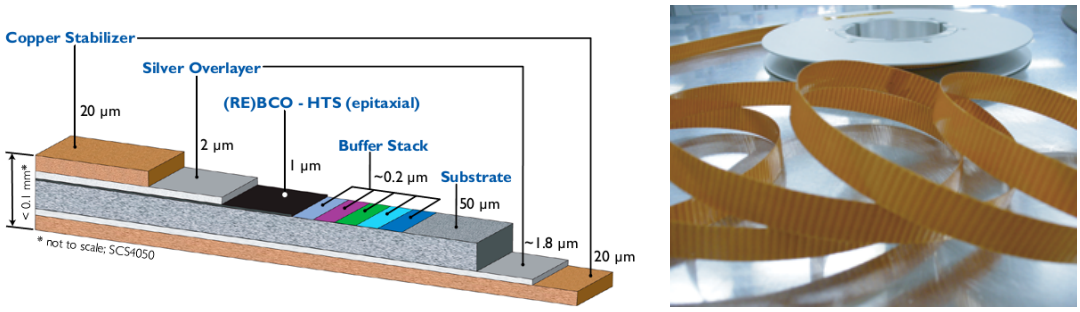

a) Layers diagram b) Actual aspect of the tape

Figure 2.12. 2G HTS Tape manufactured by Super Power (source: http://www.superpower-inc.com/)

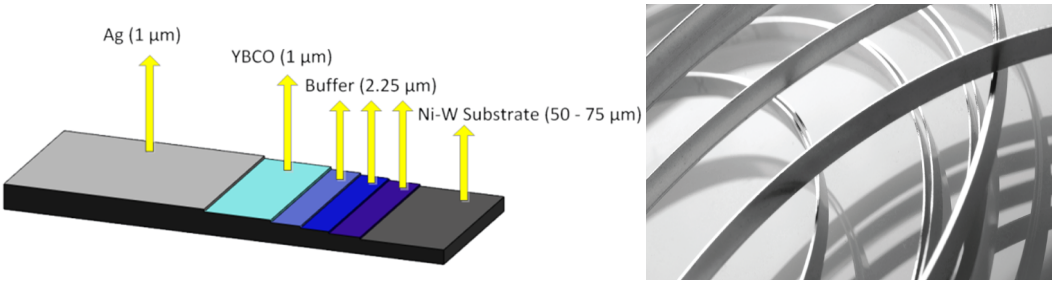

a) Layers diagram b) Actual aspect of the tape

Figure 2.13. 2G HTS Tape manufactured by AMSC (source: http://www.amsc.com/)

2.1.5. Modelling of high temperature superconductors

Accurate models are often needed when designing devices employing superconducting materials, in order to verify their behaviour. Even if a consensual theory is not yet formulated to explain the current transport mechanism in HTS, there are several models that describe the behaviour of these material with accurate results.

2.1.5.1. Critical State Models

Critical state models are the simplest option to describe the behaviour of high temperature superconductors. Based in macroscopic properties of the material, these models are obtained by experiments verifying the relation between current density and magnetic field in the superconductor. They assume that the local current density can only have three different values, namely $+J_C$, 0 or $-J_C$ where J_C is critical current density. When a superconductor is exposed to a magnetic field an outer layer of the superconductor is in a critical state, i.e., has a critical current density, and the interior of the superconductor is shielded from this applied field and does not transport any current. Increasing the applied magnetic field, the superconductor layer transporting current will also increase till this layer occupies the entire superconductor, i.e. till the magnetic field fully penetrates the superconductor. These are common characteristics of all critical state models. Since in a power system application, the main interest is the macroscopic behaviour of the superconductor, these models are very used in engineering and results obtained are usually in a close range to the real behaviour of the system. The simplest and more used critical state model is the Bean model described in next section. After that description, other critical state models will be shortly summarized.

Bean Model

Bean Model considers that current density and flux density are independent (Bean 1964). This means that when a magnetic field is applied, the value of current density in the superconductor will always assume the critical value, as already stated. To simplify the model, Bean assumed that the superconductor slab has infinite dimensions in x and z directions and width $2a$ in y direction and is immersed in a magnetic field oriented in z direction, as shown in Figure 2.14.

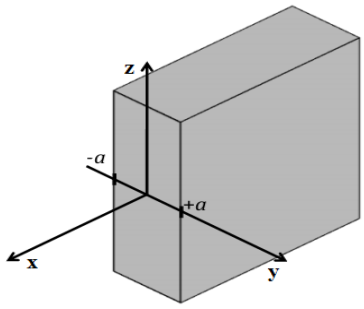

Figure 2.14. Superconducting slab with infinite dimensions in y and z and 2a width in x.

Since dimension $2a$ is very thin compared to other dimensions of the slab, only the magnetic field component which is parallel to the slab cross section (x direction component of the magnetic field) needs to be considered.

Ampère Law is still valid in the interior of the superconductor and can be written as follows.

$$\nabla \times \vec{B} = \mu_0 \vec{J} \tag{2.2}$$

This happens because macroscopically a superconducting material can be considered as non-magnetic, and it is assumed that there is a uniform penetration of flux density in the superconductor, in the operating zone, as shown in Figure 2.15.

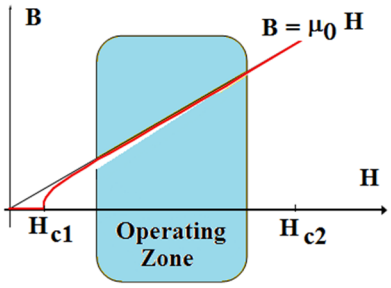

Figure 2.15. B-H relation in a superconductor.

Since the only variation will happen in *x* direction, equation (2.2) can be rewritten as

$$\frac{dB(y)}{dy}\mathbf{e}_x = \mu_0 J_x(y)\mathbf{e}_x \tag{2.3}$$

Equation (2.3) suggests that the magnetic field will linearly decrease to zero until the current density disappears along the width direction of the slab. If the magnetic field changes direction there will be an induced current with opposite signal in the surface of the superconductor. With

the increasing of the magnetic field the current density penetrates more in the superconductor till it reach full penetration. Figure 2.16 demonstrates this behaviour.

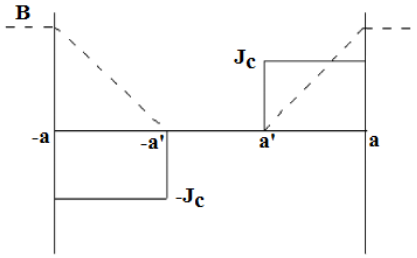

Figure 2.16. Current Density and magnetic field distribution in a superconducting slab considering Bean Model.

Other Critical State Models

In addition to Bean Model there are other more complex critical state models. One of these models also very used in engineering applications is the Kim Model (Kim et al. 1962; Kim et al. 1963). Unlike Bean Model, in this case the current density is not independent from the applied magnetic field. Instead, there is a relation between those entities given by:

$$J_C(B) = \frac{J_{C0}}{1 + B/B_i} \tag{2.4}$$

In this equation J_{C0} is the critical current density obtained at self-field; B_i is a constant obtained experimentally.

Other critical state models like Exponential Model (Fietz et al. 1964), Power Model (Irie & Yamafuji 1967) or Linear Model (Watson 1968) can also be chosen, but are not used so often as the previous two.

2.1.5.2. E-J Power Law

Critical state models are based on the assumption that currents in the superconductor always assume its critical value. However, in type II superconductors and especially in HTS, the current does not always present its critical value and the latter does not represent an abrupt transition between a superconducting state and a normal state. To achieve higher precision, it was experimentally verified that superconductors could be modelled using a power law (Rhyner 1993). This power law describes the dependence between current density and electric field as

$$E = E_C \left(\frac{J}{J_C} \right)^n \tag{2.5}$$

where E_C is the value of electric field in which the critical current density J_C is achieved. Usually, in HTS, it is used a criterion of $E_C = 1$ μV/cm to define critical current. Parameter n is a material property and defines the shape of the $E - J$ curve. Figure 2.17 shows a plot of $E - J$ curves for different values of n. It is easy to notice that if $n \to \infty$ then the $E - J$ power law becomes the Bean Model. In the other hand, if $n = 1$ this curve represents Ohm's Law, i.e. a linear variation of resistance.

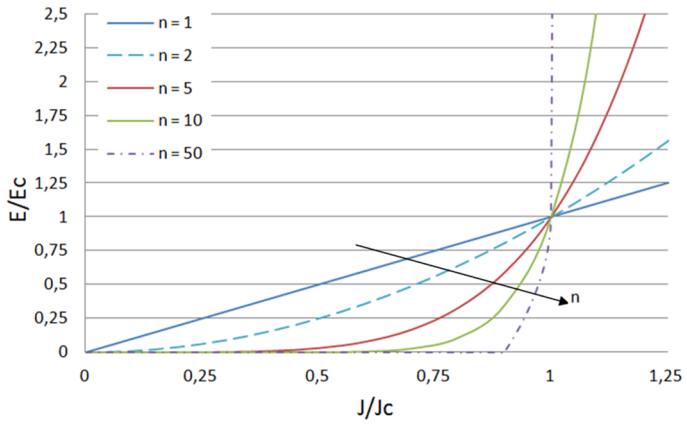

Figure 2.17. E-J Power Law for different values of n parameter.

2.1.5.3. Numerical Modelling

Numerical techniques such as finite element methods (FEM) are used to find approximate solutions of partial differential equations (PDE). FEM can be used to solve Maxwell equations for superconducting materials in order to obtain the magnetic field and current density distributions. The method for solving Maxwell equations in superconductors using FEM is usually an *H Formulation*. With an *H Formulation* it is possible to couple magnetic field equations with $E - J$ Power Law (Hong et al. 2006). This can be briefly explained as follows.

Consider a cross section view in the $x - y$ plane of a superconductor, infinite in z direction, as shown in Figure 2.18.

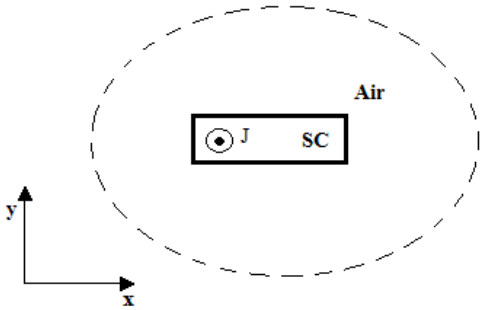

Figure 2.18. Cross section (x-y plane) of an infinite superconductor in z direction.

According to Faraday's Law:

$$\nabla \times \mathbf{E} = -\frac{\partial \mathbf{B}}{\partial t} = -\mu_r \mu_0 \frac{\partial \mathbf{H}}{\partial t} \tag{2.6}$$

Ampere's Law gives

$$\nabla \times \mathbf{H} = \mathbf{J} \tag{2.7}$$

In this specific case, since the superconductor is infinite in z direction, the problem simplifies to a two dimensional one. Considering also that the current density flows in z direction, inside the superconductor, equation (2.7) becomes

$$J_z = \frac{\partial H_y}{\partial x} - \frac{\partial H_x}{\partial y} \tag{2.8}$$

Considering also that inside a superconductor the current density can be modelled using the $E - J$ power law expressed here as

$$E_{sc} = E_C \left(\frac{J_{sc}}{J_C} \right)^n \tag{2.9}$$

where E_{sc} and J_{sc} are respectively electric field and current density inside the superconductor and J_c is the critical current density (obtained with the criterion $E_c = 1$ μV/cm). Combining equations (2.6), (2.8) and (2.9) it is possible to obtain a pair of coupled equations to describe current density and magnetic field inside the superconducting region as follows.

$$\frac{d\left(E_C \left(\dfrac{\dfrac{\partial H_y}{\partial x} - \dfrac{\partial H_x}{\partial y}}{J_C} \right)^n \right)}{dy} = -\mu_0 \frac{dH_x}{dt} \tag{2.10}$$

$$-\frac{d\left(E_C \left(\dfrac{\dfrac{\partial H_y}{\partial x} - \dfrac{\partial H_x}{\partial y}}{J_C} \right)^n \right)}{dx} = -\mu_0 \frac{dH_y}{dt} \tag{2.11}$$

Since equations (2.10) and (2.11) only model the characteristics inside the superconductor it is necessary to obtain another pair of coupled equation to model the behaviour of the outside region. Outside the superconductor a linear Ohm's law, $E = \rho J$, is used instead of the $E - J$ power law, where ρ is the resistivity of the medium (in this case air). In this case, the coupled equations for the non-superconducting region can be expressed as follows.

$$\frac{d\left(\rho\left(\frac{\frac{\partial H_y}{\partial x}-\frac{\partial H_x}{\partial y}}{J_C}\right)\right)}{dy}=-\mu_r\mu_0\frac{dH_x}{dt} \tag{2.12}$$

$$-\frac{d\left(\rho\left(\frac{\frac{\partial H_y}{\partial x}-\frac{\partial H_x}{\partial y}}{J_C}\right)\right)}{dx}=-\mu_r\mu_0\frac{dH_y}{dt} \tag{2.13}$$

By solving equations (2.10) to (2.13) one can compute the magnetic field and current density distribution in the whole space. Several software packages, for both 2D and 3D simulations, use finite element analysis (FEA) based on these equations to solve problems regarding superconductivity applications. Such software packages are powerful tools to fully simulate superconducting devices since one can model completely the system and consider not only electromagnetic but also mechanical and thermal characteristics.

2.2. Superconducting devices for power systems applications

In the last decades, with the increasing demand and high quality requirements for electric energy it became very clear that the existing power grids have many limitations. Most of the devices and equipment used to generate and transport energy are now running for decades, so the existing grid is an old grid that must be modernized. According to the International Energy Agency a large percentage of the energy we consume is produced using fossil fuels (IEA 2012) that, as it is well known, are a major source of pollution. As an effort to try to stop the planet degradation there are several laws that force electricity producers to obey a variety of rules like generate energy using a mix of sources, reduce their carbon footprint and assure an adequate response to an increasing power demand. In fact, it is estimated that consumption of electric power will increase 75% by the year 2020, compared to the year 2000 (Garrity 2008). In addition to this increasing demand other aspects are affecting efficiency in power grids. Only one third of potential energy contained in energy sources is successfully transformed into electricity and about 8% of this total electricity is lost only in transmission lines (Farhangi 2010). This brings up an obvious conclusions: electric grids are inefficient, and need to change in order to achieve the increasing quality requirements. This context, represents an opportunity for the implementation of new devices or at least for a different application of existing ones.

One such technology whose devices have a potential application into power grids is Superconductivity, mainly due to its particular characteristics which are unreproducible using conventional materials or technologies (Hassenzahl et al. 2004). Different superconducting devices can be successfully integrated in power grids, bringing new and unique characteristics:

- Superconducting Magnetic Energy Storage (SMES) systems store energy in a superconducting coil, and have the ability to discharge such energy into the grid whenever necessary, having different possible applications (Buckles & Hassenzahl 2000; Molina et al. 2011; Chen et al. 2014; Ishiyama et al. 2001).
- Superconducting Fault Current Limiters (SFCL) operate in the grid with a negligible impedance in normal operation conditions but switch to a high impedance in a faulty condition, limiting short-circuit currents (Morandi 2013; Noe & Steurer 2007). The inclusion of an SFCL in a power grid then allows the increase of short-circuit power in a grid while simultaneously protects the grid from the consequences of a fault, which increases the possibility to expand grids without changing its protection elements (Granados et al. 2002; Kovalsky et al. 2005; Arsenio et al. 2013; Pina et al. 2010).
- Superconducting Cables allow the transport of high amounts of energy with virtually zero losses, particularly when operating in DC conditions. Such characteristics creates the possibility to have (as an example) virtual bus bars with hundreds of meters of length, which can be interesting particularly for highly dense population regions. Examples of HTS cables operating in power grids can be looked at in (Stovall et al. 2001; Honjo et al. 2011; Maguire et al. 2007; Tønnesen et al. 2004).
- Superconducting Transformers: although conventional transformers already have a very high efficiency, due to the high dissemination of these devices, a small increase in efficiency might allow great economical savings (Morandi et al. 2008). Utilization of superconducting transformers allow a simultaneous decrease in size and height of the device, which can also be an interesting characteristic, particularly for urban substations (Yamamoto et al. 2000; Donnier-Valentin et al. 2001).

- Superconducting Machines: rotating machines employing superconducting technology have several advantages when compared to conventional solutions: are lighter, more compact and potentially more efficient (Kalsi 2002; Campbell 2014). These advantages originated research efforts for different classes of rotating machines and it is possible to see prototypes of different machines such as: small motors (Granados et al. 2008), machines for ship applications (Frank et al. 2006) and wind turbine generators which can reach a power rating of 10 MW (Snitchler et al. 2011; Abrahamsen et al. 2010).
- Systems with shared cryogenics: superconducting devices combining more than one superconducting solution are also a possible candidate for applications in power systems. It is possible to use a Superconducting Fault Current Limiting Transformer (SFCLT), which brings together the characteristics of SFCL's and transformers (Hayakawa et al. 2000; Hayakawa et al. 2011). It is also possible to use together different superconducting devices, which will benefit from the fact that there is a shared cryogenic system, decreasing the overall costs (Zhang et al. 2011; Zhang et al. 2012; Xiao et al. 2012).

Although there are different classes of superconducting devices with possible applications in power systems, the dissemination of these devices in power grids (when leaving the prototype concept to full-scale grid applications) is still not as high as expected. There are still many technological and economic challenges. The price of the HTS materials is one of the most limiting factors, even considering that it is expected that the price will decrease over the next few years (Malozemoff et al. 2002). Considering that superconducting materials are expensive it is also fundamental to reach protection systems with high reliability (Tsukamoto 2005). AC losses are one of the most important technological challenges that need to be overcome for the successful dissemination of HTS devices in power systems. Researching superconducting devices means always researching AC losses associated to those devices, and it is common to check the existence of AC losses in cables (Terzieva et al. 2010; Amemiya et al. 2007; Vojenčiak et al. 2011), SMES systems (M. Park et al. 2007; M.-J. Park et al. 2007; Xu et al. 2013), SFCL devices (Yasuda et al. 2005; Dommerque et al. 2010), rotating machines (Barnes et al. 2005; Jiang et al. 2006) and transformers (Perez et al. 2003; Iwakuma et al. 2001). Most of the presented devices are constituted by HTS coils, which makes this a very important and common field of research in superconductivity. This work also aims to contribute to such study.

2.3. AC Losses

Superconductors are known for having virtual zero resistance. However, this condition is only valid when the superconductor is operating in DC conditions. When an AC current is applied, the superconductor generates losses, commonly denominated as AC losses, which need to be taken into account in superconducting projects. Since superconductors operate at cryogenic temperatures, all heat generated must be extracted from the system and AC losses might have a great contribution in the generated heat. Thus, it is important to study AC losses, their origin, and possible strategies to minimize them. This section will describe the different mechanisms that originate AC losses and the systems that are used to measure them. Some common models that are vastly used in the literature will also be presented.

2.3.1. Classification of losses in superconductors

AC losses in superconductors are originated from different phenomena. Considering this, it is common to classify losses according to the mechanism that originates them. This section briefly describes the classification of AC losses in HTS tapes, since this form of superconducting materials is the one focused in this work.

There are two main mechanisms that originate AC losses in superconductors. Therefore, the losses are usually classified into two categories (Ceballos 2010):

- **Magnetization losses:** due to variations in the magnetic field;
- **Transport current losses:** arise from variations in the transport current in the superconductor.

These two types of AC losses have several subcategories, which will be briefly addressed. The total amount of AC losses in a superconductor is the sum of these two contributions.

2.2.1.1. Magnetization losses

Magnetization losses appear due to variations in the magnetic field in which the superconductor is immersed. This variation in the magnetic field can have two origins:

- Variation of the current generating the field, i.e. an AC current generates a variable field, which will generate losses;
- If the applied field is constant, i.e. created by a DC current, the movement of the superconductor and/or the source of the magnetic field will also generate losses.

The variation of the magnetic field, by any of the two previous mechanisms will originate AC losses that can be divided into three different categories:

Superconducting hysteresis losses

The variation of the magnetic state in a superconductor originates a hysteresis loop, similar to the hysteretic behaviour of ferromagnetic materials. This hysteretic behaviour will demand a constant input of unrecoverable energy, originating losses (Takacs & Campbell 1988; Clem & Sanchez 1994; Müller 1997; Poole et al. 2007).

Ferromagnetic hysteresis losses

As seen in section 2.1.4, 2G HTS tapes fabricated using the RABiTS™ technique contain a Ni-W substrate, which is ferromagnetic. This originates a hysteresis loss component in the ferromagnetic materials that is not negligible for tungsten concentrations below $9\,\%$, as demonstrated in (Ijaduola et al. 2004).

Resistive (Joule) losses

The existence of non-superconducting (but still conducting) materials in HTS tapes, which are subjected to a variable magnetic field, origins parasitic currents which dissipate energy by Joule effect. This phenomenon is slightly different in 1G and 2G tapes, so it is appropriate to make a distinction.

- 1G tapes – coupling currents (eddy currents) losses

1G tapes, composed by superconducting filaments and a silver matrix, when subjected to variable magnetic fields, produce shielding currents in the superconducting filaments and coupling currents in both, the superconducting regions and the silver matrix. Figure 2.19 depicts the existence and location of this parasitic currents. It is possible to make a separation between these two losses components as well (Rabbers 2001), however that is not the purpose of this work.

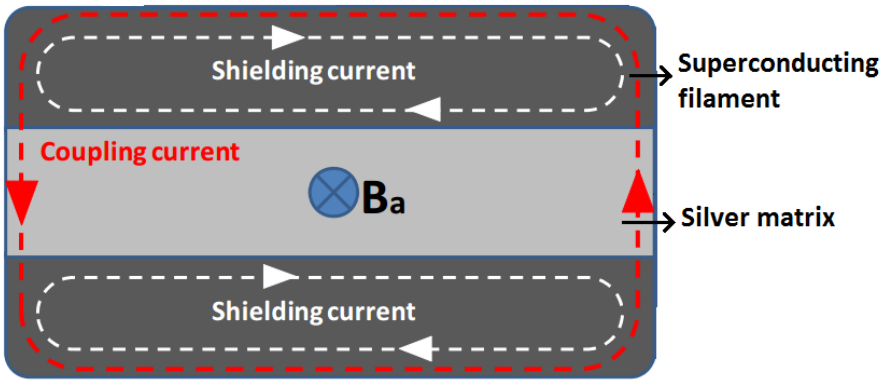

Figure 2.19. Shielding and coupling currents in a 1G HTS tape. Adapted from (Ceballos 2010)**.**

The magnitude of these losses depend on the resistivity of the silver matrix but also on the time derivative of the magnetic flux across the area between the filaments. This means that the longer the filaments the greater is this area, which results in higher losses (Ceballos 2010).

As demonstrated in (Ishii et al. 1996), these losses can be expressed as shown in equation (2.14):

$$P_{ed} = \frac{2\pi^2 \mu_0{}^2 f^2 I_p{}^2 d^3}{\rho l} \text{ (W/m)} \qquad (2.14)$$

In this expression, μ_0 is vacuum permeability, f is frequency, I_p is current amplitude through the tape, d is sheath thickness, ρ is resistivity of silver and l is perimeter of the outer superconducting filament layer.

- 2G tapes – eddy currents losses

2G tapes have several layers that, when subjected to variations of the external magnetic field, produce eddy currents that dissipate energy by Joule effect. The magnitude of AC losses depends on the thickness of the layers, so these losses are more important in the substrate than in intermediate layers. If the tape contains a stabilizing layer, losses in this layer are also important (Majoros et al. 2008). However, the contribution of these losses to the total amount of AC losses in the tape is usually negligible at low frequencies, including 50 Hz (Duckworth et al. 2005).

Although the mechanisms that originate these losses in 1G and 2G tapes are different, it is common to designate this component as eddy currents losses in both kinds of HTS tape.

2.2.1.2. Transport current losses

An AC current flowing in a superconductor originates the so-called transport current losses. These can also be divided into three categories:

- Self-field losses: originated due to the variation of the magnetic field created by the HTS tape;
- Flux-flow losses: due to the movement of the magnetic vortices in the superconductor;
- Resistive losses: both, in the superconductor (when close to the critical current) and in the other conductive layers.

The three types of transport current losses can be briefly described as follows.

Self-field losses

When an AC current flows through the HTS tape, it generates a magnetic field, denominated as self-field. This magnetic field originates hysteretic losses similar to those created by an external field presented in the previous section.

Flux-flow losses

Like all type II superconductors, high temperature superconductors usually work in the mixed state. This means that the flux penetrates the superconductor in some specific areas known as vortices. When a transport current is applied, these vortices tend to move towards the boundaries of the superconductor. If the current is sufficiently high, the interaction force surpasses the force pinning the vortex, which will cause the vortex to move through the superconductor dissipating energy (Poole et al. 2007).

Resistive losses

When the transport current gets close or exceeds the critical current of an HTS tape, some current starts to flow through the non-superconducting regions of the tape (the silver matrix in 1G tapes and the stabilizing layers in 2G tapes). The current flow through a non-zero resistivity region originates resistive losses that will be dissipated by Joule effect. For values of current close to the critical current even in the superconductor some resistive regions start to appear, which is determined by the n-value of the superconductor. Usually such resistive losses are considered for applied-to-critical current ratios higher than 0.8 (Stavrev & Dutoit 1998).

2.3.2. Models of AC losses

In the design phase of a superconducting device project, it is important to model all characteristics of the used superconductors. This will allow saving resources in the implementation phase and find possible sources of difficulties during the project. AC losses must be a part of this project and therefore models for AC losses are often used to obtain results for the total amount of losses in the superconductor. This is extremely important, considering that all generated heat must be extracted from the cryogenic environment where the superconducting device will work. Considering this, a continuous investigation effort has been dedicated in the last decades to achieve accurate models for AC losses in superconductors. This section contains a brief description of the most common models.

2.3.2.1. Analytical models

Analytical models are the most straightforward methods to calculate the total amount of AC losses in superconductors. Even if the models are not too accurate, they can be used to have a first idea of the total amount of losses.

Norris Model

Norris model is the most common analytical model for AC losses in superconducting tapes (samples of tape, not coils). As demonstrated by W. T. Norris in (Norris 1970), hysteretic AC losses of superconducting tapes with an elliptical section can be calculated as:

$$L_C = \frac{{I_C}^2 \mu_0}{\pi}\left\{(1-F)\ln(1-F)+(2-F)\frac{F}{2}\right\} \text{ (J/m/cycle)} \qquad (2.15)$$

with $F = {I_{peak}}/{I_C}$, I_C is critical current. L_C is loss per length of tape per cycle.

Even considering that this equation was formulated for low temperature superconductors in 1970 (HTS was not yet discovered), it is accurate for HTS tapes and almost every research group uses it as comparison, when calculating AC losses in samples of HTS tape.

Clem Model

Since the calculation of AC losses in HTS coils is of utmost importance, the existence of analytical models with this purpose provides a straightforward tool for obtaining an approximate value for the total amount of AC losses in a superconducting coil, more particularly in pancake coils. In (Clem et al. 2007) the so called Clem Model considers a finite Z stack of HTS tape to calculate the total AC losses in superconducting coils, considering two different situations: currents flowing in the coils with a high or a low density (close to zero or to the critical current). The model considers as starting points the Norris Model and the Bean Model. This model has different assumptions, the most important is to consider that the thickness of each superconducting filament is much smaller than the width of that filament, which is verified in 2G HTS tapes, making this model a good candidate to access AC losses in superconducting devices employing this kind of tape.

Other models

In the last years other analytical models to calculate AC losses not only in samples of HTS tape but also in coils have appeared. (Rabbers et al. 2001) presents an engineering formula that describes AC losses in 1G HTS tape considering a simultaneously applied magnetic field and current (with different orientations). In (Yuan et al. 2009) an extension of the Clem Model is presented, in order to successfully calculate magnetization and transport current AC losses in HTS coils.

One other simple analytical model is that presented in (Pardo 2008). Using as a starting point the Norris model for the calculation of the loss per length of a superconducting slab (equation 34) (Norris 1970), and considering a superconducting coil with internal radius much larger than its width and a high number of turns, the AC loss per tape length can be calculated as:

$$Q = \frac{\mu_0 w^3 d^2 J_C^2 (I_{ap} / I_c)^3}{6(d+h)} \text{ (J/m/cycle)} \qquad (2.16)$$

where w, d are respectively the width and thickness of the superconducting layer, h is the separation between superconducting layers of adjacent turns, J_C is the critical current density and I_{ap} / I_c is the ratio of applied current to the critical current. Equation (2.16) is particularly useful for HTS coils wound using 2G HTS tape, in which the superconducting layer is very narrow comparing to the total dimension of the tape consequently the coil.

2.3.2.2. Numerical Models

Numerical models are more accurate than analytical models, so they should be used in a final stage of the design of a superconducting device, to achieve results close to the real system. There are a large variety of numerical models, which include different mathematical formulations which will result in different methods for computation of AC losses (Sirois & Grilli 2015). The main drawback of these models is that they are usually very time-consuming, and simulations based on FEA take several days/weeks. Usually these models are used to simulate the superconducting device as a whole and AC losses are also studied during these simulations. Different approaches can be considered. In this document only the used numerical models will be briefly explained, however there is a common starting point to several numerical methods which is relevant to state. Usually the numerical models for calculation of AC losses in HTS coils use as a starting point the field dependence of the critical current in a short sample of tape, and expand that behavior to a more complex system such as a coil (Šouc et al. 2009; Shevchenko et al. 1998). This field dependence is even more important considering that its orientation and penetration depth will determine the total amount of AC losses (Alamgir et al. 2005).

2.3.3. AC Losses – from tapes to stacks and coils

AC losses presented by complex superconducting components like stacks or coils do not relate in a linear way with those presented by the HTS tapes that compose these devices. It is then of utmost importance to experimentally verify the total amount of losses in a superconducting device, and if possible to create models that can be used to scale those losses to even more complex systems. A common starting point is to measure AC losses in samples of HTS tape (1G or 2G, according to the tape used in the device) and then extrapolate obtained data using known and valid models (or use experimental data to create new models). This section will briefly describe the evolution pattern of AC losses when stacking HTS tapes and creating coils from samples of HTS tape. Some particularities and new sources of losses will be briefly addressed.

In section 2.3.1 the different origins of AC losses in HTS tapes were addressed. However, the utilization of HTS tapes in more complex systems generate other losses than must be accounted for, to calculate the total losses in a superconducting device. Bending HTS tapes to form pancake coils (as an example) increase their mechanical tension. In addition to this, there are thermal contractions to which the tapes are subjected during the cooling processes. These mechanical loads will increase AC losses, even when considering bending radius higher than the minimum bending radius of the used HTS tape (Kim et al. 2006). When winding HTS coils, a common process followed is to impregnate the coil with epoxy to reduce the amount of losses generated by the vibration of the tape (Tanaka et al. 2004). However, a full impregnation is also not an ideal situation because the coil will have a worse heat evacuation which will result in a decrease in the critical current (Polák et al. 2006). This is even more important considering that the total amount of AC losses also depends on the working temperature of the superconducting coil (Doan N. Nguyen et al. 2009). Models used to calculate AC losses in HTS coils generally are unable to calculate these mechanical losses which will result in a deviation when comparing its results with those obtained from the implemented system (Zhao et al. 2011). Nonetheless, the mechanical losses have to be considered and should be minimized in order to achieve an optimal efficiency.

When creating stacks of HTS tape (or coils), the self-field of the device will increase when comparing to a single sample of HTS tape. This results in a different behaviour in AC losses. The total amount of AC losses in a sample of HTS tape inside a stack (or coil) depend not only in its current and self-field but also on those created by adjacent samples (or turns) (Suárez et al. 2008). This phenomena can be verified for both, 1G and 2G tapes (Suarez et al. 2009). Such behaviour results in different evolutions of the total AC losses when stacking tapes together: magnetization losses will rapidly increase when stacking a few samples of HTS tape (Grilli et al. 2006). However, after a certain number of samples, a shielding effect starts to appear which will decrease the growth rate of magnetization losses and the stack behaviour approaches that presented by a superconducting slab (Yuan et al. 2009). In addition to this, the considered stack arrangement also influences the total amount of AC losses (Suenaga 2002). On the other hand the behaviour demonstrated by transport current losses is as follows. Stacking a few samples of HTS tape (or creating a coil with a few turns) results in a total amount of AC losses which can be several order of magnitude higher than those presented by a sample of tape multiplied by the number of turns (Choi et al. 2002). With the increase of the number of turns the total amount of AC losses per unit length will reach a saturation point and after that point, there is almost no increase in AC losses with the increase of the number of turns (Šouc et al. 2009). Finally, when

considering double pancake coils, when total amount of AC losses is around three times higher than for a single one, which might also be an important factor to consider (Pardo et al. 2012).

All these stated factors must be taken into account in the calculation of AC losses (and in used models), which demonstrates the complexity of the behaviour demonstrated by superconducting systems.

2.3.4. Methods of measuring AC losses

Measuring AC losses accurately is essential to successfully design and execute superconducting projects. There are different methods for measuring AC losses in superconducting tapes, usually classified in two different types. This section contains a state of the art description of most usual methods. A comparison of those methods is also performed.

2.3.4.1. Calorimetric

Calorimetric methods for determining AC losses are based on measuring the amount of energy that a superconductor dissipates in the form of heat. There are two common ways of applying a calorimetric method for measurement of AC losses:

- Measuring the amount of cryogenic liquid evaporated (boil-off method);
- Measuring the temperature of the superconducting sample (thermometric method);

Boil-off method

This method consists on measuring the amount of cryogenic liquid that evaporates due to heat generation in the superconductor. By measuring the amount of emitted gas with a gas flow meter, it is possible to determine the amount of AC losses in the superconductor. This means that the cryostat must be closed, in order to minimize the heat losses and allow the measurement of evaporated gas.

In low temperature superconductors, using liquid helium as coolant, this method is often used with good results. However, in HTS, using liquid nitrogen as coolant, accurate results are more difficult to achieve. This is due to the fact that nitrogen has a higher latent heat and liquid density than helium, which results in a smaller gas emission, for the same amount of thermal energy released (Okamoto et al. 2006). Even with a closed cryostat there are always heat leaks due to the temperature difference between the inside and the outside of the cryostat. In order to minimize this, it is also possible to place the test chamber of the cryostat inside another cryostat, also using liquid nitrogen as coolant. This eliminates the temperature difference between the inside and the outside of the test chamber, eliminating heat leakages (Kim et al. 2011).

The characteristics of the boil-off method, which result in a lower sensitivity when compared to electromagnetic methods make this a method only feasible for large coils and other large superconducting systems, where the amount of heat generated by AC losses is high, thus allowing accurate results. Small or medium size coils require a high sensitivity, which makes this method not as appropriate as other available methods.

Thermometric method

Another common calorimetric technique for measuring AC losses is the thermometric method. It consists on measuring the temperature rise in a section of the HTS tape, using a thermocouple. However, in order to be possible to measure the temperature rise, the tape must be insulated from the coolant, i.e., the section of the tape in which the temperature is measured cannot be inside the liquid coolant. To achieve this, that section of the tape can be insulated using (as an example) blocks of expanded polystyrene and some sealant, as demonstrated in (Ashworth & Suenaga 2001). This section of the HTS tape is cooled down by thermal conduction from the uninsulated section of that same tape.

In addition to the two aforementioned methods there are other possible approximations: (Wang et al. 2015) presented a calorimetric method to measure AC losses in 2G HTS tapes using optical fibre and (See et al. 2011) describes an innovative calorimetric method to measure AC losses in small samples of HTS tape with accurate results. In the latter work, temperature rise is measured using a commercial temperature sensor. However, the size of the tape sample is strongly limited by the size of the chamber used for measuring purposes.

2.3.4.2. Electromagnetic

Electromagnetic methods are the most common ways to measure losses in superconducting devices. These are also the methods that present the highest sensitivity, allowing an accurate measurement of AC losses. The different electromagnetic methods will now be presented in detail.

Lock-in Amplifier (LIA) Method

This is the most common way to measure AC losses in high temperature superconductors. Its configuration is depicted in Figure 2.20. The operating principle can be briefly explained as follows.

Using the internal oscillator of the LIA it is possible to generate a signal with different amplitudes and frequencies. This signal is easily controlled using LabVIEW. By means of a power amplifier and a transformer the signal is amplified to adequate values and the superconducting sample (tape or coil) is connected to the secondary of the transformer. Using the signal from a Rogowski coil (pure inductive signal) as reference in one of the LIA channels, it is possible to measure (on the other LIA channel) the resistive and inductive components of the voltage drop in the HTS sample. By allowing a separation of resistive and inductive components, this method allows the measurement of AC losses because these are correspondent to the resistive part of the voltage drop. The inductive part corresponds to the self-inductance of the sample.

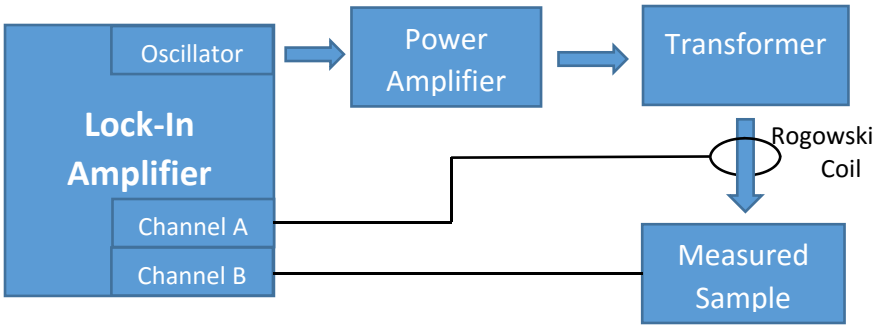

Figure 2.20. Lock-in Amplifier method for measurement of AC losses configuration.

The LIA method is especially useful for measuring AC losses in samples of HTS tape and small coils, in which measured voltages are in the range of μV. As some examples of AC losses measuring systems using this method one can look at (Yoshida et al. 2003; Choi et al. 2002; Duckworth et al. 2003b; Majoros et al. 2007; Souc et al. 2006).

Pick-up coil Method

The LIA method previously presented allows a measurement in the source, by providing information of the transport current. However, there is another method for measuring AC losses using electromagnetic quantities: measuring the information coming from the variations of the magnetic field. This is called the pick-up coil method and uses coils that are sensitive to the magnetic field variation. The pick-up coils are placed in strategic locations (which depend on the application) to measure the variations of the magnetic field in the superconducting sample. Several authors use this method for measuring magnetization losses in superconductors. See as examples (Šouc et al. 2009; Suarez et al. 2010; Suenaga 2002).

2.3.4.3. Comparison of AC losses measuring methods

The different characteristics of these methods allow a comparison between them, highlighting some advantages and drawbacks of each one.

In general, calorimetric methods have a lower accuracy than electromagnetic methods, which means that they should be used in larger systems, where the total amount of AC losses is high enough to neglect small differences in achieved results. The method that presents a higher accuracy is the LIA method, mainly due to the characteristics of this device, which minimizes noise values allowing measurements in the order of μV. Calorimetric methods are also much more time consuming than electromagnetic methods. The main drawback of electromagnetic methods is that there are often small limits for measured values. As an example, a typical LIA allows as input a maximum value of 1 V, so if the total voltage measured in the HTS tape or coil is higher than this value some kind of signal conditioning is required, which implies that more elements are added to the measuring system. Since the phase error is a very important aspect when measuring AC losses, this might represent a problem. Another drawback of the LIA method is related to the apparatus itself. The LIA works by locking-in a frequency, ignoring all other. This means that this method cannot be used for systems were the AC losses might be generated by different harmonics.

Considering the advantages and limitations of the several methods, it is also common to use simultaneously more than one method for AC losses measurements. Such combination allows not only to overcome the limitations of each method but also to easily verify the accuracy of used methods (Majoros et al. 2011; Kim et al. 2011; Vojenčiak et al. 2006; Yinshun Wang et al. 2014).

2.3.5. Strategies for minimization of AC losses

AC losses represent an important challenge for the utilization of superconducting devices. Because it is necessary to consider the refrigeration costs necessary to extract AC losses from a superconducting system, these losses lead to a decrease in the overall efficiency of the device and therefore need to be minimized or mitigated. There are different techniques to reduce AC losses and different research groups focus their interest in this topic. Methods to reduce losses through improvements of the HTS tape manufacturing process are one of the topics that concentrate a higher research effort and although this is a topic for materials science engineering, considering its importance, it will be briefly addressed. Techniques used in already manufactured superconductors and methods that can lead to a decrease of AC losses though changes in the superconducting tape will also be briefly described in this section.

2.3.5.1 Use of flux diverters

As seen in section 2.1.4, the critical current (and therefore AC losses) is dependent on the applied magnetic field. This magnetic field can be the self-field (generated by the HTS tape or coil) or an external field, but no matter its origin, it will degrade the critical current of an HTS tape and increase its AC losses. Bearing in mind this fact, one used strategy to decrease AC losses is the utilization of magnetic materials to divert the field from the superconducting tape. The materials used to divert the magnetic field (commonly designated as flux diverters) can be made of weak or strong magnetic materials and the reduction of AC losses is higher when a material with a high saturation field and low remnant field is used (Ainslie et al. 2013).

Different approaches can be considered to decrease AC losses using this magnetic shielding technique. The flux diverters can be placed at the level of the superconducting filaments, which will shield each individual filament from the magnetic field (Majoros et al. 2009); at the level of the superconducting tape, in which the full tape or only its edges can be covered with a ferromagnetic material. In this case it is important to mention that even if AC losses are reduced, when the tape is fully covered with a ferromagnetic material its critical current will decrease and the optimum point is reached when around 20% of the tape width (starting from its edge) is covered (Gömöry 2006; Gömöry et al. 2009; Alamgir et al. 2006). The last possible approach is to use flux diverters in the superconducting device as a whole and not in the superconducting tape or individual filaments. It is common to use such approach in HTS coils, where plates of ferromagnetic foils can be used in the top and bottom of the coil (Pardo, Šouc, et al. 2009) or in superconducting cables (Vojenčiak et al. 2011).

2.3.5.2 Roebel transposition

First proposed by Ludwig Roebel in 1914 for the reduction of AC losses in copper cables, this transposition shows an interesting behaviour when considering the reduction of AC losses in superconducting tapes (Goldacker et al. 2007). Superconducting cables with a Roebel transposition have the configuration presented in Figure 2.21 and in order to achieve this shape, the superconducting tape must be cut or punched into shape before the winding process.

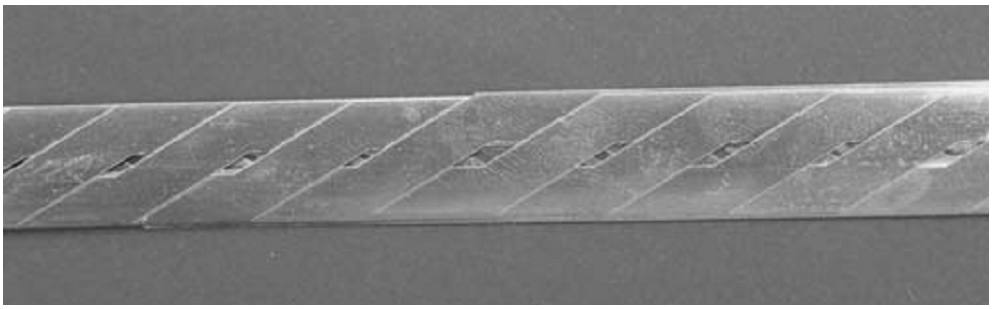

Figure 2.21. Roebel transposition consisting on sixteen 2G HTS tapes. Source: (Goldacker et al. 2007).

In the last years different research groups considered the Roebel configuration for HTS cables achieving reduced AC losses (Schuller et al. 2007; Terzieva et al. 2010; Frank et al. 2008).

2.3.5.3 AC loss minimization in the manufacturing process

Since AC losses are associated to the superconducting filament disposition in the HTS tape it is possible that different filaments configurations lead to different values of AC losses. In (Gömöry et al. 2004) the total hysteresis losses were decreased due to an optimization of the filament arrangement. As seen in section 2.1.4 superconducting tapes (1G and 2G) can have magnetic substrates. The existence of magnetic materials in the HTS tape will lead to the appearance of an AC loss component in the substrate. Considering this, different research groups focus in improving the substrate of superconducting tapes, in order to decrease the overall AC losses. In order to evaluate and decrease this loss component it is first necessary to distinguish it from the overall AC losses in an HTS tape, which usually is performed trough the comparison of experimental data with numerical modelling techniques results (Pardo, Souc, et al. 2009; Doan N Nguyen et al. 2009). Results obtained seem to indicate that the substrate is an important source of losses both in 1G and 2G tapes (Suarez et al. 2010; Gomory et al. 2009) and a continuous research effort is placed in finding optimal substrate compositions in order to decrease AC losses (Ijaduola et al. 2004; Duckworth et al. 2005). Finally, it is important to state that the source of AC losses in non-superconducting components in and HTS tape is not limited to the substrate. In tapes manufactured using the IBAD technique (in which no magnetic substrate is used), the addition of copper stabilizing layers will also generate AC losses and those can be even higher than the ones originated in the magnetic substrates (Majoros et al. 2008).

2.3.5.4 Other possible approaches for AC loss minimization

In these last sections, it was verified that the total amount of AC losses in a superconducting device can be decreased by changing the tape manufacturing process (or its constituents), or by adding ferromagnetic materials to divert the flux from the HTS tapes. There is still another approach that can be used in order to decrease AC losses in superconducting devices employing HTS coils. In a superconducting magnet constituted by more than one coil, the field distribution is not the same in each coil, and coils in specific positions (extremities in the case of a solenoid magnet) are more subjected to the magnetic field. One possible way to decrease the total AC losses in the system is then to change the aspect ratios of the coils. Different aspect ratios can be considered depending on the application and the magnetic field profile (Fukui et al. 2006; Fukui et al. 2008). One common topology is to use double or multiple pancake coils connected in parallel to form a larger coil. AC losses of each coil are strongly influenced the distance to adjacent coils and the introduction of an air gap between coils might also be used to decrease the overall losses in the system (Alex et al. 2010).

3

Modelling of High Temperature Superconductors

This chapter aims to give a description of all models used/implemented during this project. To achieve accurate results, both analytical and numerical models were used. As a first basis to model the superconducting coil, an analytical model was implemented, based on classical formulas for coil designs. This model was implemented using a Matlab script. To validate results achieved with the analytical model, the designed coil was also simulated using a numerical model, implemented with the software package FLUX2D from Cedrat Company. This numerical model was also used for calculation of AC losses, together with another numerical solution. Simulated coils were implemented and results will be described in the corresponding section. The next two sections contains an explanation of all implemented models, together with a description of models that were used but were not created in this work. Finally, in section 3.3, a short summary about the used models will be presented.

3.1. Analytical models

Analytical models provide a straightforward tool to achieve a first idea about the characteristics of the superconducting coil, namely its inductance. By using analytical expressions to calculate inductance of air core coils, it might be possible to achieve a first result for the HTS coil inductance. These analytical expressions are used for several decades, for the design of conventional coils (i.e. coils wound from materials like copper). If such formulas can be applied to HTS tapes, then they might provide a very useful tool to calculate the inductance of a superconducting coil. However, since analytical methods do not offer a reliability as high as numerical methods, results obtained with this method should be verified using a numerical solution.

One main goal when designing a superconducting device is to maximize the amount of stored energy, minimizing the volume of the HTS coil, i.e. minimizing the required amount of HTS tape. Considering this, an analytical method, based on classical formulas for the design of air core disk (pancake) coils, was implemented, to achieve the maximum value for the inductance of the HTS coil, given a specific amount of HTS tape. These formulas are based only on the geometry of the coil, as will be seen.

Consider a pancake coil, with mean radius a, height b, and total width c, as shown in Figure 3.1.

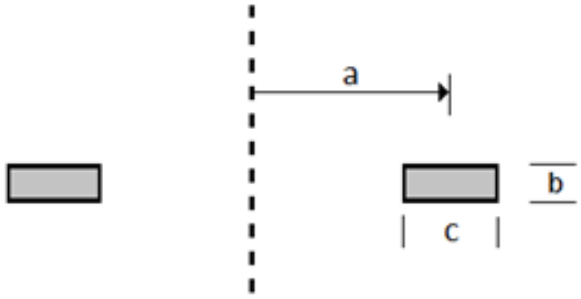

Figure 3.1. Dimensions of a pancake coil: mean radius (a), height (b), and total width (c).

The inductance L (in mH) of this coil can be determined by Weinstein Formula (Rosa & Grover 1948)

$$L = 4\pi a N^2 (\lambda + \mu) \tag{3.1}$$

where λ, μ are two constants calculated as follows.

$$\lambda = \log\left(\frac{8a}{c}\right) + \frac{1}{12} - \frac{\pi x}{3} - \frac{\log\left(1+x^2\right)}{2} + \frac{\log\left(1+x^2\right)}{12x^2} + \\ + \frac{x^2 \log\left(1+\frac{1}{x^2}\right)}{12} + \frac{2}{3}\left(x - \frac{1}{x}\right)\tan^{-1} x, \tag{3.2}$$

and

$$\mu = \frac{c^2}{96a^2}\left\{\left[\log\left(\frac{8a}{c}\right) - \frac{\log\left(1+x^2\right)}{2}\right]\left(1+3x^2\right) + 3.45x^2 + \frac{221}{60} - \right. \\ \left. -1.6\pi x^3 + 3.2x^3 \tan^{-1} x - \frac{\log\left(1+x^2\right)}{10x^2} + \frac{x^4 \log\left(1+\frac{1}{x^2}\right)}{2}\right\}, \tag{3.3}$$

with

$$x = \frac{b}{c} \tag{3.4}$$

Variable N in equation (3.1) represents the number of turns of the coil.

Equation (3.1) allows the calculation of the inductance of a coil, given the dimensions of that coil. However, in this particular case, the dimensions of the coil are not known. The only known parameters are the length of HTS tape used and the dimensions of that tape (width and thickness). Considering this, extra calculations must be considered, to obtain the prospective dimensions of the coil.

Consider a coil with internal diameter D, wound from HTS tape with thickness esp. The total length l of the HTS tape used to wound the coil can be calculated as the sum of the tape used in all turns, i.e. the sum of all perimeters. It is implicit that the packing factor is considered as 1, i.e. there is not any gap between two successive turns. The total length l can then be calculated as

$$l = \pi \times D + \pi(D + esp) + \pi(D + 2 \times esp) + ... + \pi(D + (N-1)esp) \tag{3.5}$$

Simplifying this equation and replacing the internal diameter D with the internal radius $R_i = D/2$, one has

$$l = N^2 \pi \times esp + N\pi(2 \times R_i - esp) \tag{3.6}$$

Equation (3.6) allows the calculation of the total length of tape used, considering the internal radius of the coil and number of turns. However, in this specific case, one wants to calculate the number of turns, knowing the total length. Reversing the equation, i.e. solving for N as a function of l, a second order polynomial equation is obtained, which will give two solutions, one positive and one negative. For this particular case the solution chosen is always the positive one, since the unknown variable is the number of turns. Considering this, N becomes

$$N = \frac{\pi(esp - 2R_i) + \sqrt{(\pi(2R_i - esp))^2 - 4\pi \times esp \times l}}{2\pi \times esp} \tag{3.7}$$

Knowing the number of turns, N, it is now possible to calculate the variables a and c used in expressions (3.1) to (3.4), by calculating first the external radius, R_e, of the coil

$$R_e = R_i + N \times esp \tag{3.8}$$

Thus

$$a = R_i + \frac{(R_e - R_i)}{2} \tag{3.9}$$

and

$$c = R_e - R_i \tag{3.10}$$

Considering that the variable b is the width of the HTS tape, it is now possible to determine the inductance of the coil, using expression (3.1).

This series of equations allows the calculation of inductance of a coil, given its dimensions. Since most HTS devices have more than one pancake coil, it is also necessary to compute the mutual inductance between coils. In solenoidal configuration, all coils are concentric, and the

mutual inductance L_M (in mH) of a set of two coils is given by the following equation (Babic et al. 2004):

$$L_M = \frac{\mu_0 N_1 N_2}{(R_2 - R_1)(R_4 - R_3)} \times \int_0^{\pi} \int_{R_1}^{R_2} \int_{R_3}^{R_4} \frac{\cos(\theta) r_1 r_2}{\sqrt{g^2 + r_1^2 + r_2^2 - 2 r_1 r_2 \cos(\theta)}} dr_1 dr_2 d\theta \qquad (3.11)$$

In this equation N_1 and N_2 are the number of turns of each coil and the other geometric entities (in meters) are depicted in Figure 3.2 . In this expression the coils are approximated as thin disks, i.e. the distance between coils, g, is larger than the HTS tape width. Since in HTS pancake coils these values are in the same order of magnitude, this will introduce some error. It is then necessary to evaluate the accuracy of this formula, which will be verified by comparing obtained values with those measured in experiments.

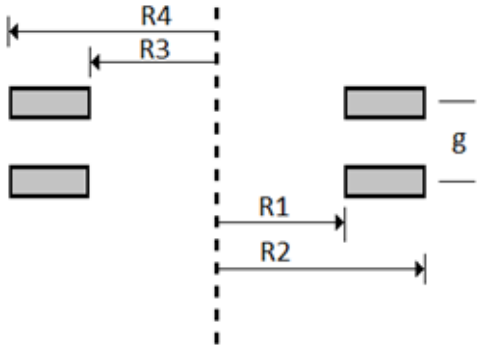

Figure 3.2. Dimensions of a set of two concentric coils.

Using equations (3.1) to (3.11), a Matlab script was programmed to compute the total inductance of a set of coils. A flowchart of this script is depicted in Figure 3.3.

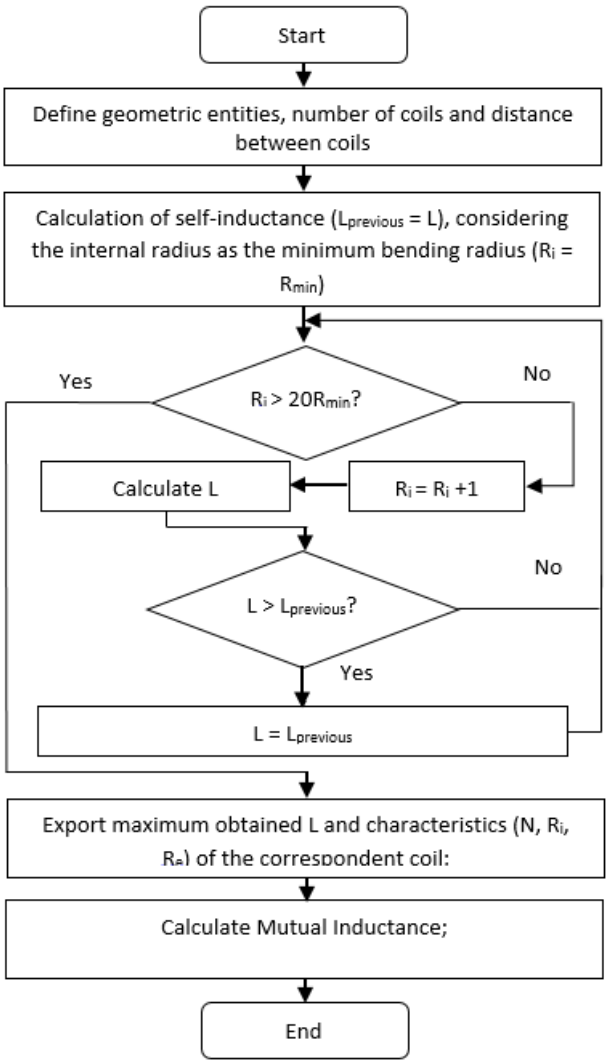

Figure 3.3. Computation of the inductance of an HTS coil.

In a brief way, the program work as follows. After introducing the characteristics of the HTS tape, such as length, width, thickness and minimum bending radius, the number of coils and distance between them, the self-inductance of the coil is computed using expression (3.1). The first step of an iterative loop considers the internal coil radius as the minimum bending radius of the tape. The internal radius of the coil is then incremented by 1 mm and the self-inductance is calculated again. If the calculated value is higher than the previous one the program saves that configuration (number of turns and internal radius). This iterative loop continues till the internal radius is twenty times the initial one. Figure 3.4 depicts results of this loop for a coil considering 37.5 m of superconducting tape, with a minimum bending radius of 30 mm, a width of 4.2 mm and a thickness of 0.25 mm. The discontinuities on this figure are due to the fact that the number of turns is always considered as integer. This loop allows the computation of the maximum value of inductance, for a specified amount of HTS tape.

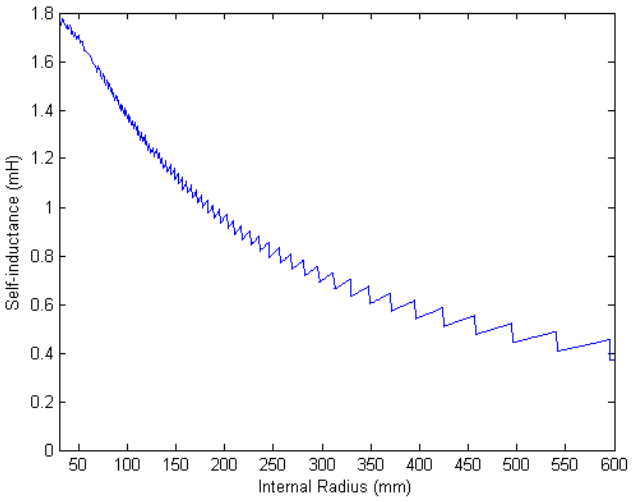

Figure 3.4. Computation of inductance in function of internal radius of a coil.

After the calculation of the maximum self-inductance of each coil (assuming that all the coils are similar), the algorithm computes the mutual inductance between the several coils (if more than one coil is used) and the total inductance of the HTS coil. The flowchart of Figure 3.5 describes the computation of the mutual inductance between pairs of coils. It is necessary to calculate all contributions between all used coils, in order to achieve the value of the total mutual inductance of the system.

Considering a set of N coils, connected in series, the equivalent inductance of the set, L_{eq}, is given by

$$L_{eq} = \sum_{i=1}^{N} \sum_{j=1}^{N} L_{ij} \tag{3.12}$$

where L_{ii} is the self-inductance of the i-th coil, and $L_{ij} = L_{ji}$ is the mutual inductance between the i–th and the j–th coils. The mutual inductance is only calculated for a maximum index i of 5. This means that the mutual inductance is only considered between one coil and the closest 5 coils to that first one. If there are more than 6 coils, the mutual inductance between coil 1 and coil 7 (as an example) is already so small that its value can be neglected.

The expressions (3.1) and (3.11) contained in this model are used for several years, in conventional materials like copper. However, the current distribution in superconductors is different from these materials, so it is important to test if such expressions can be used for design of HTS coils. This model was used as a basis for two implemented HTS coils, and results are accurate, as will be see in the corresponding section (implementation of HTS coils).

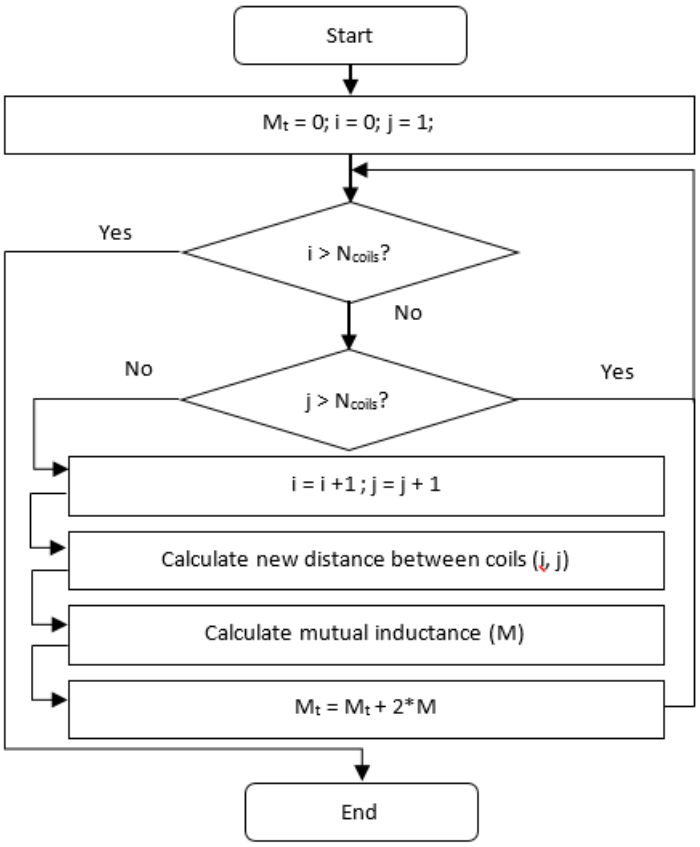

Figure 3.5. Computation of the total mutual inductance of an HTS coil, composed of several single pancake coils.

3.2. Numerical models

Numerical models provide the most reliable approach to verify characteristics of a superconducting coil. These methods should be used in a second stage of the design, in order to verify the accuracy of results obtained from analytical methods and obtain results closer to the real system. Numerical models are usually based on finite elements analysis (FEA), following an *H Formulation*, as presented in section 2.1.6.3. In this project, these models were used for simulation of HTS coils and short samples of HTS tapes. Since it is possible to use only one software project to verify all characteristics of the tape/coil, such as current density, inductance and AC losses, the implemented projects will be described in this section and the results obtained will be discussed in the respective sections, considering the characteristic in study. Thus, this section contains a description of implemented numerical methods, using the software package FLUX2D from Cedrat Company and also a short description of other numerical method used in this work. This last method was not implemented in this work, it was only used to verify and corroborate results from other methods, when measuring AC losses in HTS coils.

3.2.1. Minimum Electro-Magnetic Entropy Production Simulations

Minimum Electro-Magnetic Entropy Production (MEMEP) is a numerical method that can be applied to almost any superconducting device (including large HTS coils), developed by Enric Pardo et al., in (Pardo et al. 2015). One main disadvantage of numerical methods based on FEA (like the FLUX2D software) is the computation time, which easily is in the order of days/weeks. This strongly limits the utilization of such methods, and it is unfeasible to simulate HTS coils with more than a few hundred turns. One of the reasons for this long computation time is that the FEM methods need to set boundaries far away from the sample, which will increase the number of elements, thus increasing the simulation time. The MEMEP method, based on variational principles (Grilli & Pardo 2010), restricts the computation volume to the superconducting region in study, allowing enhancing computation times. In addition, this method allows a utilization of almost any possible $E(J)$ relation, in particular a power law $E(J)$ relation with magnetic field-dependent critical current density, J_C, which is the verified relation in HTS coils.

The MEMEP method was applied in this particular case with some simplifications: the self-field was not corrected in the $J_C(B,\theta)$ dependence and the superconducting region was approximated by one of two different approaches: an ellipse surrounding all superconducting filaments or a rectangle with the same area. The geometric parameters used in the MEMEP models are presented in Table 3.1.

Table 3.1. Geometric parameters used in the MEMEP simulations.

Geometric parameter	Value	
	Rectangular Mode	Elliptical Model
Coil internal radius (mm)	32	
Tape thickness (mm)	0.23	
Tape width / coil height (mm)	4.2	
Rectangle/Ellipse thickness (mm)	0.1328	0.1622
Rectangle/Ellipse width (mm)	3.9	4.0637
Rectangle/Ellipse area (mm²)	0.51779	
Insulating layer thickness (mm)	0.02	
Total number of turns	128	

For the simulations performed using the rectangular cross-section a mesh with a total of 80x10 elements was used whereas for the elliptical cross section model the mesh had a total of

66x13 elements. Two different n-values were simulated: $n = 10.8$, which was the measured n-value of the tape during the AC losses measurements and $n = 200$. In the MEMEP model no silver region was simulated, i.e. the model only considered the superconducting region.

Briefly, the MEMEP method work as follows: measuring the critical current (I_C) of the HTS tape under applied field B with different orientations and considering the superconducting region of the tape (which can be calculated from a microphotography of the HTS tape) it is possible to extract the critical current density $J_C(B,\theta)$ dependence. With this $J_C(B,\theta)$ dependence, the current distribution in each turn of the HTS coil is then calculated. Finally, the AC loss per cycle (which was the only characteristic verified using this method) can be calculated by the integration of the dissipation power density $J.E$ in a period and on the whole volume of the superconductor, where J is the current density and E is the electric field. Figure 3.6 depicts measured I_C of the used HTS tape, under applied field B with different orientations.

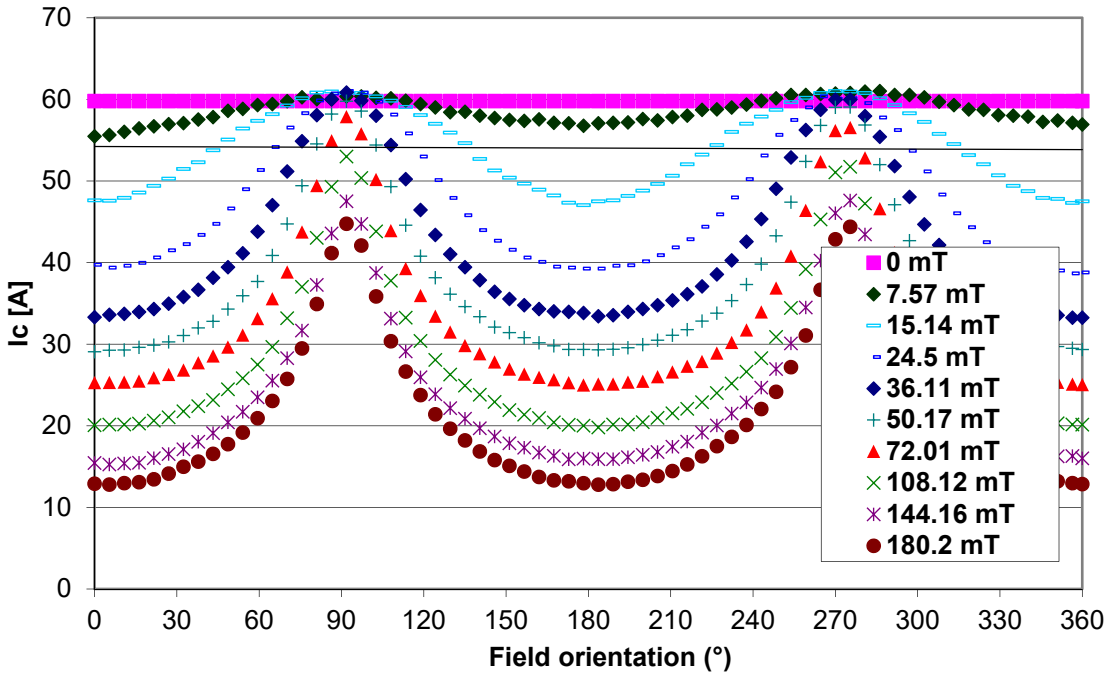

Figure 3.6. Critical current dependence of applied magnetic field for the used 1G HTS tape.

3.2.2. FLUX2D Simulations

Using the software FLUX2D from Cedrat Company, several superconducting coils were simulated and their main characteristics like critical current, generated magnetic field and AC losses were extracted. This section briefly describes the method followed for the coil design and simulation. This software package has been used in the last years to simulate HTS systems, by different research groups, with accurate results (Stavrev et al. 2003; Nibbio et al. 2001; Stavrev et al. 2002).

The geometry of the simulated HTS coils was constructed using as a basis the HTS tape design depicted in Figure 3.7 (Cedrat 2001). Since at the time of first performed experiments the

available tape was mainly 1G HTS tape, this will define the kind of tape used during the whole work and obviously also in the simulation process. Another possible approach is to define the different superconducting filaments, and create the correspondent geometry. However, such approach will lead to more complex models, which will increase even further the simulation times.

Figure 3.7. FLUX2D model of a cross section of 1G HTS tape.

Using several geometric parameters, it is possible to easily design an HTS coil with a given number of turns, using as basis the tape. Since a pancake coil corresponds to a series of turns with increasing concentric radius, it is possible to use an axisymmetric geometry. Different size coils were tested and the only difference between them is the number of turns, i.e. each additional turn is created in the same way, using the same materials. Figure 3.8 depicts the full geometry simulated for an HTS coil with eight turns. As can be seen, a large air region must be used, in order to define the boundary conditions for the simulation, which will increase simulation time. In these simulations, the condition used was an imposed zero magnetic flux in the external boundaries of the simulated region. Since the external boundaries are far away from the test device, this condition can be applied.

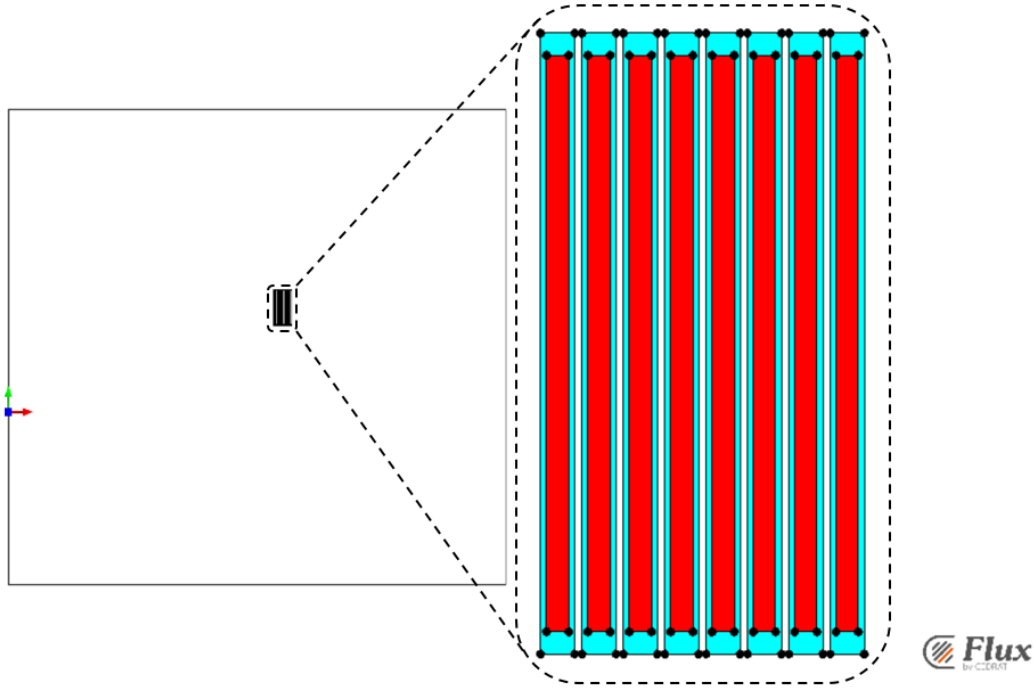

Figure 3.8. Geometry of an HTS coil with 8 turns.

Table 3.2 contains the values of the several geometric parameters used in the several FLUX2D simulations performed.

Table 3.2. Geometric parameters for FLUX2D simulations of HTS coils.

Geometric parameter	Value (mm)
Coil internal radius	32
Tape thickness	0.23
Tape width / coil height	4.2
Superconductor thickness	0.133
Superconductor height	3.9
Insulating layer thickness*	0.02

*Air was used as insulator.

The materials used in the simulation were superconductor and silver only (and air as insulator). The main characteristics of these materials are presented in Table 3.3.

Table 3.3. Characteristics of materials used in simulations.

Material	Characteristic	Value
Silver	Resistivity (Ω.m)	3×10^{-9}
Superconductor	Model: Power Law	$E(J) = E_C(\frac{J}{J_C})^n$
	n value	15*
	J_C (A/mm^2)	90
	E_C (V/m)	1×10^{-4}

* variable n value, depending on the tape characteristics

The regions associated to silver and superconductor were simulated as solid conductors, placed in series with a programmable current source. The utilization of a programmable current source allows a great flexibility, being possible to use DC or AC currents, also considering several harmonics. Figure 3.9 shows the electric circuit used to simulate the coil. The upper solid conductors correspond to those associated to silver regions and the lower to superconducting regions. In a normal operation, due to the lower resistivity, all current flows through the superconducting regions. However, if the applied current surpasses the critical current, then the surplus current will start flowing through the regions with higher resistivity (silver regions). Using the circuit of Figure 3.9, it is also possible to simulate a problem in one turn, by changing the characteristics of the superconducting material used in that turn (as an example). In this case, the current would flow through the silver in that turn only.

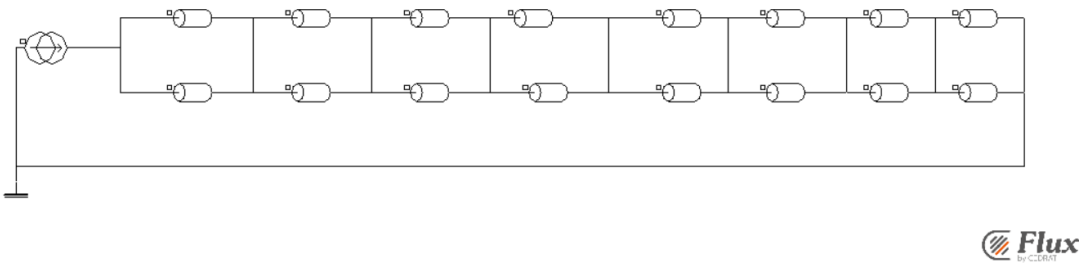

Figure 3.9. Equivalent electric circuit for a coil with 8 turns.

The software works by dividing the full region in smaller elements and solving the PDE in those regions. This is done by constructing a mesh in the whole simulated region. The mesh used in this case (of a coil with 8 turns) can be seen in Figure 3.10. Mesh elements in the superconducting region are rectangular, in opposition to the triangular elements of the

remaining regions, as defined by Cedrat Company (Cedrat 2001). This is an important condition to correctly simulate the superconducting behaviour. The used mesh had a total of 80x10 elements in the superconducting region.

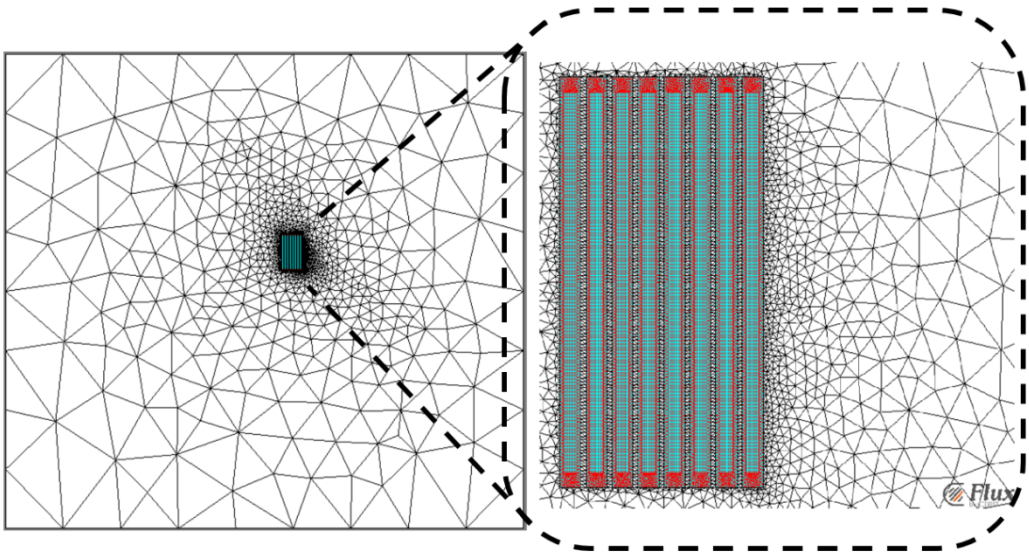

Figure 3.10. Mesh size for simulation of a coil with 8 turns.

The described method allows the simulation of HTS coils of different sizes. In all simulations performed the model characteristics remained the same, except for the number of turns, number of solid conductors and the n-value of the superconductor.

3.3. Concluding remarks

This section presented an overview of used models for simulation of HTS tapes and coils. An analytical method, for a first approach to determine the inductance of the coil was presented. This method, based on classical formulas and implemented in Matlab, allows an optimization of HTS tape used, i.e. a maximization of inductance value for a specified amount of HTS tape. Results obtained with this method might not be as accurate as desirable, especially because the used formulas were only applied in conventional materials and in superconductors the current distribution is different, so numerical methods also need to be considered. Two different numerical methods are used in this work (and were presented in this section): a MEMEP based method, which was not implemented by the author of this work (it was only used in the context of this project) and a FLUX2D software project that allows the simulation of HTS coils, with a different number of turns. The MEMEP method was used only to measure AC losses. The FLUX2D model was used to verify different characteristics of HTS coils and is used as a basis to verify experimental data regarding the coils and also AC losses.

4

Experimental Setups

This part of the document aims to give a description of all implemented experimental setups. One main characteristic in a superconducting device is its critical current, so the setup implemented/used to verify the critical current of HTS tape and coils need to be described. For simulation purposes, it is necessary to know the critical current of superconducting tape not only in self-field conditions but also with an applied external field. Both setups will be described in this section. One other characteristic that requires attention in a superconducting device is the total amount of AC losses, as previously explained. Two different setups for measuring AC losses were used, one based in an electromagnetic method, using a LIA and another one based on calorimetric methods. Results obtained using all these setups were compared not only with the results obtained from simulations (using the different models described in the last section) but also with values found in the literature. This sections contains a description of the used experimental setups and results achieved will be described in the corresponding sections.

4.1. Critical current measurements

In order to successfully design a superconducting device, one main characteristic of the constituting HTS tape that needs to be verified is the critical current. Although the critical current (or critical current density) is always given by the tape manufacturer, tape ageing, heterogeneities in the tape manufacturing process, and so on, can decrease its critical current value. Considering this, it is desirable to measure the critical current of the HTS tape, at the moment of implementation of a superconducting device, in order to verify the exact characteristics of that device. On the other hand, if the implemented device is a coil, then its critical current (also in DC conditions) will be lower than the tape's critical current. This is due to the fact that the coil will generate a magnetic field, which will decrease the critical current value, as seen in section 2.1.2. Bearing in mind these facts, different experimental setups were implemented/used to verify the critical current of HTS tape and coils. Those setups will now be described.

4.1.1. Superconducting tape

HTS tape can be modelled, as seen in section 2.1.6, using an $E-J$ relation (equation 2.5). This equation can also be written in terms of voltage, U, and applied DC current, I, as

$$U = U_C \left(\frac{I}{I_C} \right)^n \tag{4.1}$$

where U_C is the critical voltage (which results from the criterion of $E_C = 1$ μV/cm and considering the length of the sample) and I_C is the critical current.

Using expression (4.1), increasing the applied current and measuring the sample voltage allows the determination of critical current and n value of the superconducting tape. The critical current is the value of current in which the critical electric field is verified and the n value can be determined adjusting the experimental data to a power law curve, using a curve fitting application like *cftool* from Matlab.

4.1.1.1. Self-field

Critical current is usually measured in self-field conditions, i.e. the only magnetic field in the tape is the field generated in by the tape itself. The experimental setup used is based in the four-point method according to international standards (IEC 2006). This method consists on measuring the applied current in the HTS tape and the voltage drop across a specific length of tape. Voltage is measured be means of two voltage taps, usually soldered in the superconducting tape. This configuration is depicted in Figure 4.1. Different samples were used, in different phases of tape utilization (to verify tape ageing effect). In the setup shown in Figure 4.1, voltage taps are separated by 4 cm, which means that the critical current is reached when the measured voltage is 4 μV. The voltage level in this experiments required the existence of a high sensibility voltmeter, such as a Keithley 2001 voltmeter or equivalent.

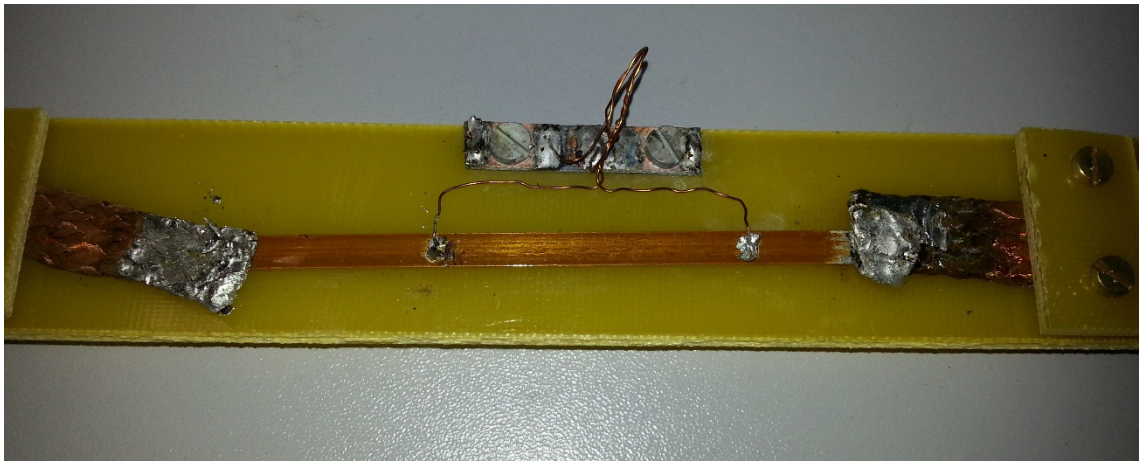

Figure 4.1. HTS sample for critical current measurement.

4.1.1.2. Applied external field

In order to simulate the HTS coils using the MEMEP method, described in section 3.2.1, it is necessary to determine the $J_C(B,\theta)$ dependence. This can be determined by measuring the critical current of a sample of HTS tape with an applied magnetic field.

The procedure used for measuring the critical current is the same as used in the previous section, with a difference: the sample is placed inside a copper coil, which generates a known variable magnetic field. A stable magnetic field value must be provided for the whole HTS sample. Using a step motor, it is possible to rotate the sample, thus rotating the orientation of the applied magnetic field. This experimental setup was not implemented in this project. It was already implemented at the Slovak Academy of Sciences, where it was used. Critical current was measured for applied fields ranging from 0 to 180.2 mT. Each motor step corresponded to a rotation of 1.8 °.

4.1.2. Superconducting coils

Due to the generated magnetic field by the superconducting coil itself, the critical current is expected to decrease, as seen in section 2.1.5. This means that after the wound process, the critical current should be measured, prior to the coil utilization. The critical current of implemented coils was measured using the same experimental setup as tapes (four point method), and the same criterion for the critical electric field of $E_C = 1$ μV/cm. The voltage taps were placed close to the coil ends.

4.2. AC losses measurement system

AC losses are expected to be one of the main limiting factors for the dissemination of superconducting devices in power systems. Since these devices work at cryogenic temperatures, all generated heat must be extracted, increasing the required cryogenic power requirements. Thus, it is important so verify the amount of AC losses in superconducting devices. Two different methods for measuring AC losses were used in this project: an electromagnetic method, using an LIA, and a simple calorimetric method. These methods will now be discussed.

4.2.1. Electromagnetic method

Electromagnetic methods offer the highest accuracy when measuring AC losses. The utilization of an LIA offers the possibility to measure voltages of the order of μV, allowing a precise measurement of losses in superconducting tapes or coils. The method used in this work is similar to the classic LIA method, with a few changes necessary for signal conditioning. Measurements made using this method were performed in two different places (Slovak Academy of Sciences (SAS) and FCT-UNL so the same method was applied two different times, with different (but similar) instruments. The main difference between the two methods is the used transformer, connected in series with the power amplifier, and the used Rogowski coils. These differences will be discussed now.

The LIA method, depicted in Figure 4.2, was used for AC losses measurements of both, samples of HTS tape and HTS coils. Figure 4.3 shows the experimental setup used at SAS.

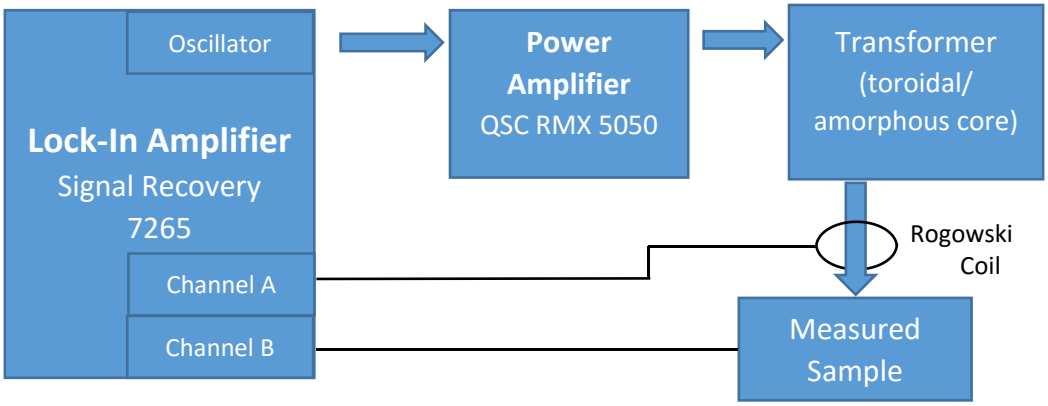

Figure 4.2. LIA Method for AC loss measurement.

The Lock-In Amplifier is connected to a PC, using a GPIB interface. A LabVIEW program is used in the computer. This program is obtainable at the LIA manufacturer website (available at http://www.signalrecovery.com/downloads/labview.aspx). The LIA oscillator (controlled through the LabVIEW interface) is connected to a power amplifier. In this particular case, the

used power amplifier is a QSC RMX 5050 audio amplifier, which has a maximum output of 5 kW, using a bridge connection (between its two outputs) and considering a 4 Ω resistive load. Since the load is not pure resistive (especially in the case of coils) the currents achieved at the amplifier output are not high enough to fully test the superconductor, i.e. to achieve its critical current. Considering this, it is necessary to add a transformer, in order to increase the current to desired values. Two different transformers were used, because the measurements were realized in two different laboratories. The reason for the choice of two different transformer types was only based on availability of these devices. No visible differences were noticed in the different measurements realized, using both transformers. Besides the transformers, the other different element in the system is the Rogowski coil. Initially, at SAS, a laboratory implemented prototype was used. At FCT-UNL, a commercial Rogowski coil (Fluke i3000s) was available. Results obtained using the two different Rogowski coils were similar.

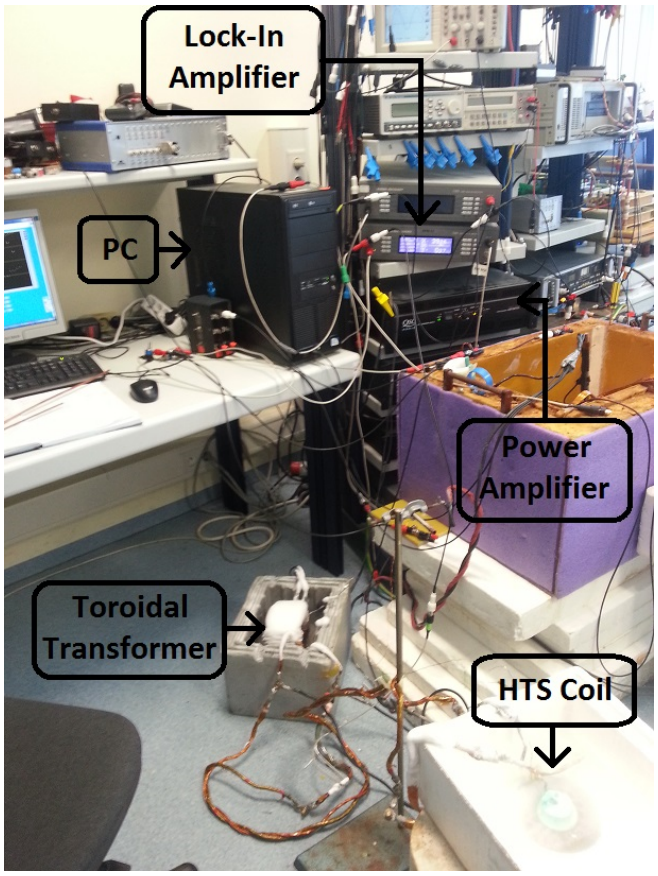

Figure 4.3. AC losses measurement system used at the Slovak Academy of Sciences.

When measuring losses in HTS coils, measured voltages easily surpass 1 V, which is the typical maximum voltage input for a LIA. Considering this, different strategies had to be followed, to decrease the measured value. One fundamental aspect to take into account is the maximum phase error. In a coil, the measured values of inductance and resistance (in phase and quadrature with the Rogowski coil signal, respectively) easily have differences higher than one order of magnitude. Thus, the maximum allowed phase error must be very low, because a slight change in the phase represents a large error in the measured loss value. Then, the elements added for signal conditioning (to decrease the measured voltage to readable values under 1 V) must not change the phase of the measured signal. In all experiments performed, the phase error was limited to a maximum of 0.1°.

AC losses were measured in a frequency range of 50 Hz to 1152 Hz, and different methods were used for signal conditioning, briefly explained as follows.

- Resistive divider (Bourns 3540s-440-130): for frequencies up to 288 Hz, a resistive divider was used to decrease the measured value. This proved to be a simple solution to decrease the measured value to levels under 1 V. However, for frequencies higher than 288 Hz the resistive divider started to change its frequency response, which changed its gain, thus changing the measured value. This characteristic made this approach unfeasible, for frequencies higher than 288 Hz.
- Voltage taps at representative turn: Šouc et al, in (Šouc et al. 2009) demonstrated that losses measured in some specific turns (representative turns) can be extrapolated to obtained losses in the whole coil, with accurate results. Considering this, a configuration using 4 cm voltage taps was also used. The voltage taps were placed in a representative turn, which usually can be defined as 2/3 from the total number of turns. Using this configuration, the large inductive component is avoided, allowing the safe utilization of an LIA.
- Contactless loop: The utilization of voltage taps has some disadvantages when used in medium/large sized coils. The necessity to remove the electric insulation from the tape generates a weak point due to the high inductive voltages presented in these coils. Measuring AC losses in superconducting tape samples using contactless methods has already been done for several years (Gomory et al. 2001) and in HTS coils Nguyen et al. also demonstrated the applicability of such methods (Nguyen et al. 2013). However, in the later work, the loop is located in the last turn of the coil, which results in the need to determine a calibration factor. Considering this, different contactless loops were also used to measure AC losses, having as goal the elimination of the necessary calibration factor. This was proven and it was possible due to the utilization of contactless loops in representative turns. Figure 4.4 has a detail of one of the contactless loops used. The copper wire was placed in the centre of the superconducting tape and Kapton tape was used to hold it.

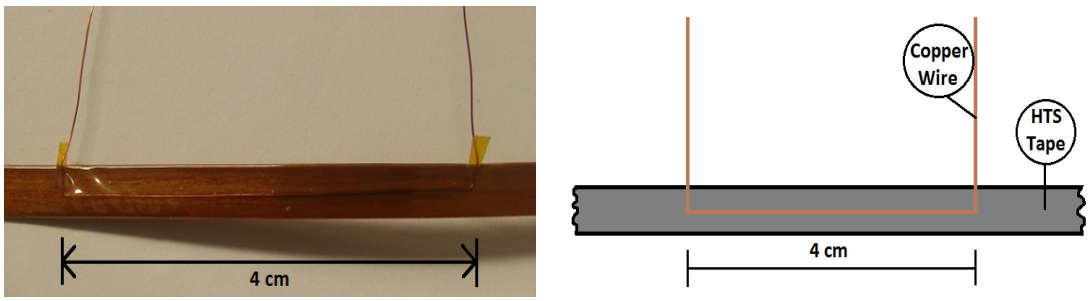

Figure 4.4. Detail of copper wire position in a 4 cm contactless loop: real tape (left) and schematic (right).

Figure 4.5 shows one used HTS coil and the position of the contactless loop (and also the voltage taps in the representative turn).

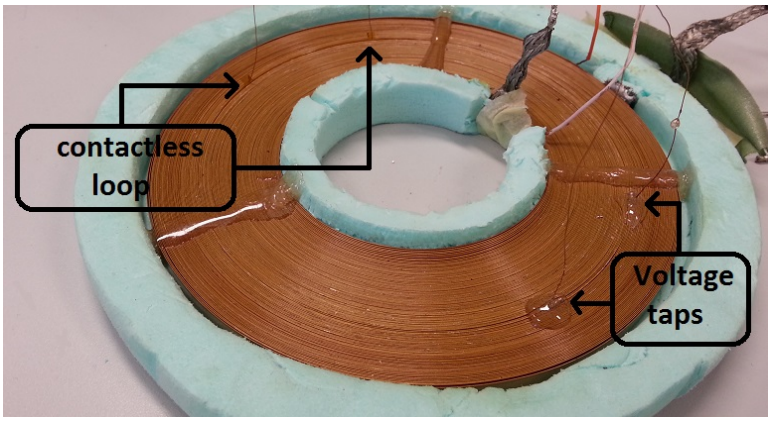

Figure 4.5. Position of AC losses measuring methods in the HTS coil.

Results obtained used the different methods, in both HTS tape and coils, will be presented in the respective sections.

4.2.2. Calorimetric method

The LIA method allows a great accuracy for measurement of AC losses. However, the utilization of an LIA has some limitations. The device locks a specific frequency (hence the name lock-in) and measure voltages in that frequency only. This means that if a multi-harmonic system is considered, i.e., if one wants to measure AC losses in a superconducting device considering different harmonics, the LIA method cannot be used.

To measure AC losses considering different harmonics, the more feasible way is to use a calorimetric method. Even if calorimetric methods do not offer the same accuracy as the electromagnetic ones, they can provide an approximate value of the total amount of AC losses. Specifically when the device is large enough to have a measurable amount of AC losses, like an HTS coil. Considering this, a very simple calorimetric method was implemented, to verify the total amount of AC losses in a superconducting coil, when applied currents with more than one harmonic. The method is based on the measurement of the liquid nitrogen evaporation rate, using a cylindrical capacitor, to evaluate the level of coolant. This method can be explained as follows.

Consider a cylindrical capacitor with length L, internal radius r_1 and external radius r_2, as shown in Figure 4.6.

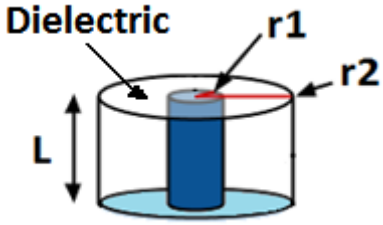

Figure 4.6. Cylindrical capacitor.

The total capacitance can be calculated as (Halliday et al. 2011):

$$C = \frac{2\pi \times L \times \varepsilon}{\ln(\frac{r_2}{r_1})} \text{ (F)} \tag{4.2}$$

As it is well known, the equivalent capacitance value of a parallel connection of capacitors is the sum of all capacitances. Considering now the situation depicted in Figure 4.7, where the cylindrical capacitor has two different dielectrics.

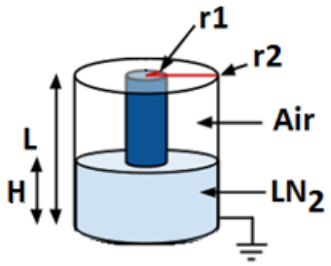

Figure 4.7. Cylindrical capacitor with two different dielectrics.

The total capacitance can then be calculated as:

$$C_T = \frac{2\pi \times (L-H) \times \varepsilon_1}{\ln(\frac{r_2}{r_1})} + \frac{2\pi \times H \times \varepsilon_2}{\ln(\frac{r_2}{r_1})}$$

$$= \frac{2\pi\left[(L-H) \times \varepsilon_1 + H \times \varepsilon_2\right]}{\ln(\frac{r_2}{r_1})} \text{ (F)} \tag{4.3}$$

where ε_1 and ε_2 are permittivity of both dielectrics. In this particular case, dielectric 1 is considered as air so $\varepsilon_1 = \varepsilon_0 = 8.854 \times 10^{-12}$ (F/m). If the dielectric 1 is considered as gaseous nitrogen, the relative permittivity is $\varepsilon_r = 1.002$ which represents a negligible difference.

Equation 4.2 shows that the value of total capacitance is related to the height of liquid dielectric (in this particular case liquid nitrogen). This means that knowing the capacitance value and the total height of the capacitor, L, it is possible to determine the height of liquid in the cryostat at all times. This height can be calculated by solving equation (4.2) in order of H:

$$H = \frac{\frac{C \times \ln(\frac{r_2}{r_1})}{2\pi} - L \times \varepsilon_1}{\varepsilon_2 - \varepsilon_1} \text{ (m)} \tag{4.4}$$

By only knowing the evolution of liquid nitrogen height in the cryostat it is not possible to determine the amount of AC losses. However, if a specific time is considered (two hours, as an example), and knowing the section of the cryostat, it is possible to determine the total amount of evaporated nitrogen, during that time. Realizing two different tests in the same conditions (i.e. same time and temperature room), one in DC conditions and another one in AC conditions, the difference between the amounts of evaporated nitrogen in those two tests is proportional to the amount of AC losses of the system.

Consider now the permeability of the liquid nitrogen as $\varepsilon_2 = \varepsilon_r \varepsilon_0$ with $\varepsilon_r = 1.4323$, its density as $\rho = 805.43$ kg/m^3 and its latent heat of vaporization as $\Delta H_{vap} = 198.99$ kJ/kg (Lemmon et al. 2007).

The difference of nitrogen heights during a specific time allows the calculation of the total evaporated mass of nitrogen as

$$m = (H_1 - H_2) \times S_C \times \rho \text{ (kg)} \tag{4.5}$$

where H_1 and H_2 are respectively the initial and final heights of nitrogen and S_C is the section of the cryostat.

The total energy associated with the vaporization process of nitrogen can then be calculated as

$$\Delta E = m \times \Delta H_{vap} \text{ (kJ)} \tag{4.6}$$

Since the natural evaporation of nitrogen might conceal the total amount of AC losses, the section of the used cryostat has to be as low as possible, to minimize the area of nitrogen in contact with room temperature. A low section cryostat has yet another advantage, the variation of nitrogen height is higher, which facilitates the measurement of the capacitance value (because the difference between measured values is higher). For this work, a digital RLC meter EDC 1620 was used to read the capacitance value. Two similar laboratory prototypes of cylindrical capacitors were implemented, using stainless steel tubes. To assure a uniform air gap between the tubes, insulating tape was placed at the two extremes of the inside tube. One of the implemented cylindrical capacitor is shown in Figure 4.8.

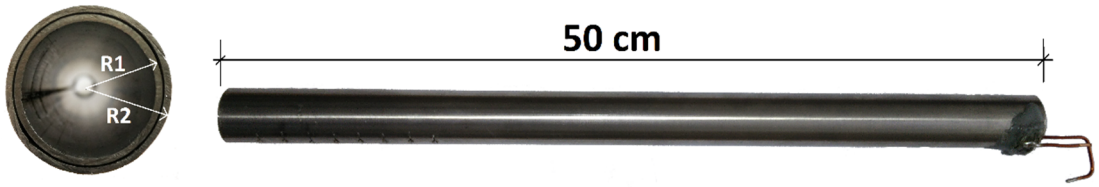

Figure 4.8. Implemented cylindrical capacitor.

The used stainless steel tubes had external diameters of 30 mm and 33.7 mm, respectively, and a thickness of 1.5 mm. This means that the external radius of the internal tube is: $R_1 = \frac{30}{2} = 15$ mm and the internal radius of the external tube is: $R_2 = \frac{33.7}{2} - 1.5 = 15.35$ mm.

Considering air as dielectric, theoretically the implemented capacitor has the following capacitance:

$$C = \frac{2\pi \times L \times \varepsilon}{\ln(\frac{r_2}{r_1})} = \frac{2\pi \times 0.5 \times \varepsilon_0}{\ln(\frac{15.35}{15})} = 1206 \text{ pF} \tag{4.7}$$

Measured capacitance values for the two implemented capacitors (henceforth referred as C_1 and C_2) are $C_1 = 1211$ pF and $C2 = 1213$ pF, which represents a total deviation of 0.4 % and 0.58 % to the theoretical value, respectively. These errors can be considered negligible.

Fully immersed in liquid nitrogen, i.e. using liquid nitrogen as dielectric, the theoretical capacitance value is 1688 pF and the measured value for the first implemented capacitor is $C1_{LN2} = 1695$ pF, which also represents a deviation of 0.4 %. The deviation in both cases (for the capacitor C_1) is a constant factor, which can easily be subtracted in order to achieve more accurate results. There are two possible causes for this deviation: the radius of one (or both) of the tubes is not exactly the theoretical value and the capacitance measuring device might have a small offset value. However, the measured capacitance for the second capacitor, when fully immersed in liquid nitrogen is $C2_{LN2} = 1673$ pF, which represents a total deviation of 0.9 % when comparing to the theoretical value. This indicates that in the case of C_2, the measured error is not a constant factor. The main reason for the difference has to be related to the dimensions of the stainless steel tubes and how they change when the tubes are immersed in liquid nitrogen. However, the measured error is still less than 1% which should represent a negligible difference, considering the accuracy of the created method. Nonetheless, results obtained with the two different capacitors will be compared to assess the importance of this difference.

4.3. Concluding remarks

This section described all experimental setups used in this thesis. A standard four-point method was used to measure critical currents, both in samples of HTS tape and HTS coils. The measurement of critical current is fundamental in any superconducting device, because it determines the maximum operating current value. Regarding the study of AC losses, two different setups were implemented and used: a standard electromagnetic LIA method was used for measurement of AC losses till a maximum frequency of 1152 Hz. Since this method has some limitations when measuring losses with different harmonic components, a very simple calorimetric method was implemented. This is based on the measurement of the total evaporated nitrogen, obtained by measuring the difference of liquid heights for a specific experiment. Even if the natural evaporation of the nitrogen might conceal the amount of AC losses, as a first idea to determine the total amount of losses during a specific time this is a good and simple method. Results obtained with these methods will be presented in the respective sections, and validated using numerical simulations, with the models already presented in section 3.

5

HTS Coils Prototypes

During this work, different pancake coils were implemented and different experiments were realized using those coils. This section briefly explains the implementation process and the measurements of critical current. Since the critical current of HTS coils is lower than the critical current of the HTS tape used to wound those coils, a simple experiment consisting on adding a ferromagnetic shielding was performed, to verify the influence of the magnetic field in the critical current of HTS coils. Different experiments performed with the implemented coils showed that the critical current was decreasing with the process of tape ageing. This characteristic will also be addressed in this section.

5.1. Coil Implementation

To implement an HTS pancake coil, it is necessary to take into account the main characteristics and limitations of the used HTS tape. In all coils implemented during this work, the used HTS tape was a BSCCO insulated tape, manufactured by InnoST, whose main characteristics (according to the manufacturer) are shown in Table 5.1.

Table 5.1. HTS tape characteristics.

Characteristic	Value
Critical current @ 77 K, self-field (A)	90
Minimum bending radius (mm)	30
Width (mm)	4.2 ± 0.1
Thickness (mm)	0.25 ± 0.01

Before implementing HTS coils using this tape, it is important to determine the real tape characteristics since the critical current might have a real value slightly different from the one given by the manufacturer. Considering the importance of the critical current value in superconducting projects, it is fundamental to make this verification.

The critical current was measured in a sample of unused tape, following the method presented in section 4.1.1 (Arsénio 2012). A tape sample with a total length of 20 cm was prepared by soldering copper voltage taps (5 cm apart from each other), as shown in Figure 5.1.

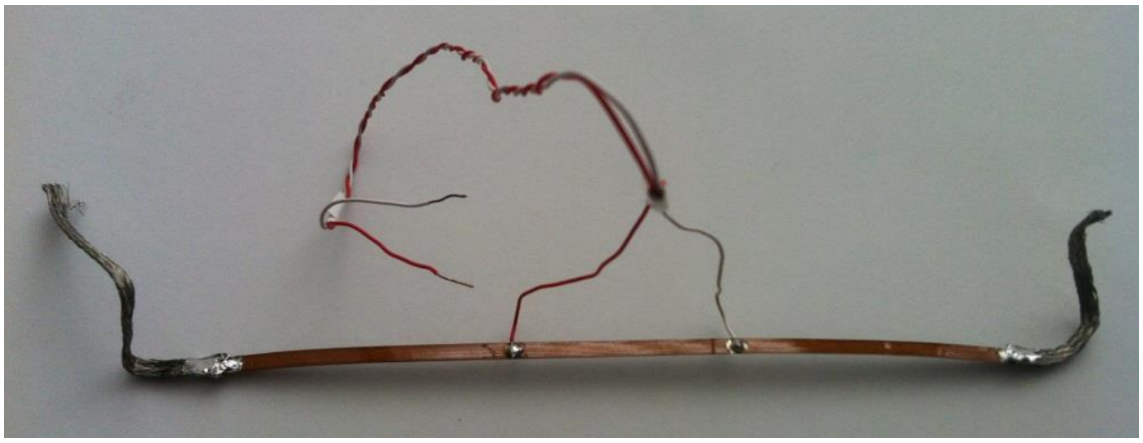

Figure 5.1. Sample of HTS tape for critical current measurement (adapted from (Arsénio 2012)**).**

Results obtained from the measurements of critical current are shown in Figure 5.2. The criterion used for the electric field was $E_C = 1$ μV/cm, as it is common to do. This results in a critical voltage of $U_C = 5$ μV. Using a fitting tool like *cftool* from Matlab, it is possible to find a power law that fits the experimental points. As result of this experiment, the critical current was determined as $I_C = 85.5$ A and the n value of the tape as $n = 15.35$ (Arsénio 2012).

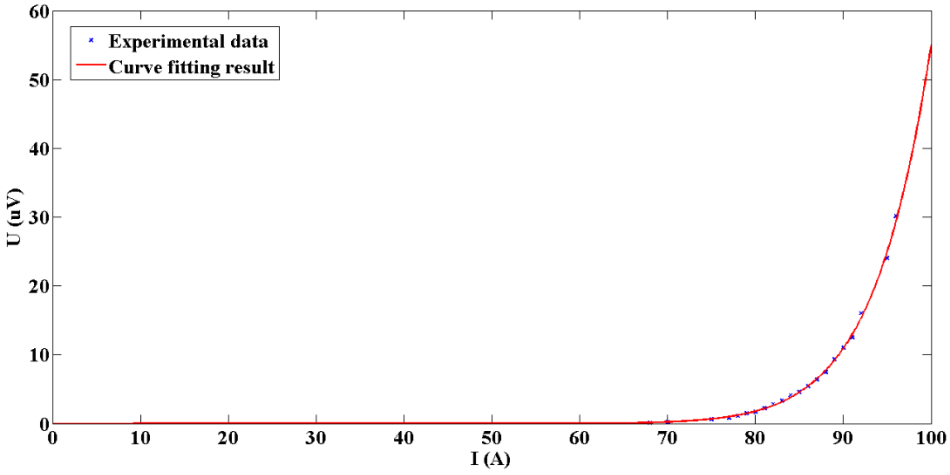

Figure 5.2. Curve fitting for critical current determination.

The measured critical current for the HTS tape is then slightly different from the value indicated by the manufacturer, in Table 5.1. One possible reason for this difference of values is the fact that usually manufacturers measure the critical current in samples of tape, and manufacturing heterogeneities can slightly change the critical current value in total length of the tape roll. Some mechanical stress associated to transport and even in the preparation of the sample for critical current measurement might also change slightly the obtained value. However, even if there is a difference, this is not determinant for the project success and the only important aspect to take into account is the minimum critical current value (which in this case was the measured value). The measured values of critical current and n-value of the HTS tape will then be considered for the modelling and implementation of HTS coils.

The total HTS tape available for implementation of a first prototype coil was 75 m. Following the analytical method presented in section 3.1, a set of two HTS coils was implemented. Each coil had a total length of 37.5 m. Considering the characteristics of the used HTS tape, shown in Table 5.1 and the available length of 37.5 m (for each coil) the results obtained using the analytical method were those listed in Table 5.2.

Table 5.2. Results of analytical method for coil design.

Characteristic	Value
Self-inductance (each coil) (mH)	1.75
Internal Radius (mm)	32
Number of Turns	128
Mutual Inductance (mH)	1.25
Total inductance (mH)	6

Two similar coils were wound inside a mould of extruded polystyrene (XPS). The implemented coils can be seen in Figure 5.3.

Figure 5.3. Implemented HTS coils.

The two implemented coils were used to verify the applicability of the analytical method for determination of inductance, as previously stated. In order to verify the method accuracy, the inductance of the coils was tested in two different ways: by measuring it, using a digital RLC Meter EDC 1620, and calculating it, after measuring the total impedance of the coil, using the LIA. Both methods produced agreeable results, illustrated in Table 5.3. The total inductance of the system was measured using the RLC meter and the mutual inductance was calculated from the other values (self-inductances and total inductance).

Table 5.3. Inductance of a set of two coils.

Characteristic	Value (mH)
Coil A Self-inductance	1.45
Coil B Self-inductance	1.8
Mutual Inductance	1.35
Total inductance	5.95

Comparing the values from Table 5.2 and Table 5.3, it can be stated that in overall the analytical method produced accurate results. Considering the predicted values, measurements have a relative error in absolute value of: 17 % for the self-inductance of coil A; 3 % for the self-inductance of coil B; 8 % for the mutual inductance and less than 1 % for the total inductance of the system. Although there is a relevant discrepancy in coil A, this effect is irrelevant in the total inductance allowing the utilization of this method, particularly for a first stage of coil design.

5.2. Critical Current Measurement

The critical current of the two implemented HTS coils was measured, using the method described in section 4.1. Measurements were performed using two DC current sources QPX1200L in parallel, and the voltage at the coil ends was measured using a Keithley 2001 multimeter. Figure 5.4 shows the configuration used for measurements in one of the coils.

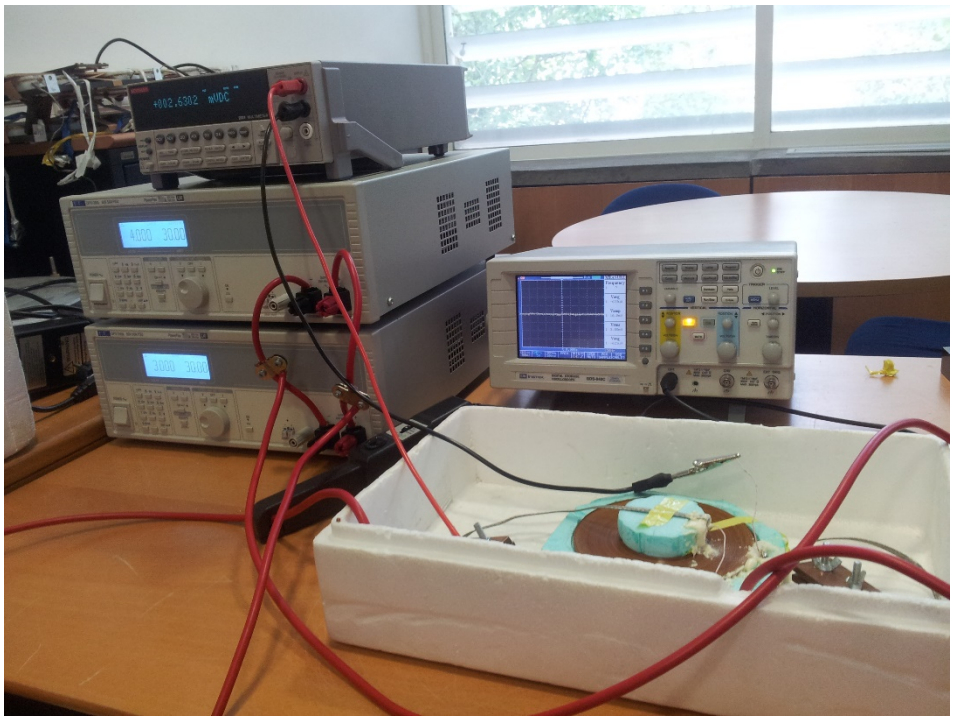

Figure 5.4. Experimental setup for measurement of critical current in an HTS coil.

Obtained results indicate that even if the coils are similar, their critical current is slightly different, as can be seen in the correspondent power laws depicted in Figure 5.5. One possible reason for this difference, in addition to the tape heterogeneities, is the fact that during the wound process some section of the tapes might be slightly more distorted, influencing its critical current value (due to the mechanical stress during the wound process).

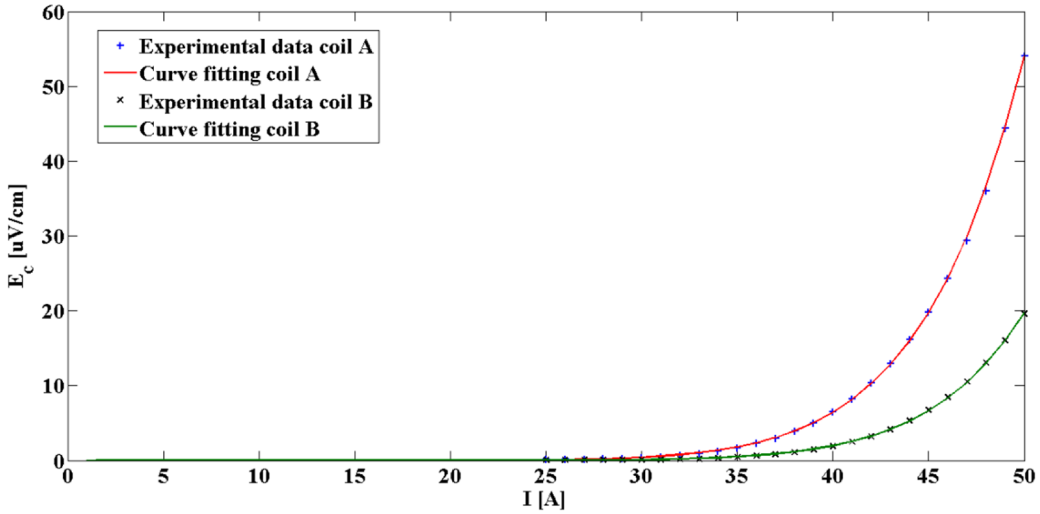

Figure 5.5. Critical current measurements in the two implemented HTS coils.

Results obtained using the curve fitting tool (cftool) from Matlab, to determine the critical current and n-value of both coils are shown in Table 5.4.

Table 5.4. Results of cftool for determination of coils characteristics.

	Characteristic	Value
Coil A	Critical current (A)	32.91
	n-value	9.54
Coil B	Critical current (A)	37.45
	n-value	10.32

The difference in the obtained values for the critical current of each coil is not significant, as long as the considered critical current value for the whole system is the lowest one. As expected, the critical current of the HTS coils is lower than that of the HTS tape. This is due to the fact that the coils generate a magnetic field, which will decrease the critical current, following the relation already presented in section 2.1.2.

The critical current measurements from Figure 5.5 were performed on each coil, individually. If the coils are connected in series, as it is common to do in a solenoidal configuration, the generated magnetic field will increase, which will further decrease the critical current. Considering this, the two coils were also measured together, connected through a copper plate, which will introduce a new source of losses. In order to accurately measure the critical current of the coil set, the critical current of each individual coil was also measured (with the coils connected). By comparing the sum of the measured voltages of the two coils and the set, it is possible to subtract the resistance of the connection between the coils, allowing an accurate measurement of critical current in the coil set. Figure 5.6 depicts the obtained results in both cases: considering the losses in the connection between coils and only in the superconducting coils.

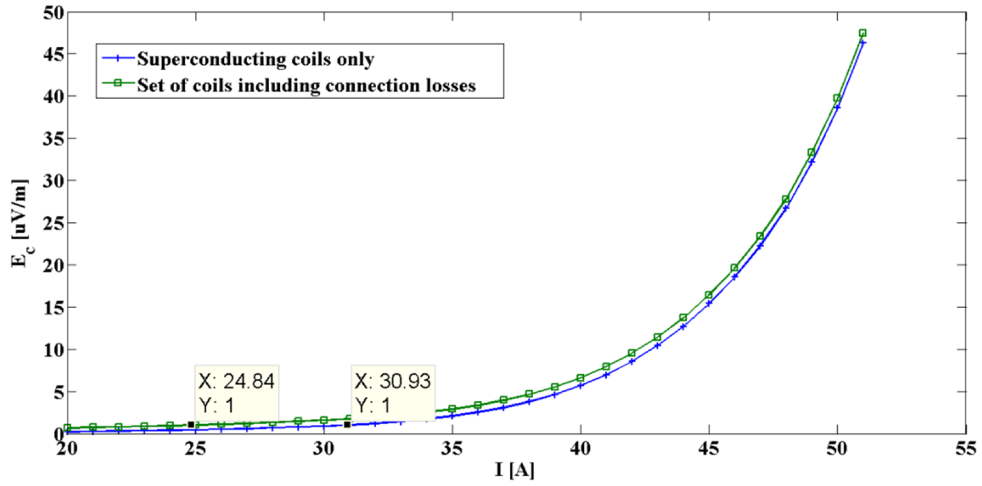

Figure 5.6. Critical current of a set of two HTS coils with and without connection losses.

By using the fitting tool *fctool* from Matlab, in the case where the connection losses were considered, the calculated critical current was $I_C = 24.8$ A and in the case where the two coils were measured without connection losses it was $I_C = 30.9$ A. Using this data, it was possible to determine the resistance of the connection between coils. This resistance was determined using all measured voltages and currents as $R_{connection} = 175 \pm 15$ mΩ. An optimization of this connection can furtherly decrease overall losses.

In order to validate the model created using the software package FLUX2D presented in section 3.2.2, a comparison between measured data and simulation results can be performed. In this FLUX2D simulation, the coil characteristics are those presented in Table 3.2 and Table 3.3 except for the n-value of the tape and its critical current, which were set as $I_C = 65$ A and $n = 11$. These two values were used since they represented better the real tape conditions at the time in which these experiments were performed (instead of the values given by the manufacturer for critical current and n-value). The difference in these values is due to the tape ageing process, which will be addressed in the next sections.

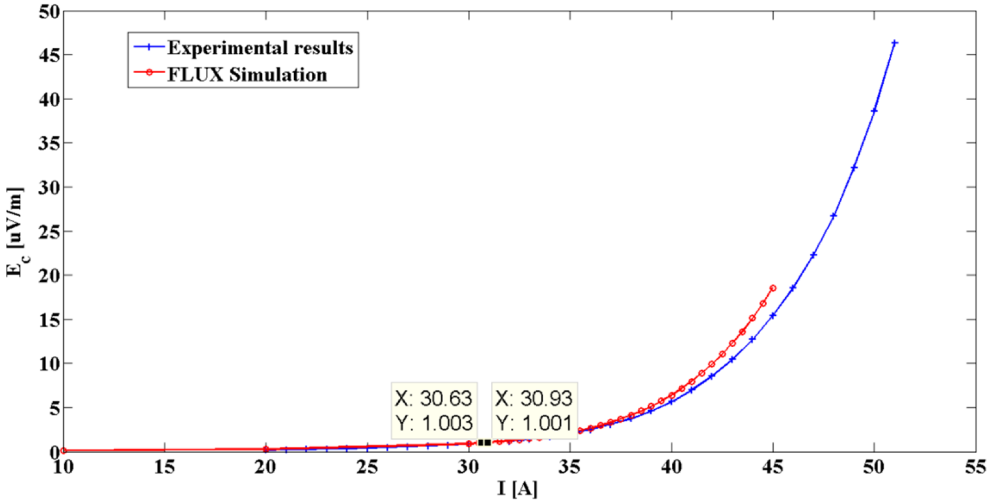

Figure 5.7. Comparison of simulated and experimentally obtained critical current of an HTS coil with 128 turns.

A comparison between results obtained experimentally and simulated shows that although the critical current value is almost the same, the n-value is not exactly the same, as can be easily seen by the slope of the two curves after reaching the critical current value. However, this difference is not critical and it can be considered that the model represents properly the coil characteristics.

5.2.1. Critical current improvement by ferromagnetic shielding

The existence of a self-field, generated by the HTS coils results in a low critical current, when compared to the value presented by the tape itself (Jiang & Jin 2011). This effect is more important in the inner turns of the coil, where the field is higher. As seen in Figure 2.9, in the case of 1G tapes, the existence of a perpendicular field can quickly degrade the critical current value. In a set of coils using different pancake coils, arranged in a solenoid configuration, the two pancake coils at the ends are those who have a higher perpendicular field component, due to the distortion of the magnetic field in this region. One possible solution to minimize this problem is the utilization of ferromagnetic materials, as flux diverters (Gömöry 2006; Pardo, Šouc, et al. 2009). If the air gap between the ferromagnetic material and the HTS tape is small enough, the flux lines will close through the ferromagnetic material and are diverted from the superconducting tape, allowing an improvement in the critical current value.

The effect of adding a ferromagnetic plate close to the coils was tested, and the critical current was measured again, to verify the real effect of this addition in the system. Two steel plates were used, without any special configuration (the steel plates were placed beneath and on top of the two HTS coils), with a separation of around 5 mm from the HTS tape. Figure 5.8 depicts the data obtained in this experiment, for the current regions close to the critical current of the coil set.

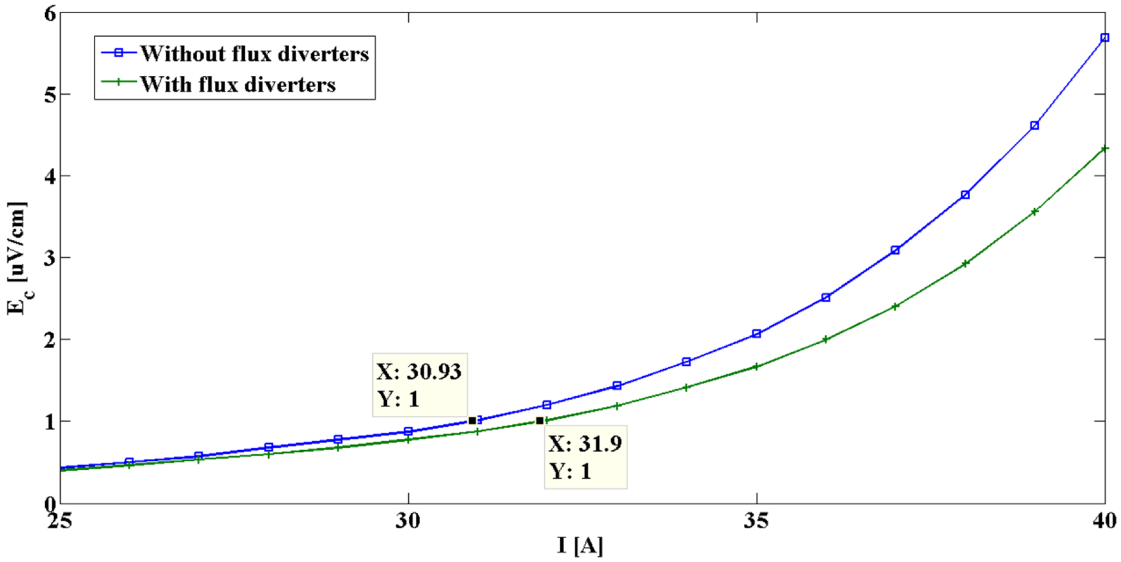

Figure 5.8. Critical current improvement by adding flux diverters.

According to obtained results, critical current indeed increased around 1 A when flux diverters are added to the HTS coil. This demonstrates that the ferromagnetic diverters have a positive effect in the field distribution. In this specific case no optimization was performed in the diverters which, if performed, can increase even further the critical current value.

5.2.2. Tape ageing and critical current degradation

During this project, the different implemented HTS coils were tested several times, and each time the coils were subjected to cool down and warm up processes, mechanical stress and current amplitudes above the critical current. These different situations lead to an ageing process in the HTS tape that constitutes the coils. In order to evaluate this ageing process, mainly due to thermal stress caused by the cooling down and warm up processes to which the HTS tape is subjected, a sample of HTS tape was prepared and the critical current was measured after 25 and after 50 thermal cycles. For every thermal cycle the tape was cooled down by directly placing it inside the liquid nitrogen and then warmed up to room temperature, just by taking it out of the liquid nitrogen. Results obtained are depicted in Figure 5.9.

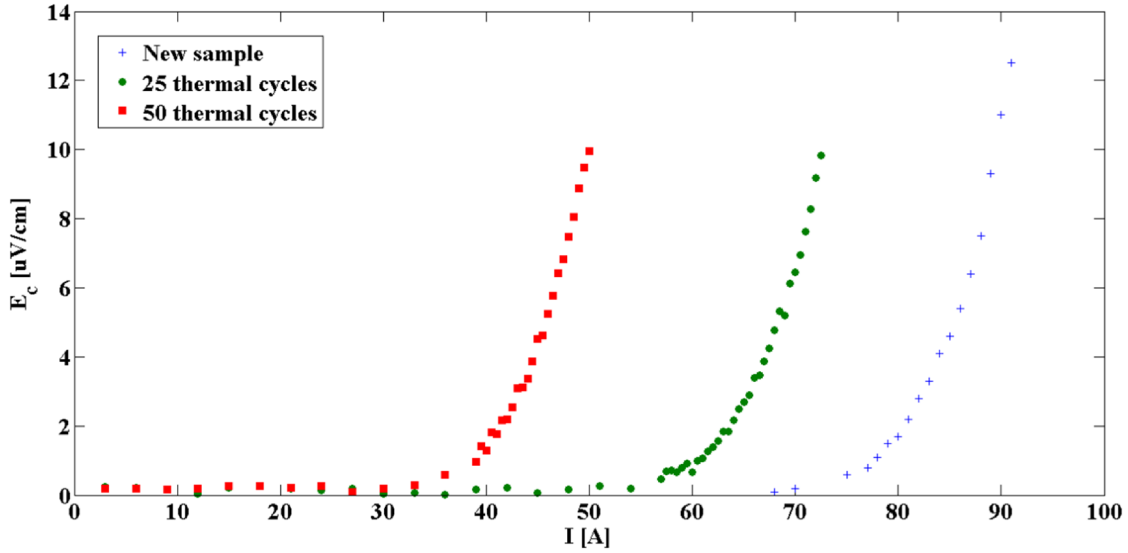

Figure 5.9. Thermal cycles effect on critical current.

The successive thermal cycles degraded substantially the critical current of the HTS tape. In fact, the critical current decreased from $I_C = 85.5$ A in the new sample to $I_C = 59.6$ A to when the sample had been subjected to 25 cycles and to $I_C = 37.9$ A after a total of 50 thermal cycles. The n-value of the tape also decreased from $n = 15.35$ (new sample) to $n = 11.73$ after 25 cycles and a lower value of $n = 8.44$ after a total of 50 cycles. This effect was already reported by other authors (Chen et al. 2003). However, in some other cases, as an example (Ceballos et al. 2014), no degradation is perceptible. There are several reasons for this disparity of results: the degradation might result from ice accumulation inside the HTS tape. If some water enters the superconducting tape, through the soldering taps as an example, the expansion of this water will degrade the superconducting filaments, which results in a degradation of critical current. Another possible aspect is the expansion (due to thermal cycles) of the material that form the mould where the tape is placed, if tests are realized using the tape attached to some mould, as it is common to do. This expansion originates mechanical stress in the HTS tape, which will also result in a degradation of its characteristics. Considering these aspects, it is necessary to continuously verify the tape characteristics, in order to assure the device proper operation. This is extremely important because the degradation of critical current and n-value represents an increase of losses, for the same operation current.

5.3. Concluding remarks

This part of the document contained a description of the creation and experiments realized in two different HTS coils prototypes. Those coil were implemented following an analytical method that allowed to obtain the inductance of a set of coils based in geometric parameters only. Obtained results, from numerical methods and experiments, corroborate such outcomes, allowing the utilization of that analytical method in a first stage of design of HTS coils. Since the critical current is one of the most important characteristics in superconducting devices, because it establish the maximum working limit, it was also measured, not only in samples of the HTS tape but also in the implemented coils. Results are as expected, with the critical current of the coil being lower than that of the tape, which is due to the magnetic field generated by the coil itself. Also as expected, the critical current is lower when the magnetic field is higher, situation that occurs when the two coils are tested in series.

In order to increase the critical current of the coil set, a simple configuration using two ferromagnetic plates was tested. The placement of two ferromagnetic places on top and beneath the superconducting coils allows the magnetic flux lines to close through the ferromagnetic material and not through the HTS tape, which increases the critical current of the coil.

Lastly, the effect of tape ageing was verified. The implemented coils were subjected to a series of tests, which included several thermal cycles. These thermal cycles can degrade the HTS tape characteristics, therefore the process of tape ageing must be monitored. To verify this effect, a sample of HTS tape was subjected to a total of 50 thermal cycles, and it was verified that the critical current of that tape and also its n-value decreased more than 50 %. However, this effect is not clearly visible in other works, because using other tapes no degradation is visible. This means that, for precaution measures, the tape should be monitored during the worktime of the superconducting device, in order to verify its characteristics, thus assuring the proper operation of the device.

6

Measurement of AC losses

AC losses are one of the most limiting factors for the deployment of superconducting devices in power systems. The flow of an AC current will generate heat in the superconductor, which must be extracted with the cryogenic system. This means that in a system that generates more losses, the cryogenic system must be more powerful, in order to be able to successfully extract all generated heat. It is then of utmost importance to study AC losses in superconducting systems, to evaluate the total amount of AC losses and, if possible, create strategies to reduce them. In this particular work, AC losses were studied in samples of HTS tape and also in coils, mainly to verify the frequency dependence of the total amount of AC losses. A large spectrum of frequencies was considered: $50-1152$ Hz, both in tape samples and coils and AC losses were also measured when considering more than one current harmonic flowing simultaneously in the HTS tape.

6.1. BSCCO tape samples

As a starting point, AC losses were measured in a sample of HTS tape. This is important to verify if the tape is operating as expected, and also to extrapolate possible values of AC losses in more complex devices such as coils. AC losses, as already explained in section 2.2, have different origins, which means that for different tapes, the total amount of AC losses might be slightly different. It is then important to verify how the tape used in this project behaves, in terms of the total amount of AC losses. If possible, the different components of AC losses should also be separated, in order to verify which mechanisms are more important for the total amount of AC losses, which is an important step to create strategies to reduce AC losses. In this section, all achieved results for measurements of AC losses in samples of HTS tape will be described, a separation of losses components will be made, whenever possible, and these experimental results are also compared to those obtained used both, analytical and numerical models. This is important not only to validate the models but also to verify the accuracy of measuring setups.

6.1.1. AC losses quantification

AC losses can be separated in different components, according to the physical mechanism that originates them, as seen in section 2.2. Since in this project only 1G tapes were used, the described measurements and AC losses components in this section are only related to that type of HTS tape. The components that are expected to give a major contribution to the total amount of AC losses are:

- *Superconducting hysteresis losses (P_h)*: linearly proportional to frequency, these appear due to variations in the superconductor magnetic state (Norris 1970).
- *Eddy currents losses (P_{ed}):* due to the existence of silver in the BSCCO/Ag tape, there are eddy currents through that metal, which also generates losses. These are quadratically proportional to frequency and, as seen in section 2.1.1, can be expressed using the expression :

$$P_{ed} = \frac{2\pi^2 \mu_0^{\,2} f^2 I_p^{\,2} d^3}{\rho l} \text{ (W/m)} \tag{6.1}$$

where μ_0 is vacuum permeability, f is frequency, I_p is current amplitude through the tape, d is sheath thickness (for this tape: 36 μm), ρ is resistivity of silver (here set as $3\times10^{-9}\,\Omega.m$) and l is perimeter of the outer superconducting filament layer (in this case: 6.5 mm).

- *Resistive losses (P_r):* at high applied-to-critical current ratios (i), resistive losses appear in the superconductor. These are frequency independent and their value depends on the characteristics of the tape (mainly *n*-value). Usually they are negligible till $i > 0.8$ (Stavrev & Dutoit 1998).

Total AC losses in the superconducting tape can then be considered as the sum of those three components. By dividing the power loss per meter (P) by frequency, one can achieve the energy loss per meter, per cycle (Q) as follows.

$$Q_t = \frac{P_t}{f} = \frac{P_h}{f} + \frac{P_{ed}}{f} + \frac{P_r}{f} = Q_h + Q_{ed} + Q_r \text{ (J/m)} \tag{6.2}$$

At frequencies below 200 Hz hysteresis energy losses (Q_h) are expected to have a main contribution. These are frequency independent. Eddy currents losses contribution for frequencies below this value are usually negligible, but they start to have a higher contribution to total losses with increasing frequencies. Resistive losses, as already stated, are frequency independent and depend on the used applied-to-critical current ratio. Their contribution to total losses is only visible for applied currents close to the tape critical current I_C.

6.1.2. Frequency dependency

AC losses were measured in a sample of HTS tape, using the LIA method, described in section 2.2.3, considering a range of frequencies from 72 Hz till 576 Hz, and currents from zero till over the tape critical current. Obtained results are depicted in Figure 6.1.

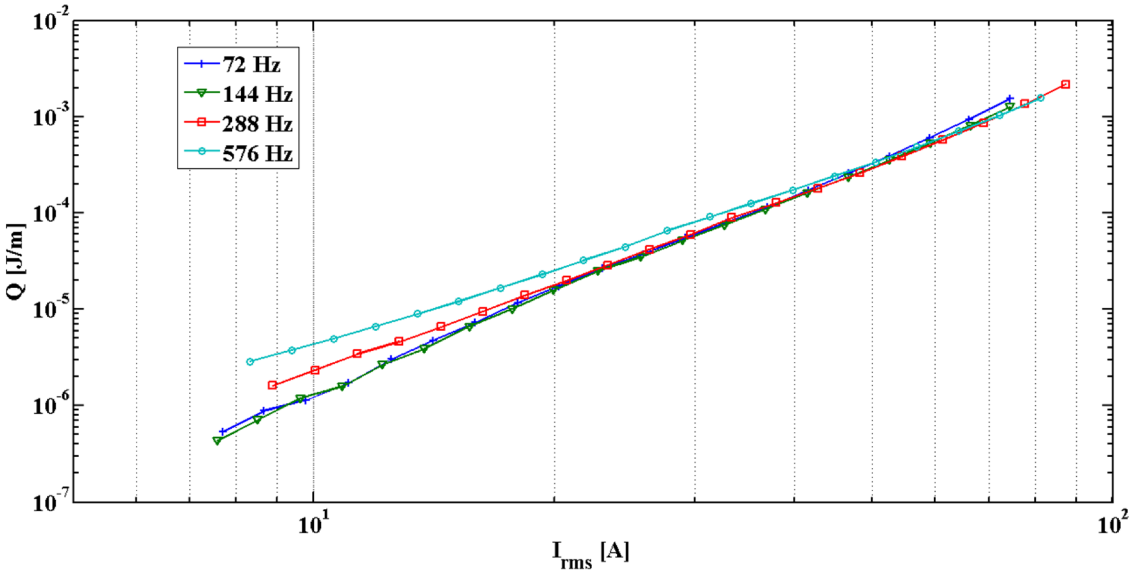

Figure 6.1. AC losses in a sample of HTS tape (experimental results).

Results obtained demonstrate a well-defined frequency dependent behaviour: measured AC losses increase with frequency, for frequencies higher than 200 Hz. This is consistent to results described in the literature since eddy currents losses are negligible for low frequencies. However, this dependency is only visible for low values of applied currents. When the applied current increases, the resistive losses start to have a major contribution in the total amount of measured losses and no difference is visible, for the tested frequencies.

Using equation (2.14) it is possible to estimate the total amount of AC losses generated due to eddy currents. In order to be able to use this expression, a microphotography of the used HTS tape was taken, to determine the values of sheath thickness (d), and the perimeter of the outer superconducting filament layer (l). The microphotography is shown in Figure 6.2.

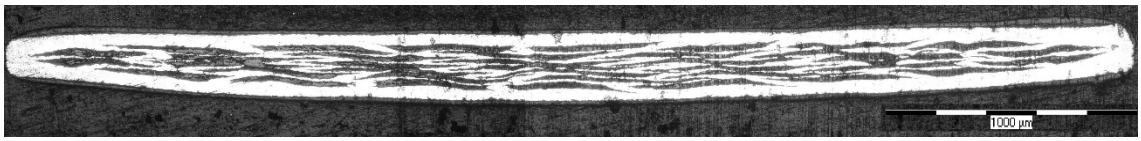

Figure 6.2. Microphotography of the used HTS tape.

Considering the data obtained from experimental measurements and using equation (2.14), the component of AC losses due to eddy currents was calculated and subtracted from the total losses. The obtained behaviour is that shown in Figure 6.3.

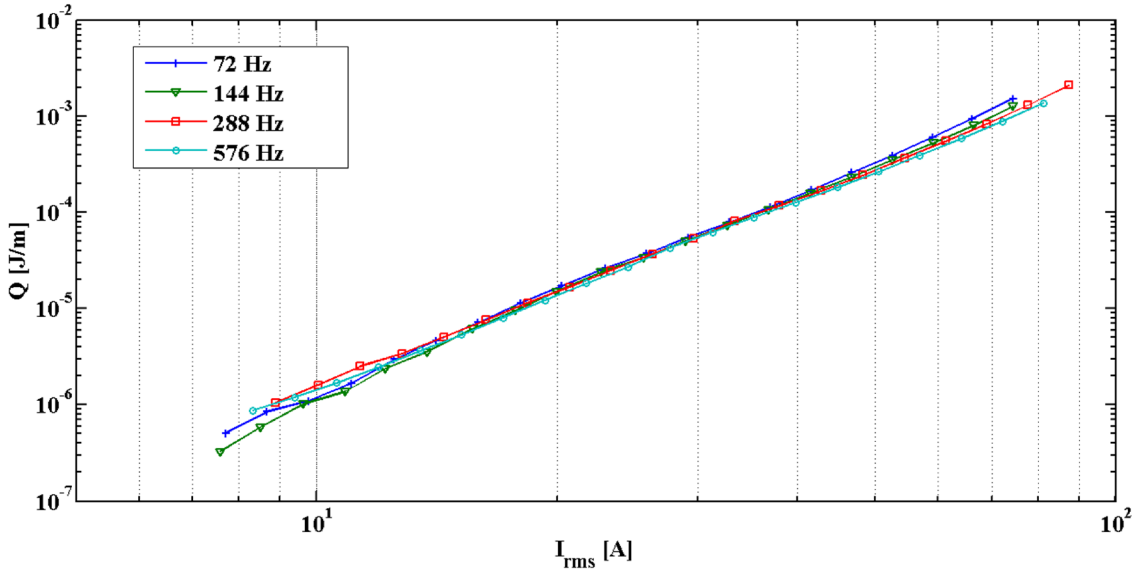

Figure 6.3. AC losses in a sample of HTS tape without the eddy currents component.

Taking out the losses component originated by eddy currents, no frequency dependent behaviour is noted, since that losses component is the only one dependent from frequency. This behaviour indicates that in order to reduce AC losses, especially when applied currents are low, strategies should focus on reducing eddy currents.

6.1.3. Comparison between models and experimental results

In order to evaluate the accuracy of experimental data obtained, results should be compared to models already demonstrated and vastly accepted in the literature. For AC losses in superconducting tapes, the model most used, as addressed in section 2.2.2 is the Norris ellipse model. Considering equation 2.15, the Norris model was used for two different critical currents: 85 A, which is the critical current of the HTS tape in non-used conditions and 60 A, which is

the critical current after a process of tape ageing, as described in section 5.2.2. Results obtained are depicted in Figure 6.4.

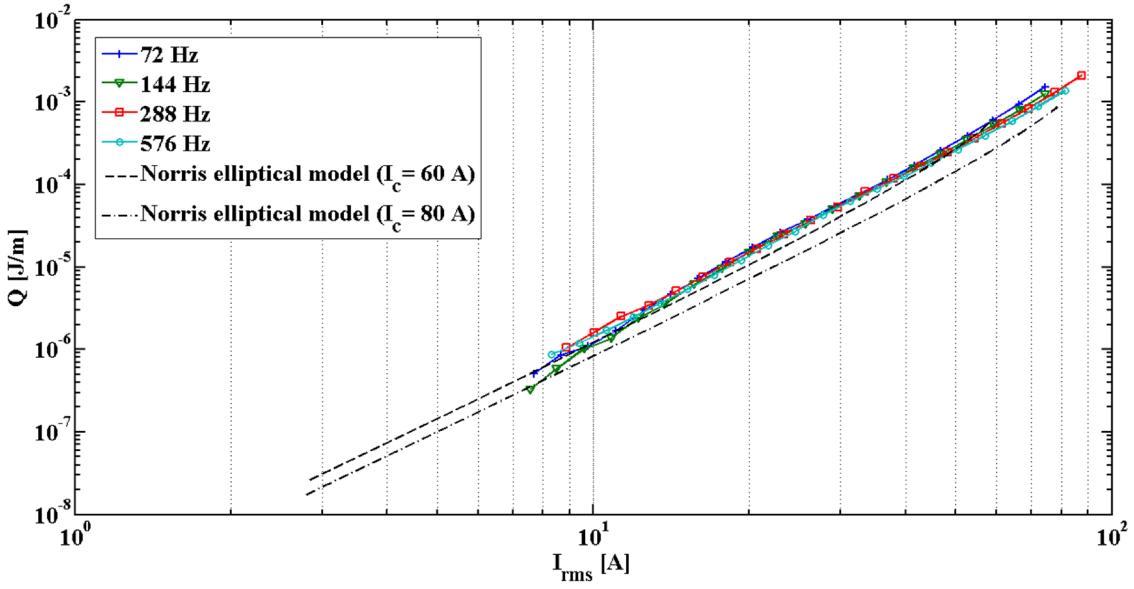

Figure 6.4. Comparison between experimental results and Norris ellipse model.

The results used for comparison with the Norris elliptical model were those calculated by subtracting the eddy currents losses component, as can be seen in Figure 6.4. The comparison of experimental data and Norris model allows one to conclude that measured AC losses are agreeable with those estimated by Norris. However, it is important to verify one important aspect, related to the critical current used in the model. In order to achieve an accurate comparison, it is important to consider the actual critical current of the HTS tape, and not the value indicated by the manufacturer (or the value measured when the tape is new). The comparison of these two models in Figure 6.4 also indicates that the process of tape ageing also increase AC losses. This is a normal behaviour since the critical current and the n-value of the tape decrease, which will increase the weight of AC losses in the system.

6.2. BSCCO coils

The process of measuring AC losses in HTS coils is usually complex, mainly due to the high inductive voltage, which limits the utilization of measuring methods. As an example, the typical LIA allows a maximum input voltage of 1 V, which is easily surpassed in medium sized coils. This fact, together with the fact that it is necessary to have a very low phase error makes the measurement process complex and often limits the experiments. It is common to see in the literature two different kinds of measurements: medium sized coils at industrial frequencies or measurements at higher frequencies but with small coils. This demonstrates that there is an important gap that still needs to be overcome: study of AC losses in medium sized coils, at high frequencies. This is even more important considering that in some devices a high frequency component might appear in the coil. In order to contribute to this gap filling, in this project AC losses were tested in medium sized coils, whose implementation was already described in section 5, at a frequency range of $50-1152$ Hz. Because the inductive voltage in the coil often exceeded the 1 V limit of the LIA, three different approaches were used to reduce the voltage to safe values for LIA measurements, as described in section 4.2.1. Data obtained using those

different methods will be presented and compared. Experimental data obtained will also be compared with results obtained from models for validation purposes. Finally, a simple calorimetric method will be used to measure AC losses considering multi-harmonic currents.

6.2.1. Magnetization losses

As seen in section 2.2.1, AC losses are usually divided into two categories: magnetization losses and transport current losses. In order to evaluate the contribution of magnetization losses to the total amount of AC losses in the system, a stack of 19 samples of HTS tapes was prepared and magnetization losses were experimentally obtained, considering parallel and perpendicular applied magnetic fields, as depicted in Figure 6.5. Under applied perpendicular field, the HTS tape show a frequency dependent behaviour, which is not noticed under parallel field. This behaviour indicates that the perpendicular field has more influence in the characteristics of the HTS tape.

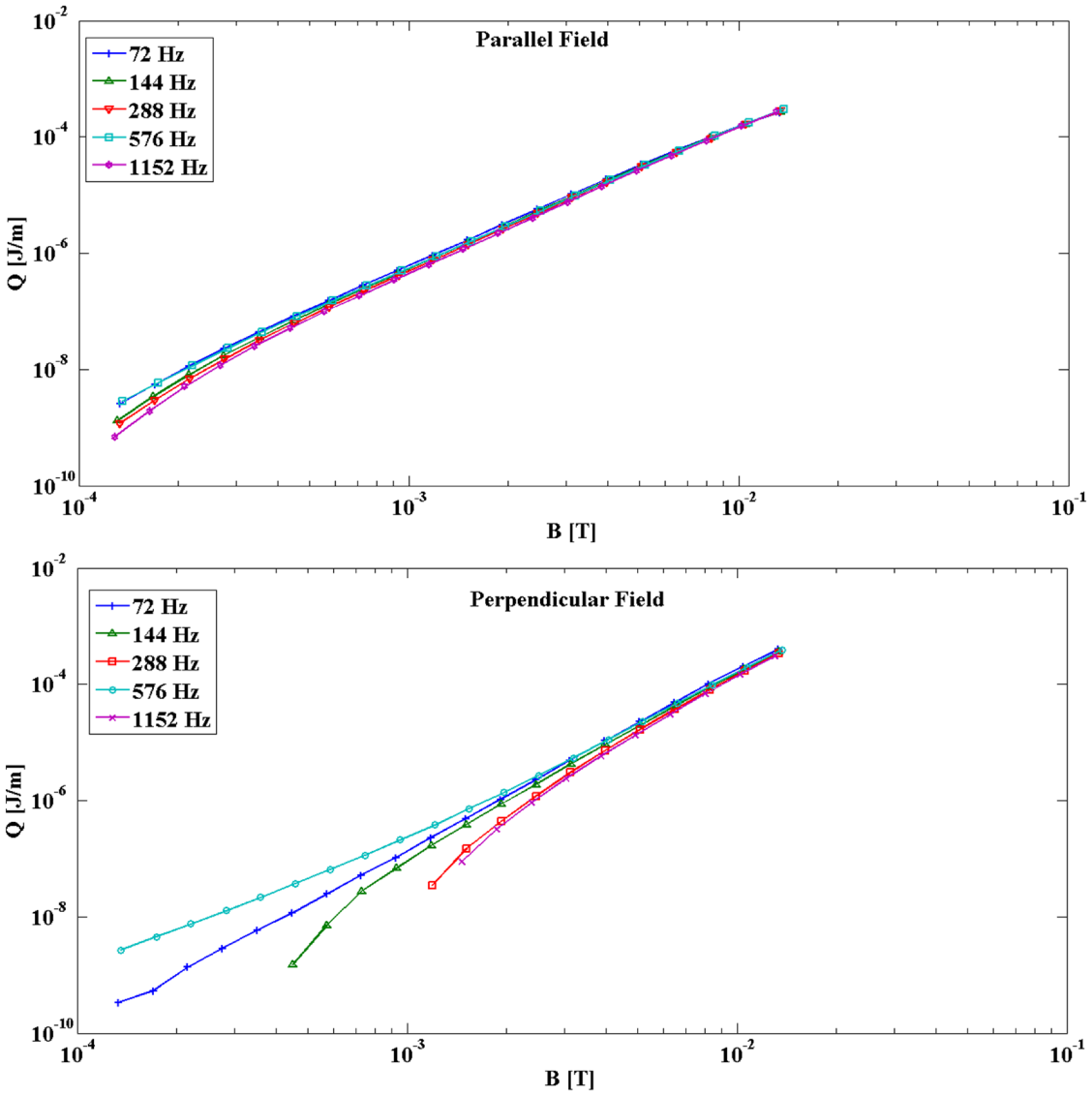

Figure 6.5. Magnetization losses under applied magnetic field.

6.2.2. Transport current losses

Transport current losses were those which concentrated a higher research effort, because as already stated, to measure losses in medium sized coils using the LIA method is a complex task. Three different approaches were followed, to verify the total amount of AC losses in the implemented HTS coils, whose characteristics were presented in section 5. In order to verify the frequency dependence in the implemented coils, losses were measured considering a range of $50-1152$ Hz. However, at 50 Hz losses were only measured as part of the multi-harmonic dependent behaviour. For currents considering only one harmonic, the study was realized within a frequency range of $72-1152$ Hz.

6.2.2.1. Single frequency behaviour

Transport current losses were experimentally verified in two similar coils, wounded with BSCCO tape, whose implementation process and main characteristics were already given in section 5. It is important to mention that the critical current of the two coils is slightly different. Using the same denomination as in section 5, the coils critical currents are: Coil A – 32.9 A; Coil B – 37.45 A. Even if the critical currents of the coils is different, the behaviour of the two coils, in terms of measured AC losses, is very similar. Figure 6.6 shows results obtained in the two coils for measurements at two different frequencies.

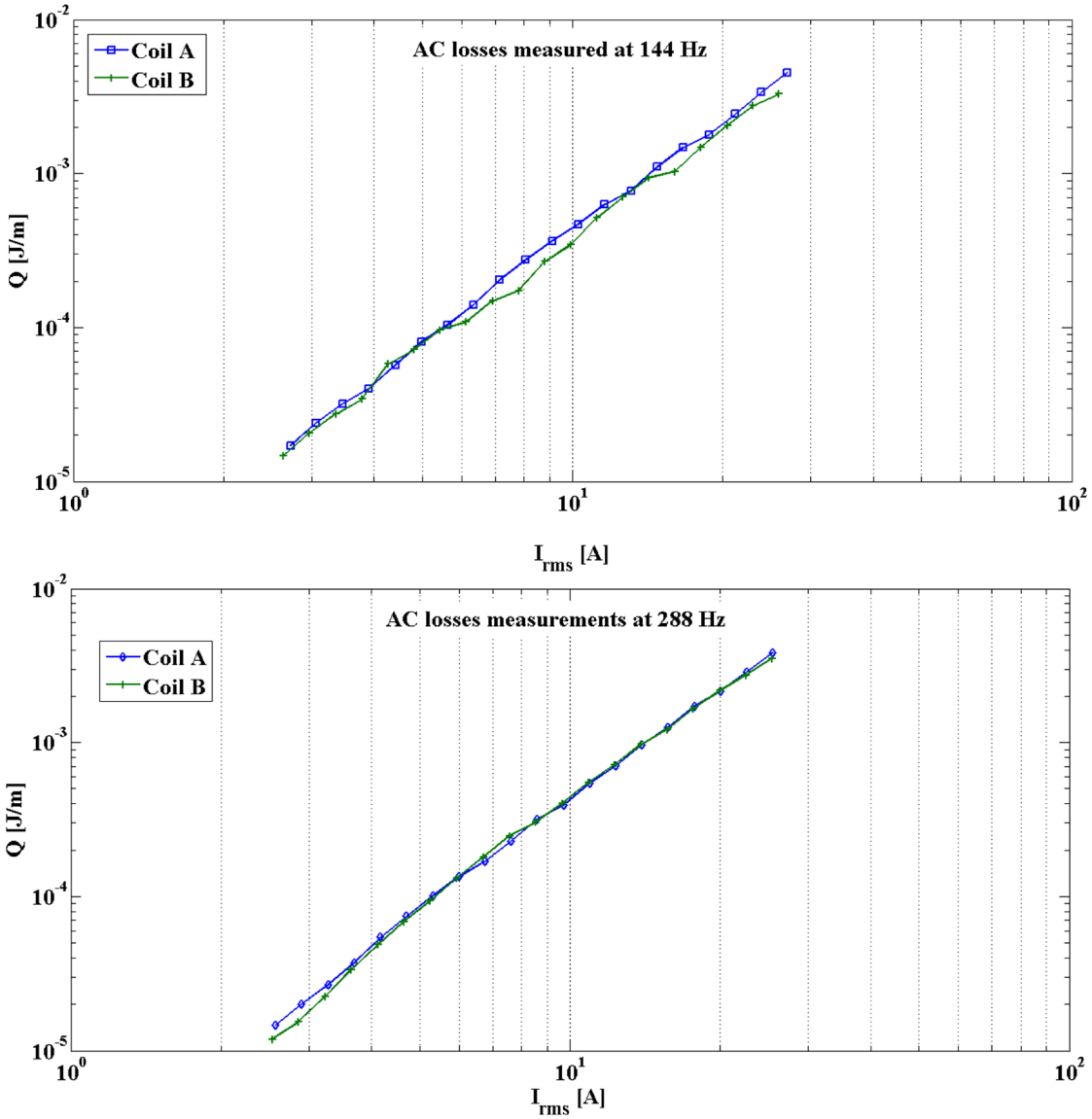

Figure 6.6. Measurements of AC losses in two implemented coils.

Since no differences are visible in the results obtained in the two coils, henceforth in this section, no reference to the used coil will be given, unless considered important for the study.

AC losses were measured using different approaches, described in section 4.2.1, with the same goal: minimize the phase error (which is a fundamental condition in measurements with the LIA) without overcomplicating the measuring setup. As a first approach, a resistive divider was used, to decrease the measured voltages by 100 times, in order to obtain safe values for the LIA. This proved to be a valid approach for frequencies up to 288 Hz. For frequencies higher than this value, the resistive divider started to change its frequency response, which changed measured results, making this an unfeasible approach. As a second approach, in order to be able to measure AC losses for frequencies higher than 288 Hz, a voltage loop with voltage taps separated by 4 cm was placed in a representative turn ($2/3$ of the total number of turns, in this particular case the 86^{th} turn was chosen) and losses were measured in this tape section. The total amount of losses in the HTS coil was then extrapolated from the measured values using the 4 cm voltage taps configuration. The main advantage of this method, when compared to the previous one, is the fact that measuring losses in a tape length of 4 cm results in much lower

measured values, which can be directly inserted in the LIA, without any signal conditioning techniques. However, this configuration have one potential drawback: if the tape used to wound the HTS coil is not homogenous, the total AC losses in the whole coil will be different from those extrapolated from a 4 cm tape section. The two previous methods imply that an electrical connection is necessary between the voltage taps and the HTS coil. In medium-to-large sized coils, the inductive component of the voltage in the coil is relatively high, especially for high frequencies, and removing the insulation generates weak spots in the system. As an example, in the implemented coils, considering a current with an amplitude of 10 A and a frequency of 1152 Hz, the measured voltage at the coil ends exceeds 130 V. Bearing in mind these limitations, the application of a contactless method is desirable. Since it is already common to measure AC losses in samples of HTS tape using contactless loops fabricated with copper wire, this approach was also tested to measure losses in HTS coils. The contactless loop was also placed in a representative turn (the same turn as the voltage taps).

The phase error was limited to $0.1°$ in all measurements. However, since the difference between resistive and inductive components is more than one order of magnitude, it is advisable to verify the effect of the phase error in measured data. In order to verify the accuracy of experimental measurements, i.e. in order to verify the effect of the phase error in the measured *vs.* real losses value, measurements were compared to values calculated eliminating that error. This is possible because the LIA saves the phase error in each measurement. In order to compensate the error, the argument of the measured voltage was corrected, and the resistive and inductive parts were recalculated using the real phase shift angle between voltage and current. Figure 6.7 depicts the comparison between measurements and corrected data, for a frequency of 288 Hz. Measurements were performed using the 4 cm voltage taps method in this particular case. As can be seen in this figure, no differences between measured and corrected values are observed, which indicates that the defined maximum phase error of $0.1°$ is enough to achieve accurate results. In fact, the maximum error achieved in measured *vs.* corrected losses for this particular case was 4.16 %. Results obtained using the other two previously described measuring methods have phase errors in the same range.

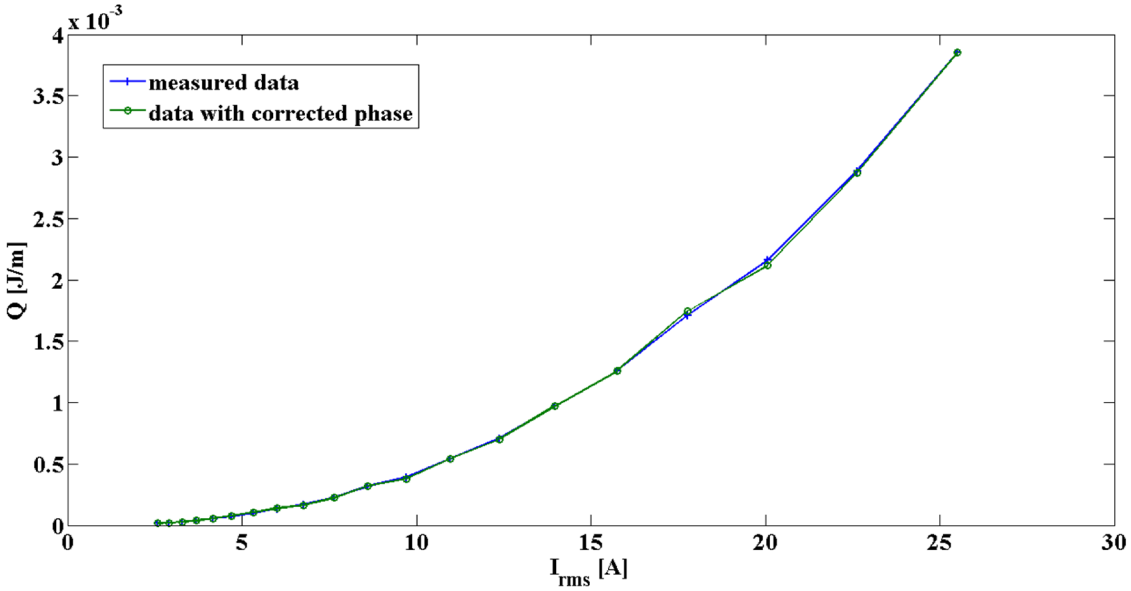

Figure 6.7. Comparison between experimental and phase corrected data.

In order to verify the accuracy of results obtained with the three different methods, measured losses were compared. The first method was only considered for the three lowest frequencies due to the aforementioned problems (72 Hz, 144 Hz and 288 Hz). Figure 6.8 depicts results obtained using the three methods, for a frequency of 144 Hz.

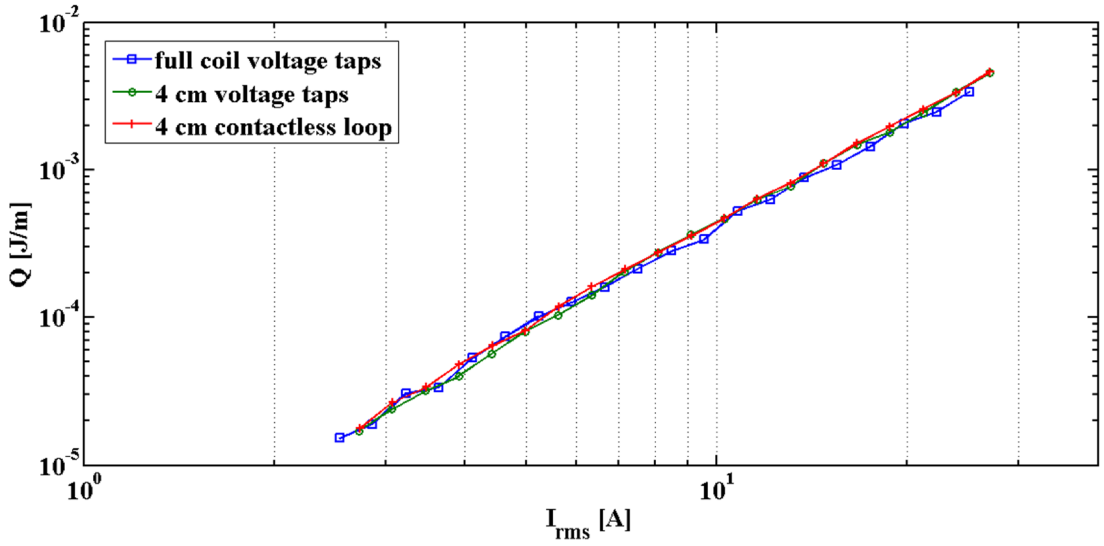

Figure 6.8. Measured AC losses at 144 Hz using three different methods.

Since the first method was only used for frequencies up to 288 Hz, a comparison of obtained results using the three methods can only be performed to frequencies up to this value. Figure 6.9 shows the frequency dependence of measured AC losses for two different values of current: 5 A and 20 A.

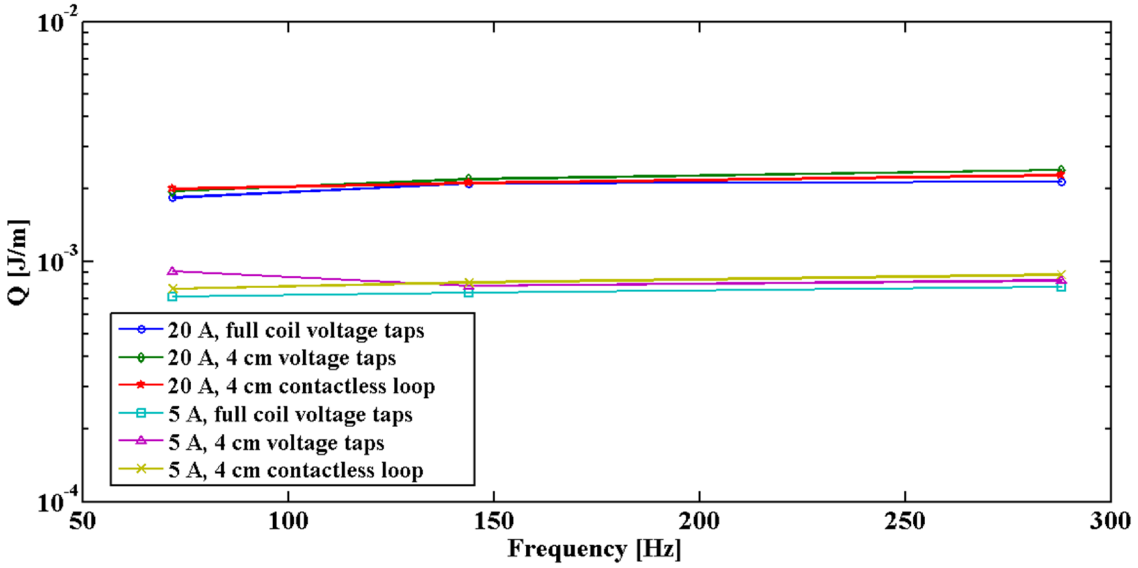

Figure 6.9. AC losses measuring methods comparison for 72, 144 and 288 Hz.

Figure 6.8 and Figure 6.9 both show that there are no relevant differences between results obtained using the three approaches, which demonstrates the applicability of the implemented methods considering voltage taps in a representative turn and a contactless loop. Factors like the tape inhomogeneity and imperfections in the soldering process (voltage taps methods) or

loop placement (contactless loop method) can explain the small differences visible mainly for a frequency of 72 Hz.

In order to evaluate the possible frequency dependent behaviour of AC losses in HTS coils, these were measured using the two latter methods for frequencies up to 1152 Hz. Figure 6.10 depicts measurements made using the 4 cm voltage taps configuration.

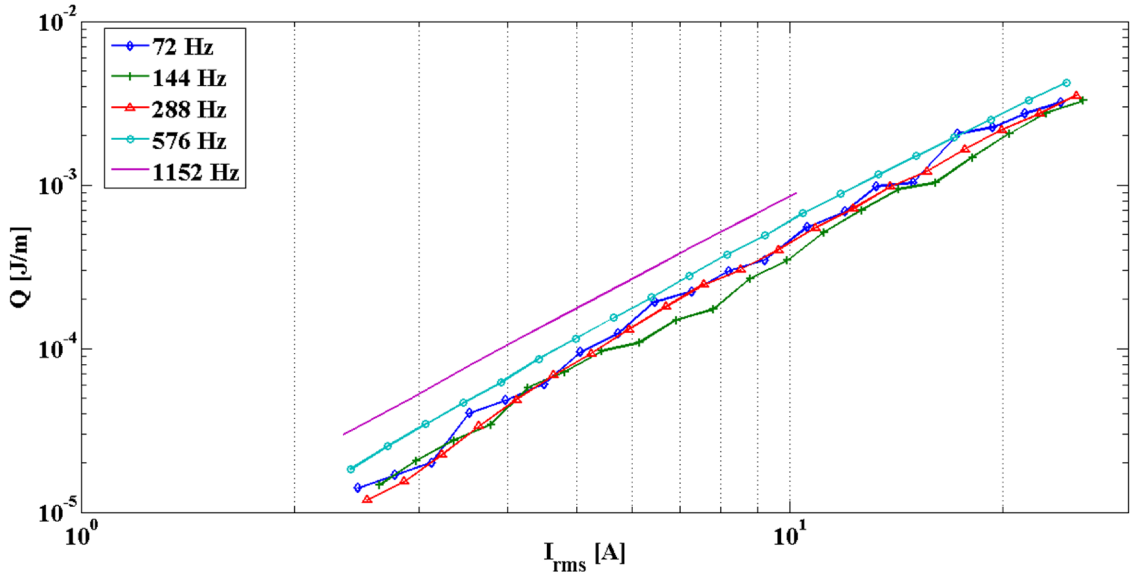

Figure 6.10. AC losses measurements for frequencies between 72 Hz and 1152 Hz.

Results indicate that there is some frequency dependent behaviour. For frequencies up to 288 Hz, AC losses present a behaviour already described in the literature (Yuan et al. 2005): first they decrease with frequency, till a certain value, then starting to increase again. The minimum loss value is reached at 144 Hz and for frequencies of 72 Hz and 288 Hz measured losses are very similar. For frequencies higher than 288 Hz, losses have an increasing value, with the increase of frequency. Some clear transition is visible between 288 Hz and 576 Hz and also between 576 Hz and 1152 Hz. To further investigate this transitions, additional measurements were performed for intermediate frequencies. Figure 6.11 shows obtained data for frequencies between 288 Hz and 576 Hz and Figure 6.12 depicts results obtained for frequencies between 576 Hz and 1152 Hz.

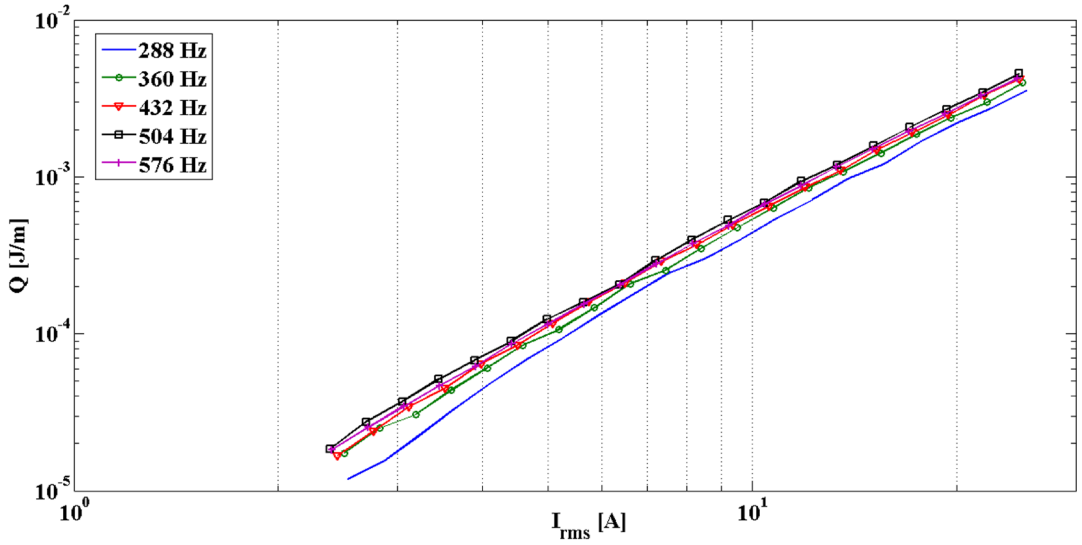

Figure 6.11. Measured AC losses for frequencies between 288 Hz and 576 Hz.

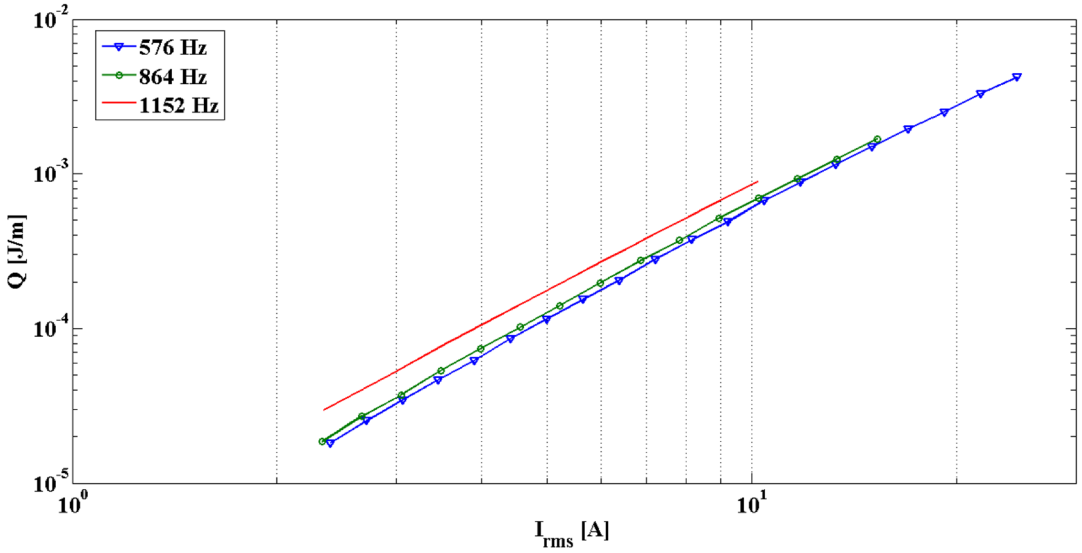

Figure 6.12. Measured AC losses for frequencies between 576 Hz and 1152 Hz.

Results obtained and presented in Figure 6.11 and Figure 6.12 indicate that clear transitions in the losses values are visible for certain frequencies. A clear transition is visible between 288 Hz and other measured frequencies (till 576 Hz) and the same behaviour is observed at higher frequencies, since losses are similar for 576 Hz and 864 Hz, and then clearly increase for a frequency of 1152 Hz. At this last frequency losses were measured only till a current value of 10 A for security reasons since for this value of frequency and current the measured voltage at the coil end already exceeded 130 V.

In order to verify the applicability of the contactless method for higher frequencies, results were compared to those obtained using the 4 cm voltage taps configuration. Figure 6.13 depicts this comparison for two different frequencies: 576 Hz and 1152 Hz.

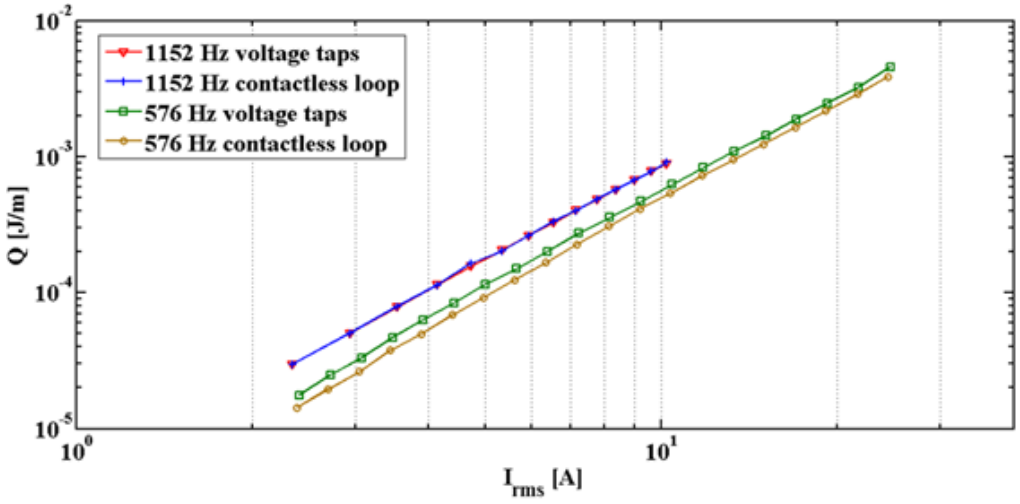

Figure 6.13. Comparison of measured AC losses using a 4 cm voltage taps and a contactless loop configurations.

Obtained results show a clear difference in losses measured using the two methods, at a frequency of 576 Hz. However, this difference might result from a displacement in the contactless loop or in the voltage taps in this measurement alone and not in the methods, since no difference is visible for other measured frequencies. In order to further investigate this issue, AC losses were also measured using these two methods in smaller coils, with 64 and 32 turns. These coils were implemented by energizing only a part of one of the implemented 128 turns coils. Figure 6.14 depicts results obtained for the measurement of AC losses in the 32 turn coil, at a frequency of 288 Hz. As can be seen in this figure, results obtained with a contactless loop match those obtained using a 4 cm voltage taps configuration. Both loops were placed in the 21^{th} turn.

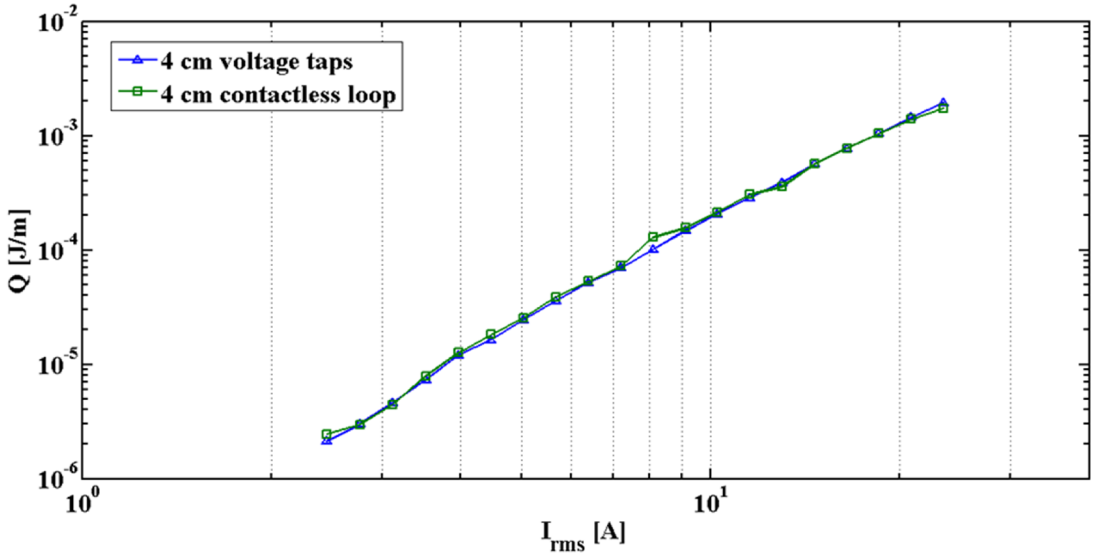

Figure 6.14. Measured AC losses in a 32 turn coil at 288 Hz.

Since obtained results are agreeable, except for one specific experiment, the applicability of a contactless method can be considered as proven. However, there is yet one important aspect to consider in the contactless method: the size of the loop, particularly when the considered loop corresponds to the length of a full turn. This particular case is of interest because both

copper wires become together right after the superconducting tape, which means that there is not any air section forming the loop. This situation was tested by measuring losses in the 64 turn coil considering two different frequencies: 144 and 288 Hz. The 4 cm loop was placed in the 42 th turn and the full turn loop in the 43 th turn. In this particular case the length of the larger loop corresponds to 26 cm. Figure 6.15 depicts results obtained for a frequency of 288 Hz. Data obtained for a frequency of 144 Hz show the same behaviour, and no difference is visible for measurements considering the two different contactless methods, which indicate that the length of the contactless loop does not influence results.

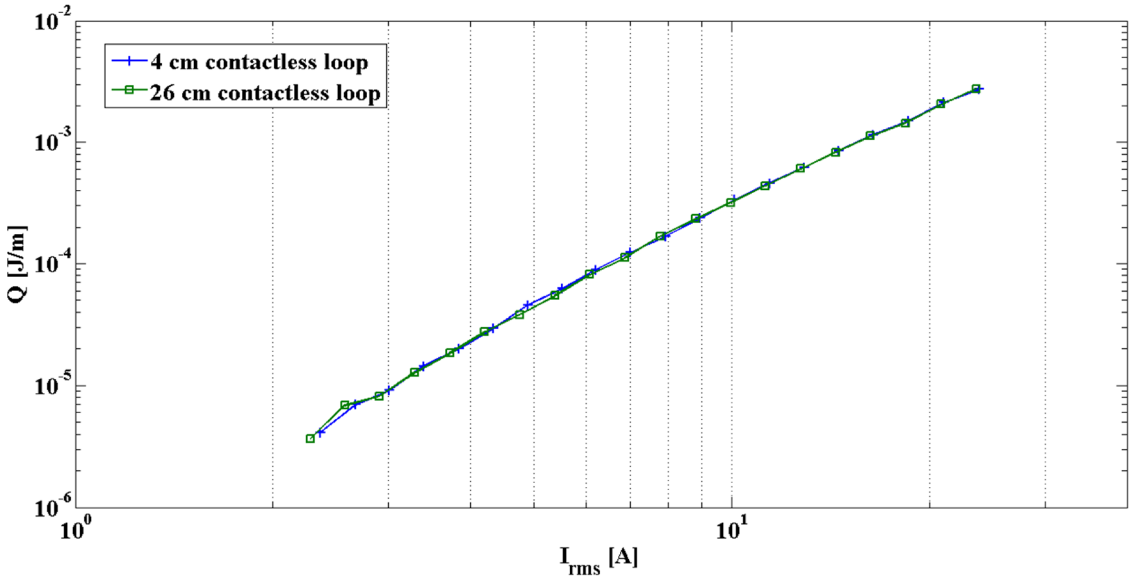

Figure 6.15. Measured AC losses at 288 Hz considering two contactless loops.

6.2.2.2. Multi-harmonic behaviour

In the last section, a comprehensive study of AC losses was performed, considering a frequency range of 72 Hz - 1152 Hz. Obtained data seem to indicate that there is some frequency dependent behaviour in measured AC losses, which will be further investigated in the next section. However, there is still another aspect considered important in the study of AC losses in HTS coils: the behaviour presented by those coils when subjected to a current with more than one frequency, i.e. a multi-harmonic current. The measurement of AC losses using a multi-harmonic current flowing through the HTS coil is complex because it is not possible to use the LIA method. Considering this, a simple calorimetric method was implemented, and AC losses were measured considering currents with a harmonic content of two different harmonics, in the same frequency range as the study presented in the last section, so that a comparison can be performed. For validation purposes, all results achieved using the calorimetric method are compared to those obtained using the LIA method, for the same frequency.

For this study three different frequencies were considered: the industrial frequency of 50 Hz and its fifth and seventh harmonics (i.e. 250 Hz and 350 Hz). AC losses were measured according to the following scheme:

- 50 Hz, considering a current of 20 A;
- 20 A at 50 Hz + 5 A at 250 Hz;
- 20 A at 50 Hz + 5 A at 350 Hz.

To generate the previous set of currents two different methods were used: for the generation of a 50 Hz current the lock-in oscillator was used as a signal source for the power amplifier, following the same technique used in the LIA method, represented in Figure 4.2. In order to obtain the multi-harmonic current, an extra step is necessary. The signal generated by the LIA internal oscillator is added to another signal generated using a different source through means of a mixer circuit, using an operational amplifier, with gain equal to one. The output signal of the op amp is then used as a reference for the power amplifier and the remaining circuit of Figure 4.2 is then used. This new configuration is depicted in Figure 6.16.

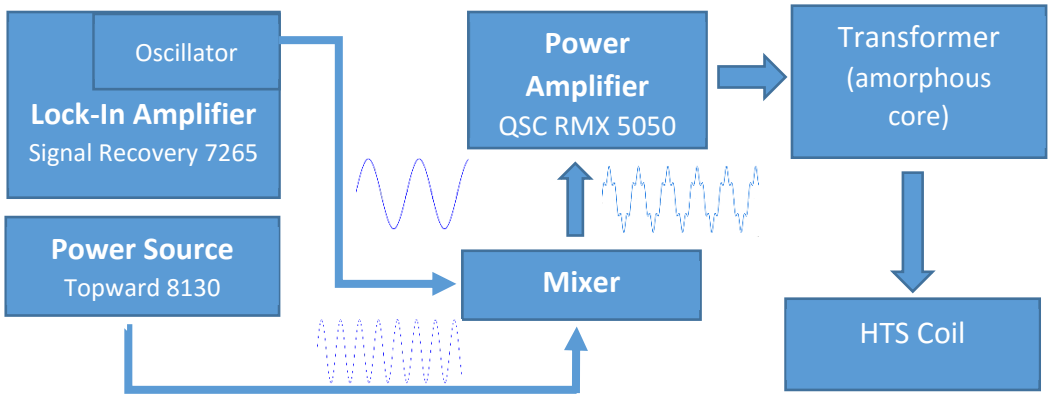

Figure 6.16. Multi-harmonic generation system.

In order to achieve a term of comparison, AC losses presented by the HTS coil at the three frequencies in study were also measured using the LIA method, for a range of currents considered as the most adequate for this particular case. Figure 6.17 shows measured data obtained for the three considered frequencies.

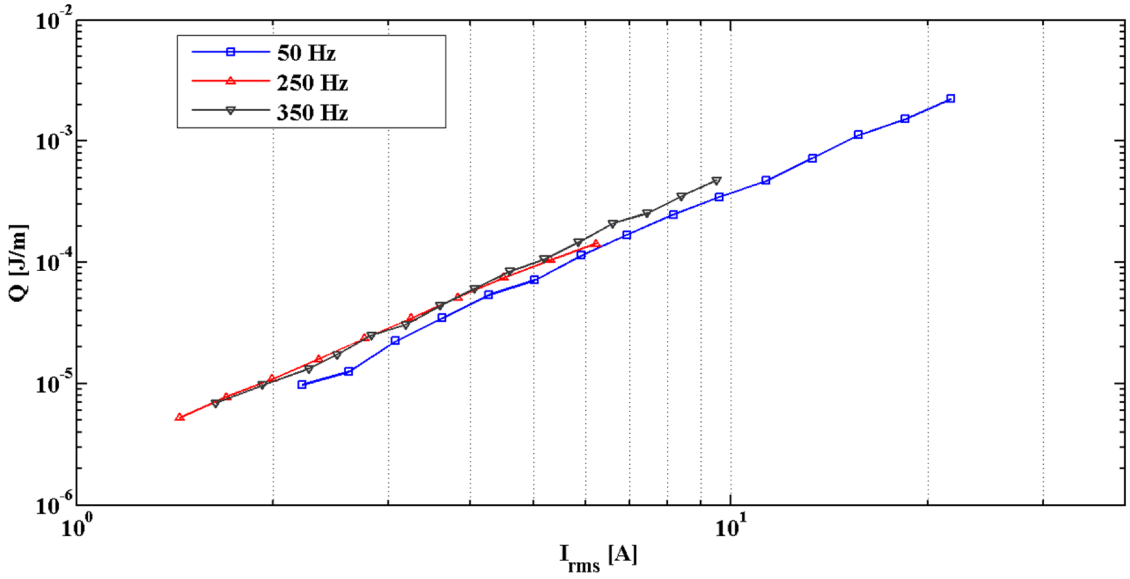

Figure 6.17. Measured AC losses for 50 Hz and its 5th and 7th harmonic.

Obtained values are within a close range of those previously obtained for similar frequencies (ex: 50 Hz and 72 Hz or 350 Hz and 360 Hz). The measured voltages for the specific currents in study are (three measured points in the above graph):

- 20 A (50 Hz): 0.167 mV;
- 5 A (250 Hz): 0.186 mV;
- 5 A (350 Hz): 0.255 mV;

Considering that the coil has a total length of 37.5 m and that the measured voltages were measured using a 4 cm voltage taps configuration, already described in section 4.2, the total amount of power dissipated can be calculated as follows (for the first case):

$$P_{20A,50Hz} = V \times I = 0.167 \times 10^{-3} \times 20 \times \frac{3750}{4} = 3.09 \text{ W.}$$

Similarly, the measured dissipated power for the other two cases in analysis are:

$P_{5A,250Hz} = 0.862$ W;

$P_{5A,350Hz} = 1.18$ W.

These dissipated power values will be used as a basis for comparison with the values obtained using the calorimetric method.

Measurement of AC losses using the calorimetric method was performed as follows: a first experiment using a DC current is performed and the initial and final capacitance values are measured. The difference between the measured values corresponds to the total amount of evaporated nitrogen. When considering a specific time interval, the evaporated nitrogen can then be related to the total amount of power dissipated. A second experiment using an AC current is then performed, considering the same time interval. The difference between the dissipated power values in those two experiments corresponds to the AC losses for that case. In every experiment performed, the time interval was set as two hours.

Consider the case of measurement of AC losses using the calorimetric method for a current of 20 A at 50 Hz.

The coil and the capacitor were placed inside a cryostat implemented using XPS (extruded polystyrene) with the following dimensions:

- Height = 44 cm;
- Width = 20 cm;
- Thickness = 4 cm;

For the first experiment a current of 20 A DC was considered. The initial and final capacitance measured values were (considering t = 2 h):

- $C_i = 1616$ pF;
- $C_f = 1440$ pF.

The measured capacitances correspond to a certain height of liquid nitrogen, given by equation (4.4):

$$H_i = \frac{\frac{C_i \times \ln(\frac{r_2}{r_1})}{2\pi} - L \times \varepsilon_1}{\varepsilon_2 - \varepsilon_1} = \frac{\frac{1616\times10^{-12} \times \ln(\frac{15.35}{15})}{2\pi} - 0.5 \times 8.854 \times 10^{-12}}{1.4323 \times 8.854 \times 10^{-12} - 8.854 \times 10^{-12}} = 0.425 \text{ m};$$

$H_f = 0.243$ m;

The total height of liquid nitrogen was also measured manually for this test and results are agreeable with those obtained using this equation.

Using now equation (4.5) and considering that the cryostat has a section of $S_C = 0.2 \times 0.04 = 0.008$ m², the total mass of evaporated nitrogen is:

$$m = (H_1 - H_2) \times S_C \times \rho = (0.425 - 0.243) \times 0.008 \times 805.43 = 1.175 \text{ kg}.$$

Considering that the liquid nitrogen has a latent heat of vaporization $\Delta H_{vap} = 198.99$ kJ/kg, the total amount of energy dissipated is:

$$E = m \times \Delta H_{vap} = 1.175 \times 198.99 = 233.906 \text{ kJ}.$$

Finally, bearing in mind the fact that the experiment was performed during 2 hours, the total amount of power dissipated is

$$P_{DC} = \frac{E}{t} = \frac{233906}{3600} = 32.487 \text{ W}.$$

This value corresponds to all power dissipated in the system, i.e. in the SC coil itself, the resistive joints, the copper cables connected to the coil and the natural evaporation of the nitrogen.

The experiment was then repeated, considering an AC current of 20 A at 50 Hz and the measured capacitances in this case are:

- $C_i = 1616$ pF;
- $C_f = 1423$ pF.

Following the same logic for these capacitance values, the total amount of power dissipated is $P_{AC} = 35.6$ W.

The total amount of power dissipated due to AC losses is then the difference between both obtained values:

$$P_{AC\_loss} = P_{AC} - P_{DC} = 35.6 - 32.5 = 3.1 \text{ W}$$

This process was applied for different experiments, whose results are depicted in Table 6.1. The first column indicates which capacitor was used to perform the experiment. Although the capacitor C2 has a larger capacitance error when immersed in liquid nitrogen (comparing with the theoretical value and with C1) no sound difference is noticed in obtained results.

Table 6.1. Power dissipated measured using a calorimetric method.

	P_{DC}	$P_{20A,50\ Hz}$	$P_{20A,50\ Hz}$ + 5A,250 Hz	$P_{20A,50\ Hz}$ + 5A,350 Hz	P_{AC_Loss} 50 Hz	P_{AC_Loss} 250 Hz	P_{AC_Loss} 350 Hz
C1	32.487	35.625	N/A	N/A	3,138	N/A	N/A
	32.302	35.256	N/A	N/A	2,954	N/A	N/A
	33.594	36.54	N/A	N/A	2,946	N/A	N/A
	32.856	35.809	N/A	N/A	2,953	N/A	N/A
	34.148	37.102	N/A	N/A	2,954	N/A	N/A
	31.692	34.588	N/A	N/A	2,896	N/A	N/A
C2	29.718	32.856	33.779	33.964	3.138	0.923	1.108
C1	34.836	37.655	38.662	38.863	2.819	1.007	1.208
C2	31.749	34.702	35.625	35.994	2.953	0.923	1.292

The most important aspect to notice is that obtained results suggest that the multi-harmonic behaviour of the current does not add an extra component of AC losses, i.e., the total amount of losses obtained is equal to the sum of each individual component (each individual frequency operating alone), behaviour already indicated by other research groups as well (Tsuda et al. 2015).

Obtained results seem to indicate that the implemented calorimetric method can be used to estimate the total amount of AC losses in superconducting devices. Comparing the results obtained for 50 Hz using both, the LIA and the calorimetric methods, there is a maximum error of 8.76 % (measured value of 2.819 W). Maximum error for obtained results at a multi-harmonic current flow (50 Hz + 250 Hz and 50 Hz + 350 Hz), when comparing to values obtained when those frequencies were tested operating in single frequency mode are respectively 16.8 % and 9.4 %. The main reason for the increasing error in these results is related to the fact that measured values are in the range of 1W, which is a small value compared to the overall value of total dissipated power measured (higher than 30 W). This is the major drawback of this method: the natural evaporation of the nitrogen will conceal AC losses of low magnitudes or, as in this case, lead to some error in the obtained results. In order to reduce the uncertainty of results (when comparing to the LIA method) some improvements are possible: the cryostat can be implemented of a rigid material whose dimensions are known and exact (which is not the case in the performed experiments), in order to accurately calculate the amount of evaporated nitrogen. Nonetheless, as a method designed to roughly estimate the total amount of AC losses in a superconducting device and considering its great simplicity, obtained results are accurate and agreeable with other techniques.

6.2.2.3. Frequency dependence analysis

Measured AC losses in HTS coils present a frequency dependent behaviour. Considering the studied frequency range from 72 Hz to 1152 Hz, AC losses increased to the double (in average, considering the full current range tested). Comparing the loss value obtained at 144 Hz (because this was the frequency with lower loss values) and at 1152 HZ, for a current of 10 A, the difference increases to 2.5 times. However, just like verified in section 6.1.2 for samples of HTS tape, it is expected that the eddy currents component plays a major role in such increase (Dai et al. 2005). In order to verify the contribution of eddy currents component in the measured AC losses, equation (2.14) was again used to subtract that component from the measured

values, and obtained results are depicted in Figure 6.18 for three different frequencies: 144 Hz, 576 Hz and 1152 Hz.

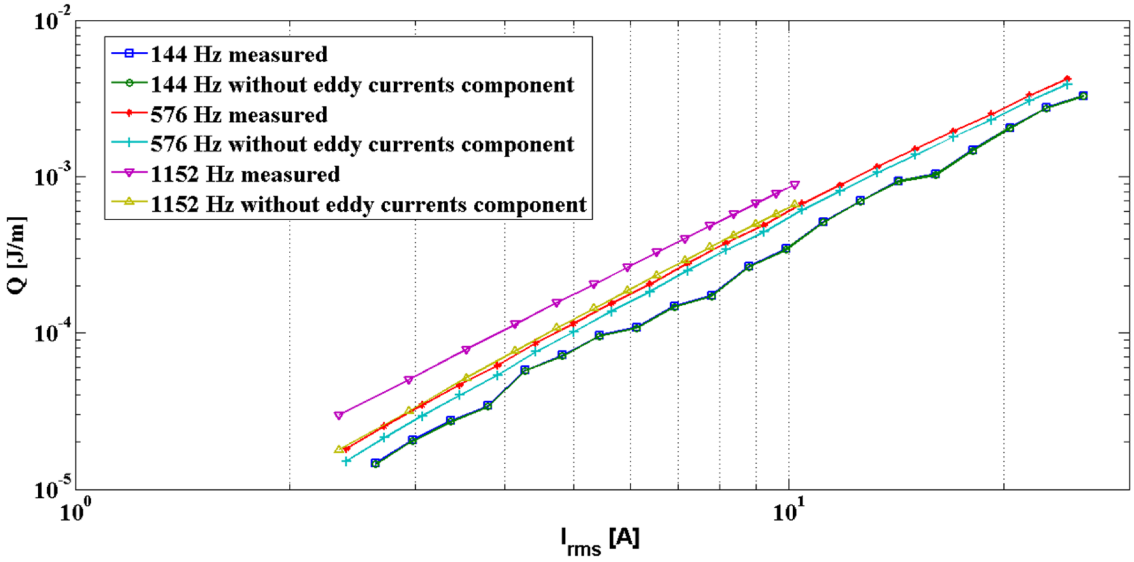

Figure 6.18. Eddy currents component subtraction in measured AC losses in HTS coils.

As expected, eddy currents component has a greater importance for the total amount of AC losses at higher frequencies. For 144 Hz, this component is practically inexistent. However, even subtracting this component from the total measured losses, there is still some frequency dependent behaviour in losses. In order to easily perceive this frequency dependent behaviour Figure 6.19 depicts measured losses with and without the eddy currents component, for two different currents. The shape of the curves seem to indicate that the HTS coils have a similar behaviour to that demonstrated by HTS tapes in the literature, even taking out the eddy currents component. First the losses decrease with increasing frequency, till a certain value (in this case 144 Hz) and for higher frequencies AC losses show a proportional behaviour, increasing with the frequency. To increase legibility, in Figure 6.19 AC losses were normalized using the average loss value of each current (5 A and 20 A), i.e., each value was divided by the average value of losses obtained (at different frequencies) for that current. It is also possible to see that the eddy currents component has a higher importance for low currents. As an example, for a frequency of 576 Hz, eddy currents represent 11.7 % of the total measured losses at 5 A but if the current increases to 20 A this weight decreases to 7.89 %. This is also expected because at higher currents resistive losses start to have a higher importance, as already seen.

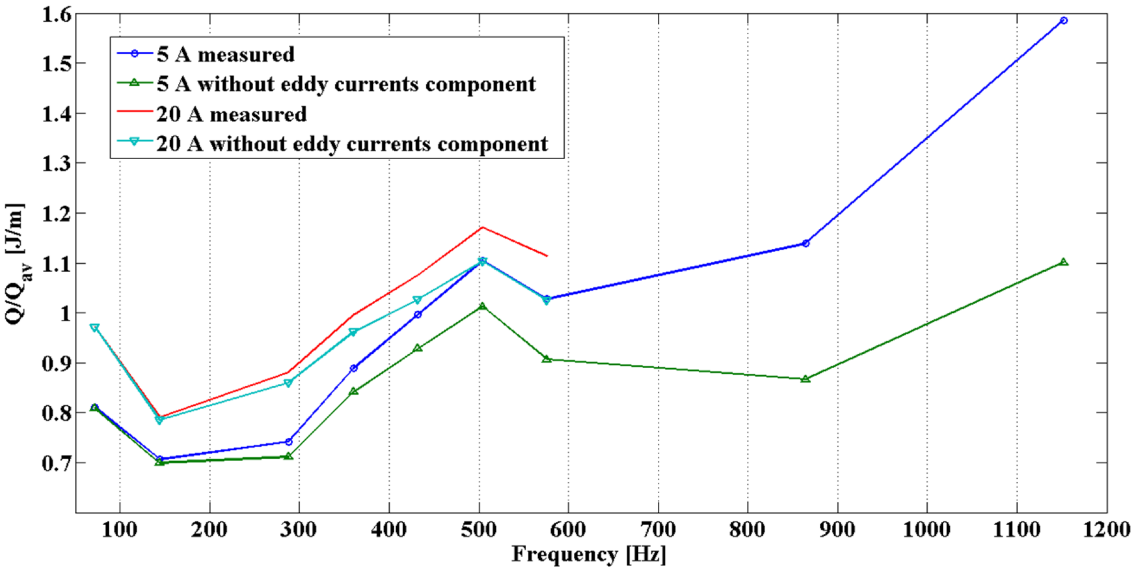

Figure 6.19. Frequency dependence behaviour of AC losses.

As seen in the previous section a multi-harmonic current profile does not add losses components to the HTS tape, and the total amount of AC losses can be calculated summing the different individual harmonic components present in the current flowing through the coil. This fact is relevant for devices in which a current with a non-sinusoidal profile is used.

6.2.3. Comparison between models and experiments

In science fields like superconductivity, where characteristics of used materials combined with the complexity of devices present important technological and economic challenges, modelling acquires an important step in development projects. In order to validate results obtained using two different numerical models presented in section 3.2, MEMEP and FLUX2D simulations, a comparison between measured AC losses and results obtained from those models is performed, but first, a small comparison between obtained experimental data and the analytical model presented in equation (2.16) will also be performed.

Following equation (2.16), considering the dimensions of this particular HTS tape as: $w = 3.9$ mm; $d = 0.1328$ mm; $h = 0.054$ mm. Also considering $I_C = 32.91$ A (critical current of coil A) and J_C calculated diving the critical current by the superconducting region used in the MEMEP ellipse model (0.51779 mm^2), the AC losses per length of HTS tape can be calculated. Results obtained are depicted in Figure 6.20 for comparison purposes.

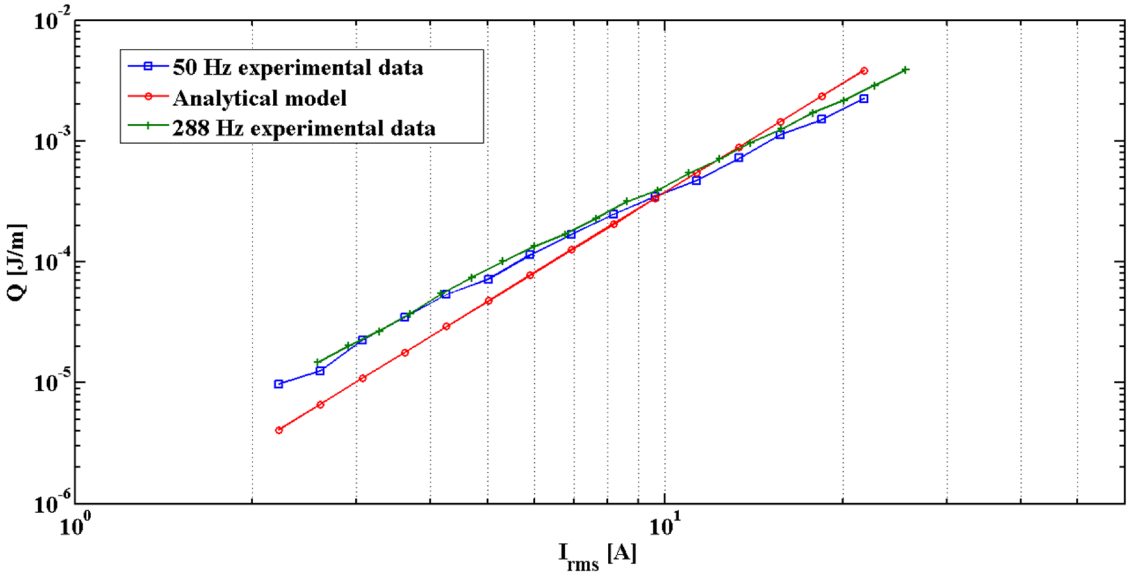

Figure 6.20. Comparison of AC losses obtained experimentally and by an analytical model.

Results obtained indicate that there are differences between results obtained experimentally and using the analytical model. Such differences can be explained according to two reasons: firstly, the superconducting coil has a total of 128 turns, which are in the lower limit of the saturation of AC losses with the number of turns (Pardo 2008) and this analytical model produce better results for a high number of turns (inside that saturation region); in addition to this, the model also produce better results when the internal radius of the HTS coil is much larger than its width (which is not the case of this coil) and when using 2G HTS tape (instead of 1G tape which was used in this case). However, even considering the differences obtained, the simplicity of this analytical model when comparing to numerical models allows its utilization as a first step to verify the general amount of AC losses in HTS coils with a size similar to those used in this work.

Considering that the results obtained using the analytical model have relatively high error when comparing to the experimental data obtained, this data was also compared to the two considered numeral models. The used FLUX2D model considered a coil with a total of 128 turns whose dimensions and main characteristics are given in section 3.2.2 and AC losses were computed following a common approach given by (Grilli 2003):

$$P = f \int_T \int_S \mathbf{J}.\mathbf{E} \; dS \; dt \;\; \text{(W)} \tag{6.3}$$

where f is frequency of the source, T is the second simulated period (to avoid the transient in the first period) and S is total superconducting section.

Regarding MEMEP simulations, whose characteristics are given in section 3.2.1, different models were considered: the superconducting region was simulated using two different approaches, a rectangular and an elliptical cross-section. This allows a direct comparison not only with experimental data but also with the FLUX2D model, in which a rectangular cross-section was used (to decrease the simulation time). Also in the MEMEP model, two different n-values for the HTS tape were considered, in order to evaluate the impact of this variable in this simulation method.

Figure 6.21 shows a comparison between measured AC losses for a frequency of 72 Hz and results obtained using the MEMEP modelling method considering two different n-values for the HTS tape.

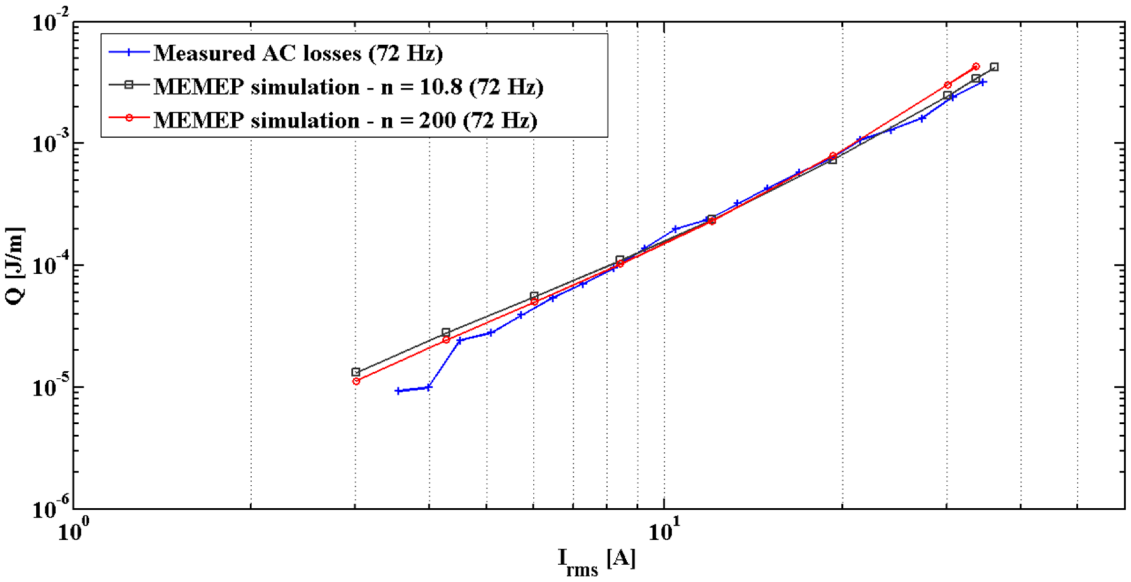

Figure 6.21. MEMEP simulations: different n-values comparison.

Obtained data suggest that n-value does not represent a fundamental variable in the MEMEP model. However, it is possible to see that results computed using an n-value of 10.8 are closer to the experimental data at higher current amplitudes, which is an expected behaviour since this is closer to the real n-value of the HTS tape. Another verified characteristic using the MEMEP method was the effect of simulating different superconducting cross-sections in the total AC losses. Figure 6.22 depicts obtained data using this simulation method considering different cross-sections for the HTS region and its comparison with experimental results for a frequency of 72 Hz.

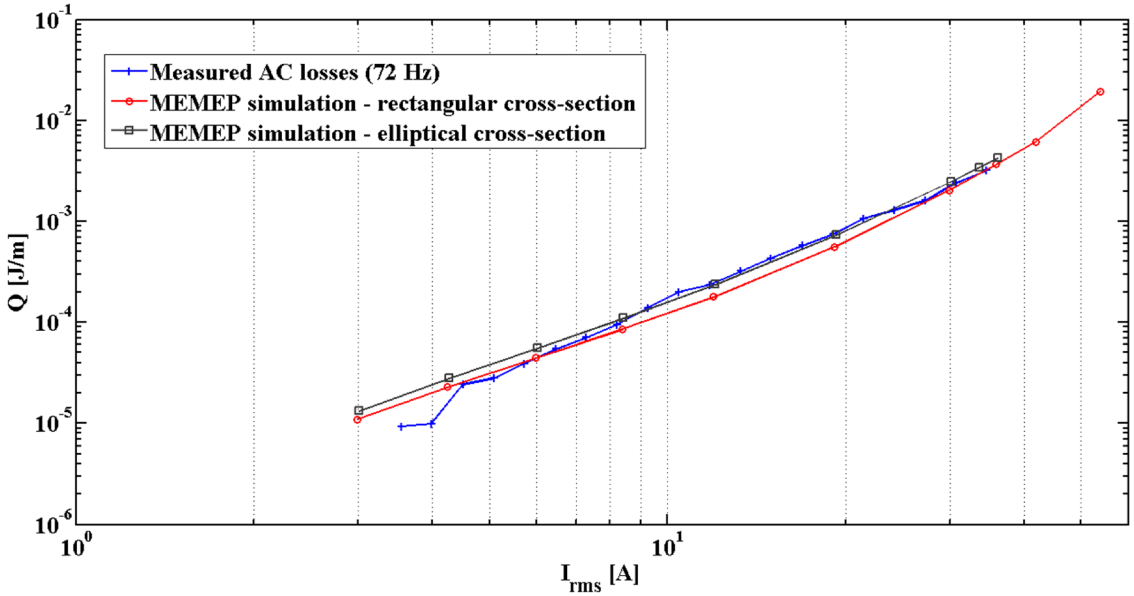

Figure 6.22. MEMEP simulations: different cross-sections comparison.

As expected, results obtained using an elliptical cross-section are closer to experimentally obtained data, for the majority of the current range considered. However, results obtained using a rectangular cross-section are not so different, which indicates that this cross-section can also be considered, if it brings other advantages like reduced computation times. In fact, the main goal of the MEMEP simulation using a rectangular cross-section was to achieve a direct term of comparison with the results obtained using the FLUX2D software package in which a rectangular cross-section was considered due to the limitations of the software (an elliptical cross-section led to non-viable simulation times). This is one of the advantages of the MEMEP method, when comparing to FEM modelling performed by FLUX2D. In average, the computation times for MEMEP simulations were in the order of 4 to 5 hours and each FLUX2D simulation took in average 74 to 75 hours, using computers with similar characteristics. Figure 6.23 and Figure 6.24 depict results obtained using both simulation methods and experimental data for a frequency of 144 Hz and 288 Hz, respectively.

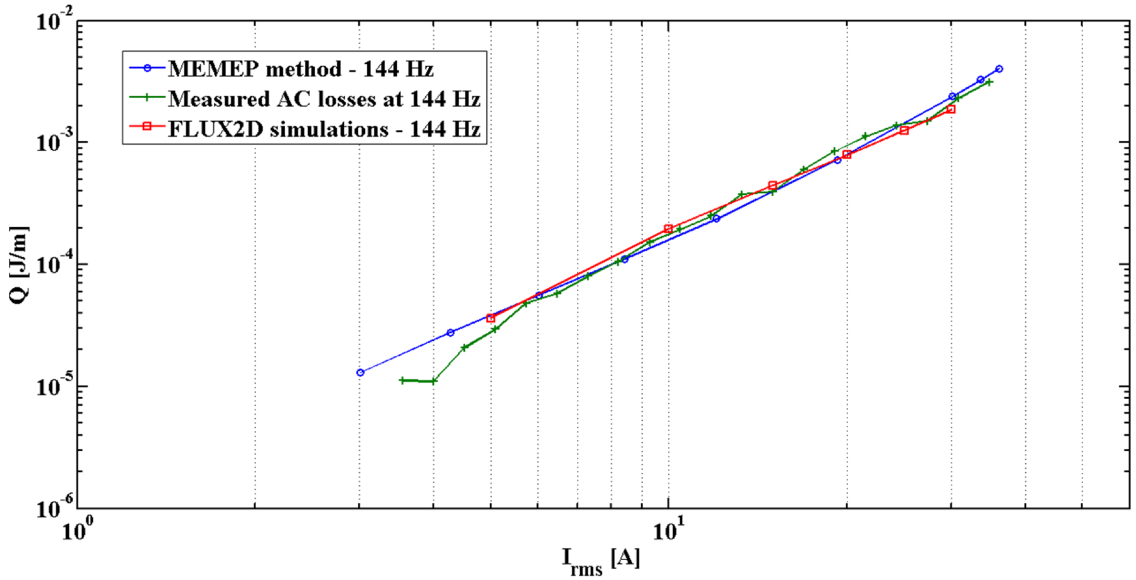

Figure 6.23. AC losses at 144 Hz: simulation results VS experimental data.

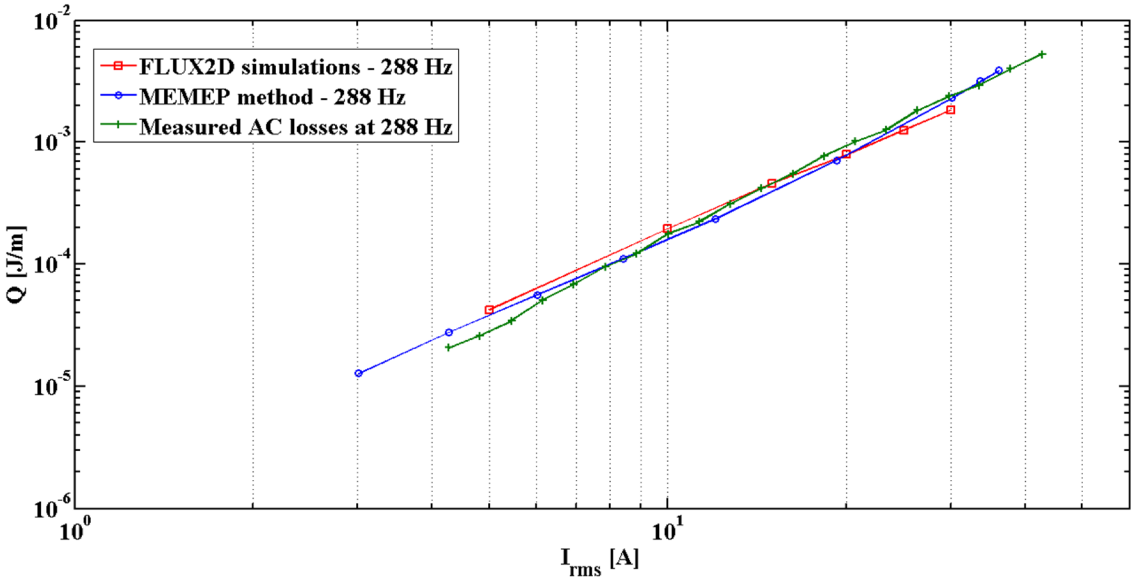

Figure 6.24. AC losses at 288 Hz: simulation results VS experimental data.

Results obtained and presented from Figure 6.21 to Figure 6.24 suggest that both models (MEMEP and FLUX2D) can be used to simulate AC losses in HTS coils, presenting good results when compared to those obtained experimentally. However, all results obtained from modelling techniques have one similar characteristic when compared to experimental data: at low current amplitudes simulated AC losses are higher than measured values. There are two causes for this phenomenon: firstly, on the measurement of the critical current of the HTS tape, presented in Figure 3.6, the effect of self-field was not corrected. This means that at low magnetic fields the critical current density in the HTS tape is higher than the one considered in the model, which will result in a lower AC loss. The second reason is that the superconducting core of the Bi-2223 tape is not homogeneous and the critical current density close to the outer perimeter of the core is usually larger than the average critical current density, which will also lead to a reduction of AC losses at low current amplitudes. Despite this difference in obtained results at low current amplitudes, in average obtained values are good, which indicates that both modelling techniques can be used to simulate AC losses in HTS coils.

6.3. Concluding remarks

This chapter presented a comprehensive study of AC losses in samples of HTS tape and coils, considering a frequency range of 50 - 1152 Hz and currents raging from zero till close the critical current. Obtained experimental values were compared to those obtained from numerical models and obtained results indicate that the considered numerical modelling methods are applicable to HTS coils, producing results close to those obtained experimentally.

Regarding the measurements in tapes, it was possible to verify that eddy currents play an important role, particularly for higher frequencies and low current amplitudes. It is possible to calculate and extract this component from the total amount of AC losses using an analytical formula which depends only on the geometry of the HTS tape and the characteristics of the materials. Subtracting this component, no frequency dependency is visible and obtained losses result in a higher predominance of hysteresis losses, which fit in the classical Norris model for superconductors with an elliptical cross-section.

When considering HTS coils, losses were measured using three different methods, which produced similar results. A standard 4 point method with voltage taps at the coil ends was first considered for lower frequencies using a resistive divider to decrease measured voltages to safe values for the LIA inputs, but it was not possible to use it in the full frequency range due to the frequency response of the divider. Taking into account this limitation, two other methods were considered: a 4 point configuration using only a section of the tape and a contactless method, which has the main advantage of eliminating electrical contacts between the measuring system and the HTS coil. Since all results obtained, except for one specific experiment, are very similar to those achieved using a standard 4 cm voltage taps configuration, the applicability of a contactless loop was demonstrated. Furthermore, the applicability of the 4 cm voltage taps configuration in a representative turn produced the same results as a standard 4 point configuration at the coil ends, which indicates that all three implemented methods can be used to measure AC losses in HTS coils. Concerning the obtained data, it is important to notice that there is a frequency dependent behaviour, even taking out the eddy currents component. This is a known behaviour in coils wound with 1G HTS, already observed and described by other

research groups. The eddy currents component acquire a higher importance at low current amplitudes, which is an expected characteristic as well, since for higher currents hysteresis and resistive losses have a greater importance.

Lastly on this section, a simple calorimetric method based on calculating the amount of evaporated nitrogen by measuring the capacitance of a cylindrical capacitor was implemented and AC losses using one and two simultaneous current harmonics were measured. Obtained results indicate that this can be a method to consider for medium to large size devices, particularly for uncommon current profiles, which difficult measurements using conventional techniques as the LIA method. Although there is some difference in obtained values, when comparing to those obtained using the LIA method, the great simplicity and low cost of this method are two important advantages, particularly comparing to other common calorimetric methods that usually need to consider a closed cryostat and a gas flux meter.

7

Conclusions and Future Work

During the different chapters of this document, small conclusions of each topic were already presented. In this chapter, only a general summary will be performed, as a way to condensate all results achieved during this work.

This performed work has as a basis the measurement of AC losses in HTS coils up to a maximum of 128 turns, wound using 1G HTS tape. Different frequencies were considered, ranging from 50 Hz till 1152 Hz and using currents from zero till over the critical current of the coils which was measured as around 30 A. Losses were measured considering three different techniques, all based in the LIA method and all results obtained seem to indicate that the three different approaches produce similar results. One of these three techniques uses a contactless loop to measure the AC losses, which has several advantages when comparing to other methods in which an electrical contact with the coil is necessary. In addition to this, AC losses were also measured when applying more than one current harmonic in simultaneous to the HTS coil. A simple calorimetric method, based on measuring the evaporation of liquid nitrogen through the utilization of a cylindrical capacitor, was used and achieved results indicate that this simple method can be used to have a rough idea of AC losses in larger superconducting devices. Although there is some error in the obtained results, considering the high simplicity of this method, it can present a valid alternative to measure AC losses, particularly for current profiles with more than one harmonic.

Experimental data achieved during this work was also used to validate analytical and numerical models commonly used to calculate AC losses. MEMEP and FLUX2D simulations were performed and both numerical methods produce results highly accurate when compared to those obtained experimentally and an analytical method was also verified. Although in this case the error between computed and experimentally obtained data is higher than in numerical simulations, the simplicity of the analytical approach presents an important advantage and it can be considering when measuring AC losses in HTS coils with a large number of turns.

Regarding the frequency dependence of AC losses, achieved results are in the same spectrum of results obtained by other research groups in different sized HTS coils and samples of HTS tape. Eddy currents losses have an important contribution to the total amount of AC losses at higher frequencies and hysteresis losses are the main contributor for the total amount of AC losses at lower frequency values. It is possible to separate the different components in the AC losses which can be used as a way to improve the manufacturing processes of superconducting tape thus decreasing the total amount of losses.

Concluding, the study of AC losses in superconducting devices such as HTS coils should be further investigated in order to achieve a minimization in this phenomenon which is a major limiting factor in the dissemination of technologies based on superconductivity.

The different experiments performed using the implemented HTS coils also allowed to reach the following conclusions: the utilization of ferromagnetic flux diverters increase the critical current of the HTS coils, thus decreasing its losses for the same operating current; the continuous utilization of the HTS tape, particularly if that tape is subjected to different thermal cycles will degrade its characteristics and to assure a proper operation of the superconducting system these characteristics should be continuously verified.

Future Work

Because no work is ever finished and there is always space for improvements the author recommends the following aspects to be considered as future work in this research line:

- Considering the study of AC losses in medium-sized HTS coils, it is important to try to study AC losses in even larger coils and considering an even larger frequency range. This is a step forward in the study of the behaviour of superconductors and will allow a good prediction of their behaviour in complex systems; the study of AC losses in systems with multiple coils will also allow to reach new results that can be used to validate literature models.
- During this work, a noticeable degradation in the tape characteristics was verified. This investigation should continue, in order to verify the origin of this degradation so that it is possible to minimize it.
- The electric method used to measure AC losses (based on the LIA approach) has different limitations: the major one is related to the fact that a power amplifier is used and that power amplifier only works in some specific conditions (optimal point of work is achieved with a 4 Ω pure resistive load, which is not the case). The study of these limitation and the improvement of the system (maybe through the integration of capacitive elements to decrease the inductive load of the HTS coils) should be performed, in order to allow the utilization of this method for higher frequencies and with larger coils.
- Finally, the calorimetric method implemented has different possible improvements: the capacitance reading process can be improved, in order to achieve highly accurate results. In addition to this, the container of the sample should be implemented using well known dimensions, in order to successfully calculate the amount of liquid nitrogen evaporated during the experiments.

O

Original contributions

The main original contributions of this work can be briefly stated as:

- Implementation of a methodology to determine maximum inductance of superconducting coils, based on geometric parameters;
- Study of AC losses in a superconducting coil with a reasonable number of turns (128) at high frequencies (up to 1152 Hz);
- Development of a contactless method to measure AC losses in HTS coils;
- Development of a calorimetric method based in the measurement of the evaporation of liquid nitrogen to measure AC losses in HTS coils considering currents with two harmonics;
- Contribution to the validation of literature analytical and numerical models for the calculation of AC losses.

During this work, and as a way to validate the different original contributions stated above, several scientific papers were published in Journals and Conferences with peer reviewing. The full list of published papers, with the correspondents digital object identifiers (DOI) is given below.

Journal Papers

- A Fast Algorithm for Initial Design of HTS Coils for SMES Applications. IEEE Transactions on Applied Superconductivity. doi:10.1109/TASC.2012.2231912
- Contactless loop method for measurement of AC Losses in HTS coils. IEEE Transactions on Applied Superconductivity. doi:10.1109/TASC.2014.2374155

Conference Proceedings

- "SUPERCONDUCTING MAGNETIC ENERGY STORAGE - A Technological Contribute to Smart Grid Concept Implementation." 1st International Conference on Smart Grids and Green IT Systems, DOI: 10.5220/0003978301130120

- A Study on Superconducting Coils for Superconducting Magnetic Energy Storage (SMES) Applications, Technological Innovation for the Internet of Things, doi:10.1007/978-3-642-37291-9_48

- AC Losses and Material Degradation Effects in a Superconducting Tape for SMES Applications, Technological Innovation for Collective Awareness Systems, doi:10.1007/978-3-642-54734-8_46

- Combined operation of an Unified Power Quality Conditioner and a Superconducting Magnetic Energy Storage system for power quality improvement, Technological Innovations for Cloud-based Engineering Systems, doi:10.1007/978-3-319-16766-4_40

- Integration of SMES devices in power systems – opportunities and challenges, CPE2015 – 9th International Conference on Compatibility and Power Electronics (to be indexed to IEEExplore)

- Improved Operation of an UPQC by addition of a Superconducting Magnetic Energy Storage system, CPE2015 – 9th International Conference on Compatibility and Power Electronics (to be indexed to IEEExplore)

The author of this work was also co-author of the following scientific papers:

- Validation and application of sand pile modeling of multiseeded HTS bulk superconductors. IEEE Transactions on Applied Superconductivity. Doi:10.1109/TASC.2014.2366073

- Device for Measuring the Thermal Cycling Degradation in 2G Tapes for Electrical Power Applications, IEEE Transactions on Applied Superconductivity. Doi:10.1109/TASC.2014.2377474

In addition to the aforementioned scientific papers two more papers are expected to be published as a result of this work (as first author): one is already submitted to the Journal "Superconductor Science and Technology" and the other one was presented at the conference EUCAS 2015 – 12th European Conference on Applied Superconductivity and is now submitted to the Journal IEEE Transactions on Applied Superconductivity.

R

References

Abrahamsen, A.B. et al., 2010. Superconducting wind turbine generators. *Superconductor Science and Technology*, 23(3), p.034019.

Abrikosov, A., 1957. Magnetic properties of superconductors of the second group. *Sov. Phys. - JETP (Engl. Transl.); (United States)*, 5:6.

Ainslie, M.D., Weijia Yuan & Flack, T.J., 2013. Numerical Analysis of AC Loss Reduction in HTS Superconducting Coils Using Magnetic Materials to Divert Flux. *IEEE Transactions on Applied Superconductivity*, 23(3), pp.4700104–4700104.

Alamgir, a. K.M., Gu, C. & Han, Z., 2005. Comparison of self-field effects between Bi-2223/Ag tapes and pancake coils. *Physica C: Superconductivity*, 424(3-4), pp.138–144.

Alamgir, a. K.M., Gu, C. & Han, Z., 2006. Experiment of enhancing critical current and reducing ac loss in pancake coil comprised of Ni-coated Bi-2223/Ag tape. *Physica C: Superconductivity*, 440(1-2), pp.35–39.

Alex, F. et al., 2010. AC losses in HTS multi-pancake coils made of BSCCO-tape. *Journal of Physics: Conference Series*, 234(3), p.032014.

Amemiya, N. et al., 2007. AC Loss Reduction of Superconducting Power Transmission Cables Composed of Coated Conductors. *IEEE Transactions on Applied Superconductivity*, 17(2), pp.1712–1717.

Arsenio, P. et al., 2013. Analysis of Characteristic Hysteresis Loops of Magnetic Shielding Inductive Fault Current Limiters. *IEEE Transactions on Applied Superconductivity*, 23(3), pp.5601004–5601004.

Arsénio, P., 2012. *Desenvolvimento e Análise de um Limitador de Corrente Indutivo Baseado em Fita Supercondutora Bi-2223 (in portuguese)*. Universidade Nova de Lisboa.

Ashworth, S.P. & Suenaga, M., 2001. Local calorimetry to measure ac losses in HTS conductors. *Cryogenics*, 41(2), pp.77–89.

Babic, S., Salon, S. & Akyel, C., 2004. The Mutual Inductance of Two Thin Coaxial Disk Coils in Air. *IEEE Transactions on Magnetics*, 40(2), pp.822–825.

Barnes, P.N., Sumption, M.D. & Rhoads, G.L., 2005. Review of high power density superconducting generators: Present state and prospects for incorporating YBCO windings. *Cryogenics*, 45(10-11), pp.670–686.

Bean, C.P., 1964. Magnetization of High-Field Superconductors. *Reviews of Modern Physics*, 36(1), pp.31–39.

Bednorz, J.G. & Müller, K.A., 1986. Possible high Tc superconductivity in the Ba-La-Cu-O system. *Zeitschrift für Physik B Condensed Matter*, 64(2), pp.189–193.

Buckles, W. & Hassenzahl, W.V., 2000. Superconducting magnetic energy storage. *IEEE Power Engineering Review*, 20(5), pp.16–20.

Burns, G., 1992. *High-temperature Superconductivity: an introduction*, Academic Press.

Campbell, A.M., 2014. Superconducting and conventional machines. *Superconductor Science and Technology*, 27(12), p.124012.

Ceballos, J. et al., 2014. Device for Measuring the Thermal Cycling Degradation in 2G Tapes for Electrical Power Applications. *IEEE Transactions on Applied Superconductivity*, pp.1–1.

Ceballos, J.M., 2010. *Analysis of AC losses in superconducting electrical components for application in the design of electrical systems*. University of Extremadura.

Cedrat, 2001. FLUX2D Superconductors technical paper. , p.36.

Chen, D.-X. et al., 2003. Frequency dependent AC loss in degraded Bi-2223/Ag tape. *Physica C: Superconductivity*, 391(1), pp.75–78.

Chen, X.Y. et al., 2014. Integrated SMES Technology for Modern Power System and Future Smart Grid. *IEEE Transactions on Applied Superconductivity*, 24, pp.1–5.

Choi, S. et al., 2002. AC transport current loss in stacked HTS tapes. *Physica C: Superconductivity*, 372-376, pp.1746–1749.

Chu, C.W. et al., 1993. Superconductivity above 150 K in HgBa2Ca2Cu3O8+δ at high pressures. *Nature*, 365(6444), pp.323–325.

Clem, J.R., Claassen, J.H. & Mawatari, Y., 2007. AC losses in a finite Z stack using an anisotropic homogeneous-medium approximation. *Superconductor Science and Technology*, 20(12), pp.1130–1139.

Clem, J.R. & Sanchez, A., 1994. Hysteretic ac losses and susceptibility of thin superconducting disks. *Physical Review B*, 50(13), pp.9355–9362

Dai, P. et al., 1995. Synthesis and neutron powder diffraction study of the superconductor HgBa2Ca2Cu3O8 + δ by Tl substitution. *Physica C: Superconductivity*, 243(3-4), pp.201–206.

Dai, T. et al., 2005. Study on ac losses of HTS coil carrying ac transport current. *Physica C: Superconductivity*, 426-431, pp.1339–1342.

Daunt, J. & Cobble, J., 1953. Superconductivity of Technetium. *Physical Review*, 92(2), pp.507–508.

Dommerque, R. et al., 2010. First commercial medium voltage superconducting fault-current limiters: production, test and installation. *Superconductor Science and Technology*, 23(3), p.034020.

Donnier-Valentin, G., Tixador, P. & Vinot, E., 2001. Considerations about HTS superconducting transformers. *IEEE Transactions on Applied Superconductivity*, 11(1), pp.1498–1501.

Duckworth, R.C. et al., 2005. Substrate and stabilization effects on the transport AC losses in YBCO coated conductors. In *IEEE Transactions on Applied Superconductivity*. pp. 1583–1586.

Duckworth, R.C. et al., 2003a. Transport ac loss studies of YBCO coated conductors with nickel alloy substrates. *Superconductor Science and Technology*, 16(11), pp.1294–1298.

Duckworth, R.C. et al., 2003b. Transport ac loss studies of YBCO coated conductors with nickel alloy substrates. *Superconductor Science and Technology*, 16(11), pp.1294–1298.

Farhangi, H., 2010. The path of the smart grid. *IEEE Power and Energy Magazine*, 8(1), pp.18–28.

Fietz, W. et al., 1964. Magnetization of Superconducting Nb-25%Zr Wire. *Physical Review*, 136(2A), pp.A335–A345.

Frank, A. et al., 2008. Roebel assembled coated conductor cables (RACC): Ac-Losses and current carrying potential. *Journal of Physics: Conference Series*, 97, p.012147.

Frank, M. et al., 2006. High-Temperature Superconducting Rotating Machines for Ship Applications. *IEEE Transactions on Applied Superconductivity*, 16(2), pp.1465–1468.

French, R.A., 1968. Intrinsic type-2 superconductivity in pure niobium. *Cryogenics*, 8(5), pp.301–308.

Fujiwara, N. et al., 2010. Development of YBCO power devices in Japan. *Physica C: Superconductivity*, 470(20), pp.980–985.

Fukui, S. et al., 2006. Numerical Study on AC Loss Characteristics of HTS Coils With Various Cross Sections and Methods of AC Loss Reduction. *IEEE Transactions on Applied Superconductivity*, 16(2), pp.139–142.

Fukui, S. et al., 2008. Study on Optimal Design of High Temperature Superconducting Coil Based on AC Loss Minimization. *IEEE Transactions on Applied Superconductivity*, 18(2), pp.1366–1369.

Garrity, T., 2008. Getting Smart. *IEEE Power and Energy Magazine*, 6(2), pp.38–45.

Goldacker, W. et al., 2007. ROEBEL Assembled Coated Conductors (RACC): Preparation, Properties and Progress. *IEEE Transactions on Applied Superconductivity*, 17(2), pp.3398–3401.

Gomory, F. et al., 2009. Magnetic Flux Penetration and Transport AC Loss in Superconductor Coated Conductor on Ferromagnetic Substrate. *IEEE Transactions on Applied Superconductivity*, 19(3), pp.3102–3105.

Gomory, F. et al., 2001. Partitioning of transport AC loss in a superconducting tape into magnetic and resistive components. *IEEE Transactions on Applied Superconductivity*, 11(1), pp.2967–2970.

Gömöry, F., 2006. Improvement of the self-field critical current of a high-T[sub c] superconducting tape by the edge cover from soft ferromagnetic material. *Applied Physics Letters*, 89(7), p.072506.

Gömöry, F. et al., 2009. Magnetic flux penetration and AC loss in a composite superconducting wire with ferromagnetic parts. *Superconductor Science and Technology*, 22(3), p.034017.

Gömöry, F. et al., 2004. The influence of filament arrangement on current distribution and AC loss in Bi-2223/Ag tapes. *Superconductor Science and Technology*, 17(5), pp.S150–S154.

Goyal, A., Parans Paranthaman, M. & Schoop, U., 2004. The RABiTS approach: Using rolling-assisted biaxially textured substrates for high-performance YBCO superconductors. *MRS bulletin*, 29(8), pp.552–561.

Granados, X. et al., 2002. Design, building up and testing of a 400 hybrid FCL. *Physica C: Superconductivity*, 372-376, pp.1680–1683

Granados, X. et al., 2008. Low-power superconducting motors. *Superconductor Science and Technology*, 21(3), p.034010.

Grilli, F., 2003. *Numerical Modelling of High Temperature Superconducting Tapes and Cables*. École Polytechnique Fédérale De Lausanne.

Grilli, F., Ashworth, S.P. & Stavrev, S., 2006. Magnetization AC losses of stacks of YBCO coated conductors. *Physica C: Superconductivity*, 434(2), pp.185–190.

Grilli, F. & Pardo, E., 2010. Simulation of ac loss in Roebel coated conductor cables. *Superconductor Science and Technology*, 23, p.115018.

Grivel, J.-C. & Flükiger, R., 1996. Visualization of the formation of the phase. *Superconductor Science and Technology*, 9(7), pp.555–564.

Halliday, D., Resnick, R. & Walker, J., 2011. *Fundamentals of Physics* 9th Edition, Wiley.

Hammerl, G. et al., 2002. Possible solution of the grain-boundary problem for applications of high-T- c superconductors. *Applied Physics Letters*, 81(17), p.3209.

Hassenzahl, W.V. et al., 2004. Electric power applications of superconductivity. *Proceedings of the IEEE*, 92(10), pp.1655–1674.

Hayakawa, N. et al., 2000. Feasibility study on superconducting fault current limiting transformer (SFCLT). *Cryogenics*, 40(4-5), pp.325–331.

Hayakawa, N. et al., 2011. Progress in Development of Superconducting Fault Current Limiting Transformer (SFCLT). *IEEE Transactions on Applied Superconductivity*, 21(3), pp.1397–1400.

Hong, Z., Campbell, a M. & Coombs, T. a, 2006. Numerical solution of critical state in superconductivity by finite element software. *Superconductor Science and Technology*, 19(12), pp.1246–1252.

Honjo, S. et al., 2011. Status of Superconducting Cable Demonstration Project in Japan. *IEEE Transactions on Applied Superconductivity*, 21(3), pp.967–971.

IEA, (International Energy Agency), 2012. 2012 Key World Energy Statistics. , p.82.

IEC, 2006. IEC International Standard 61788-3.

Ihara, H. et al., 1988. A new high-Tc TlBa2Ca3Cu4O11 superconductor with Tc >120K. *Nature*, 334(6182), pp.510–511.

Ijaduola, A.O. et al., 2004. Magnetism and ferromagnetic loss in Ni–W textured substrates for coated conductors. *Physica C: Superconductivity*, 403(3), pp.163–171.

Irie, F. & Yamafuji, K., 1967. Theory of Flux Motion in Non-Ideal Type-II Superconductors. *Journal of the Physical Society of Japan*, 23(2), pp.255–268.

Ishii, H. et al., 1996. The a.c. losses in (Bi,Pb)2Sr2Ca2Cu3Ox silver-sheathed superconducting wires. *Cryogenics*, 36(9), pp.697–703.

Ishiyama, A. et al., 2001. Research and development of HTS-SMES system. *Physica C: Superconductivity*, 357-360, pp.1311–1314.

Iwakuma, M. et al., 2001. AC loss properties of a 1 MVA single-phase HTS power transformer. *IEEE Transactions on Applied Superconductivity*, 11(1), pp.1482–1485.

Jiang, Q. et al., 2006. Design and AC loss analysis of a superconducting synchronous motor. *Superconductor Science and Technology*, 19(11), pp.1164–1168.

Jiang, Z.Q. & Jin, J.X., 2011. Critical current measurement and experimental comparison of 1 G and 2 G HTS tapes. *2011 International Conference on Applied Superconductivity and Electromagnetic Devices*, pp.145–149.

Jorgensen, J.D. et al., 1991. Defects, defect ordering, structural coherence and superconductivity in the 123 copper oxides. *Physica C: Superconductivity*, 185-189, pp.184–189.

Kalsi, S.S., 2002. Development status of superconducting rotating machines. In *2002 IEEE Power Engineering Society Winter Meeting. Conference Proceedings (Cat. No.02CH37309)*. IEEE, pp. 401–403.

Kim, H.-J. et al., 2006. AC loss characteristics of Bi-2223 HTS tapes under bending. *Physica C: Superconductivity*, 445-448, pp.768–771.

Kim, J.-H. et al., 2011. Transport AC Loss Measurements in Superconducting Coils. *IEEE Transactions on Applied Superconductivity*, 21(3), pp.3269–3272.

Kim, Y., Hempstead, C. & Strnad, A., 1962. Critical Persistent Currents in Hard Superconductors. *Physical Review Letters*, 9(7), pp.306–309.

Kim, Y., Hempstead, C. & Strnad, A., 1963. Magnetization and Critical Supercurrents. *Physical Review*, 129(2), pp.528–535.

Kovalsky, L. et al., 2005. Applications of Superconducting Fault Current Limiters in Electric Power Transmission Systems. *IEEE Transactions on Applied Superconductivity*, 15(2), pp.2130–2133.

Lemmon, E.W., Huber, M.L. & McLinden, M.O., 2007. *NIST Standard Reference Database 23: Reference Fluid Thermodynamic and Transport Properties-REFPROP, Version 8.0*, Gaithersburg.

Maeda, H. et al., 1988. A New High- Tc Oxide Superconductor without a Rare Earth Element. *Japanese Journal of Applied Physics*, 27(Part 2, No. 2), pp.L209–L210.

Maguire, J.F. et al., 2007. Development and Demonstration of a HTS Power Cable to Operate in the Long Island Power Authority Transmission Grid. *IEEE Transactions on Applied Superconductivity*, 17(2), pp.2034–2037.

Majoros, M. et al., 2008. AC LOSSES IN YBCO COATED CONDUCTORS WITH DIFFERENT SUBSTRATES AND DIFFERENT STABILIZING LAYERS. In *ADVANCES IN CRYOGENIC ENGINEERING MATERIALS: Transactions of the International Cryogenic Materials Conference*.

Majoros, M. et al., 2011. AC Magnetization Loss of a YBCO Coated Conductor Measured Using Three Different Techniques. *IEEE Transactions on Applied Superconductivity*, 21(3), pp.3293–3296.

Majoros, M. et al., 2007. Transport AC losses in YBCO coated conductors. *Superconductor Science and Technology*, 20(9), pp.S299–S304.

Majoros, M., Sumption, M.D. & Collings, E.W., 2009. Transport AC Loss Reduction in Striated YBCO Coated Conductors by Magnetic Screening. *IEEE Transactions on Applied Superconductivity*, 19(3), pp.3352–3355.

Malozemoff, A.P. et al., 2002. Power applications of high-temperature superconductors: status and perspectives. *IEEE Transactions on Appiled Superconductivity*, 12(1), pp.778–781.

McIntyre, P.C., Cima, M.J. & Roshko, A., 1995. Epitaxial nucleation and growth of chemically derived Ba2YCu3O7−x thin films on (001) SrTiO3. *Journal of Applied Physics*, 77(10), p.5263.

Meissner, W. & Ochsenfeld, R., 1933. Ein neuer Effekt bei Eintritt der Supraleitfähigkeit. *Die Naturwissenschaften*, 21(44), pp.787–788.

Molina, M.G., Enrique Mercado, P. & Hirokazu Watanabe, E., 2011. Improved Superconducting Magnetic Energy Storage (SMES) Controller for High-Power Utility Applications. *IEEE Transactions on Energy Conversion*, 26(2), pp.444–456.

Morandi, A., 2013. State of the art of superconducting fault current limiters and their application to the electric power system. *Physica C: Superconductivity*, 484, pp.242–247.

Morandi, A. et al., 2008. Superconducting transformers: key design aspects for power applications. *Journal of Physics: Conference Series*, 97, p.012318.

Müller, K.-H., 1997. Self-field hysteresis loss in periodically arranged superconducting strips. *Physica C: Superconductivity*, 289(1-2), pp.123–130.

Nguyen, D.N. et al., 2009. A new finite-element method simulation model for computing AC loss in roll assisted biaxially textured substrate YBCO tapes. *Superconductor Science and Technology*, 23(2), p.025001.

Nguyen, D.N. et al., 2013. Electrical measurements of AC losses in high temperature superconducting coils at variable temperatures. *Superconductor Science and Technology*, 26(9), p.095001.

Nguyen, D.N. et al., 2009. Temperature Dependence of Total AC Loss in High-Temperature Superconducting Tapes. *IEEE Transactions on Applied Superconductivity*, 19(4), pp.3637–3644.

Nibbio, N., Stavrev, S. & Dutoit, B., 2001. Finite element method simulation of AC loss in HTS tapes with B-dependent E-J power law. *IEEE Transactions on Applied Superconductivity*, 11(1), pp.2631–2634.

Noe, M. & Steurer, M., 2007. High-temperature superconductor fault current limiters: concepts, applications, and development status. *Superconductor Science and Technology*, 20(3), pp.R15–R29.

Norris, W.T., 1970. Calculation of hysteresis losses in hard superconductors carrying ac: isolated conductors and edges of thin sheets. *Journal of Physics D: Applied Physics*, 3(4), pp.489–507.

Okamoto, H. et al., 2006. The Nitrogen Boil-Off Method for Measuring AC Losses in HTS Coils. *IEEE Transactions on Applied Superconductivity*, 16(2), pp.105–107.

Onnes, H.K., 1913. Investigations into the properties of substances at low temperatures, which have led, amongst other things, to the preparation of liquid helium. *Nobel Prize Winning Speech*.

Orlando, T.P. & Delin, k. A., 1991. *Foundations of Applied Superconductivity*, Addison-Wesley.

Pardo, E., Souc, J., et al., 2009. AC Loss and Voltage Signal in a Pancake Coil Made of Coated Conductor With Ferromagnetic Substrate. *IEEE Transactions on Applied Superconductivity*, 19(3), pp.2223–2227.

Pardo, E., 2008. Modeling of coated conductor pancake coils with a large number of turns. *Superconductor Science and Technology*, 21(6), p.065014.

Pardo, E., Šouc, J. & Frolek, L., 2015. Electromagnetic modelling of superconductors with a smooth current–voltage relation: variational principle and coils from a few turns to large magnets. *Superconductor Science and Technology*, 28(4), p.044003.

Pardo, E., Šouc, J. & Kováč, J., 2012. AC loss in ReBCO pancake coils and stacks of them: modelling and measurement. *Superconductor Science and Technology*, 25(3), p.035003.

Pardo, E., Šouc, J. & Vojenčiak, M., 2009. AC loss measurement and simulation of a coated conductor pancake coil with ferromagnetic parts. *Superconductor Science and Technology*, 22(7), p.075007.

Park, M., Kwak, S. & Kim, W., 2007. AC Loss and Thermal Stability of HTS Model Coils for a 600 kJ SMES. *IEEE Transactions on Applied Superconductivity*, 17(2), pp.2418–2421.

Park, M.-J. et al., 2007. Analysis of magnetic field distribution and AC losses of a 600kJ SMES. *Cryogenics*, 47(7-8), pp.391–396.

Perez, B. et al., 2003. AC losses in a toroidal superconducting transformer. *IEEE Transactions on Applied Superconductivity*, 13(2), pp.2341–2343.

Pina, J. et al., 2010. High Temperature Superconducting Fault Current Limiters as Enabling Technology in Electrical Grids with Increased Distributed Generation Penetration L. M. Camarinha-Matos, P. Pereira, & L. Ribeiro, eds. *IFIP Advances in Information and Communication Technology*, 314, pp.427–434.

Polák, M. et al., 2006. The effect of epoxy impregnation on the behaviour of a Bi-2223/Ag coil carrying DC or AC current. *Superconductor Science and Technology*, 19(4), pp.256–262.

Poole, C. et al., 2007. *Superconductivity* 2nd Editio., Academic Press.

Rabbers, J.J., 2001. *AC Loss in Superconducting Tapes and Coils*.

Rabbers, J.J. et al., 2001. An engineering formula to describe the AC loss of BSCCO/Ag tape. *IEEE Transactions on Applied Superconductivity*, 11(1), pp.2623–2626.

Rhyner, J., 1993. Magnetic properties and AC-losses of superconductors with power law current—voltage characteristics. *Physica C: Superconductivity*, 212(3-4), pp.292–300.

Rosa, E.B. & Grover, F.W., 1948. *Formulas and Tables for the calculation of mutual and self-inductance*, Washington: United States Government Printing Office.

Rupich, M.W. et al., 2007. The Development of Second Generation HTS Wire at American Superconductor. *IEEE Transactions on Applied Superconductivity*, 17(2), pp.3379–3382.

Schilling, A. et al., 1993. Superconductivity above 130 K in the Hg–Ba–Ca–Cu–O system. *Nature*, 363(6424), pp.56–58.

Schuller, S. et al., 2007. Ac-loss measurement of a DyBCO-Roebel assembled coated conductor cable (RACC). *Physica C: Superconductivity and its Applications*, 463-465, pp.761–765.

See, K.W., Cook, C.D. & Dou, S.X., 2011. Innovative Calorimetric AC Loss Measurement of HTSC for Power Applications. *IEEE Transactions on Applied Superconductivity*, 21(3), pp.3261–3264.

Selvamanickam, V. et al., 2001. High-current Y-Ba-Cu-O coated conductor using metal organic chemical-vapor deposition and ion-beam-assisted deposition. *IEEE Transactions on Applied Superconductivity*, 11(1), pp.3379–3381.

Selvamanickam, V. et al., 1998. High-temperature superconductors for electric power and high-energy physics. *Journal of the Minerals, Minerals and Materials Society*, 50(10), pp.27–30.

Shevchenko, O. et al., 1998. AC loss in a high-temperature superconducting coil. *Physica C: Superconductivity*, 310(1-4), pp.106–110.

Sirois, F. & Grilli, F., 2015. Potential and limits of numerical modelling for supporting the development of HTS devices. *Superconductor Science and Technology*, 28(4), p.043002.

Snitchler, G. et al., 2011. 10 MW Class Superconductor Wind Turbine Generators. *IEEE Transactions on Applied Superconductivity*, 21(3), pp.1089–1092.

Souc, J. et al., 2006. AC loss of YBCO coated tape prepared by laser ablation. *Journal of Physics: Conference Series*, 43, pp.127–129.

Šouc, J. et al., 2009. Theoretical and experimental study of AC loss in high temperature superconductor single pancake coils. *Superconductor Science and Technology*, 22(1), p.015006.

Stavrev, S. et al., 2002. Comparison of numerical methods for modeling of superconductors. *IEEE Transactions on Magnetics*, 38(2), pp.849–852.

Stavrev, S. & Dutoit, B., 1998. Frequency dependence of AC loss in Bi(2223)Ag-sheathed tapes. *Physica C: Superconductivity*, 310(1-4), pp.86–89.

Stavrev, S., Dutoit, B. & Lombard, P., 2003. AC losses of multifilamentary Bi-2223/Ag conductors with different geometry and filament arrangement. In *IEEE Transactions on Applied Superconductivity*. pp. 3561–3565.

Stovall, J.P. et al., 2001. Installation and operation of the Southwire 30-meter high-temperature superconducting power cable. *IEEE Transactions on Applied Superconductivity*, 11(1), pp.2467–2472.

Suarez, P. et al., 2010. An Experimental Study of the Ferromagnetic Loss in 2G YBCO Tapes. *IEEE Transactions on Applied Superconductivity*, 20(5), pp.2327–2330.

Suarez, P. et al., 2009. Losses in 2G Tapes Wound Close Together: Comparison With Similar 1G Tape Configurations. *IEEE Transactions on Applied Superconductivity*, 19(3), pp.2395–2398.

Suárez, P. et al., 2008. Influence of the current through one turn of a multilayer coil on the nearest turn in a consecutive layer. *Journal of Physics: Conference Series*, 97, p.012176.

Suenaga, M., 2002. AC losses in stacked Bi2Sr2Ca2Cu3O10/Ag tapes with different stacking arrangements. *Physica C: Superconductivity*, 372-376, pp.1730–1733.

Takacs, S. & Campbell, A.M., 1988. Hysteresis losses in superconductors with very fine filaments. *Superconductor Science and Technology*, 1(1), pp.53–56.

Tanaka, H., Furuse, M. & Umeda, M., 2004. Heat Generation by Vibration and Coil Rigidity of Bi2223 Pancake Coil. *IEEE Transactions on Applied Superconductivity*, 14(2), pp.859–862.

Terzieva, S. et al., 2010. Transport and magnetization ac losses of ROEBEL assembled coated conductor cables: measurements and calculations. *Superconductor Science and Technology*, 23(1), p.014023.

Tixador, P., 2010. Development of superconducting power devices in Europe. *Physica C: Superconductivity*, 470(20), pp.971–979.

Tønnesen, O. et al., 2004. Operation experiences with a 30 kV/100 MVA high temperature superconducting cable system. *Superconductor Science and Technology*, 17(5), pp.S101–S105.

Tsuda, M. et al., 2015. Estimation Method of AC Losses in HTS Tape Against a Distorted Current and/or a Distorted Magnetic Field With Harmonic Components. *IEEE Transactions on Applied Superconductivity*, 25(3), pp.1–5.

Tsukamoto, O., 2005. Roads for HTS power applications to go into the real world: Cost issues and technical issues. *Cryogenics*, 45(1), pp.3–10.

Vojenčiak, M. et al., 2006. Study of ac loss in Bi-2223/Ag tape under the simultaneous action of ac transport current and ac magnetic field shifted in phase. *Superconductor Science and Technology*, 19(4), pp.397–404.

Vojenčiak, M., Šouc, J. & Gömöry, F., 2011. Critical current and AC loss analysis of a superconducting power transmission cable with ferromagnetic diverters. *Superconductor Science and Technology*, 24(7), p.075001.

Wang, Y., Zhou, W. & Dai, J., 2015. An applicable calorimetric method for measuring AC losses of 2G HTS wire using optical FBG. *Science China Technological Sciences*, 58(3), pp.545–550.

Watson, J.H.P., 1968. Magnetization of Synthetic Filamentary Superconductors. B. The Dependence of the Critical Current Density on Temperature and Magnetic Field. *Journal of Applied Physics*, 39(7), p.3406.

Wexler, A. & Corak, W., 1952. Superconductivity of Vanadium. *Physical Review*, 85(1), pp.85–90.

Wu, M. et al., 1987. Superconductivity at 93 K in a new mixed-phase Y-Ba-Cu-O compound system at ambient pressure. *Physical Review Letters*, 58(9), pp.908–910..

Xiao, L. et al., 2012. Development of the World's First HTS Power Substation. *IEEE Transactions on Applied Superconductivity*, 22(3), pp.5000104–5000104.

Xu, Y. et al., 2013. Distribution of AC loss in a HTS magnet for SMES with different operating conditions. *Physica C: Superconductivity*, 494, pp.213–216.

Yamamoto, M., Yamaguchi, M. & Kaiho, K., 2000. Superconducting transformers. *IEEE Transactions on Power Delivery*, 15(2), pp.599–603.

Yasuda, K. et al., 2005. Research & Development of Superconducting Fault Current Limiter in Japan. *IEEE Transactions on Applied Superconductivity*, 15(2), pp.1978–1981.

Yinshun Wang, Xiaojin Guan & Jingshu Dai, 2014. Review of AC Loss Measuring Methods for HTS Tape and Unit. *IEEE Transactions on Applied Superconductivity*, 24(5), pp.1–6.

Yoshida, T. et al., 2003. AC loss characteristics of Bi2223 twisted multifilamentary tape in AC longitudinal magnetic field. In *IEEE Transactions on Applied Superconductivity*. pp. 2372–2375.

Yuan, J. et al., 2005. Study of frequency dependent AC loss in Bi-2223 tapes used for gradient coils in magnetic resonance imaging. *Physica C: Superconductivity*, 424(1-2), pp.72–78.

Yuan, W., Campbell, a M. & Coombs, T. a, 2009. A model for calculating the AC losses of second-generation high temperature superconductor pancake coils. *Superconductor Science and Technology*, 22(7), p.075028.

Zhang, G. et al., 2011. The Construction Progress of a High-Tc Superconducting Power Substation in China. *IEEE Transactions on Applied Superconductivity*, 21(3), pp.2824–2827.

Zhang, J. et al., 2012. Construction, Testing and Operation of a 1 MJ HTS Magnet at a 10.5 kV Superconducting Power Substation. *IEEE Transactions on Applied Superconductivity*, 22(3), pp.5700504–5700504.

Zhao, Y. et al., 2011. Comparison between measured and numerically calculated AC losses in second-generation high temperature superconductor pancake coils. *Physica C: Superconductivity*, 471(21-22), pp.1003–1006.